INSTITUTO SUPERIOR DE ENGENHARIA DE LISBOA

Departamento de Engenharia Eletrónica e Telecomunicações e Computadores

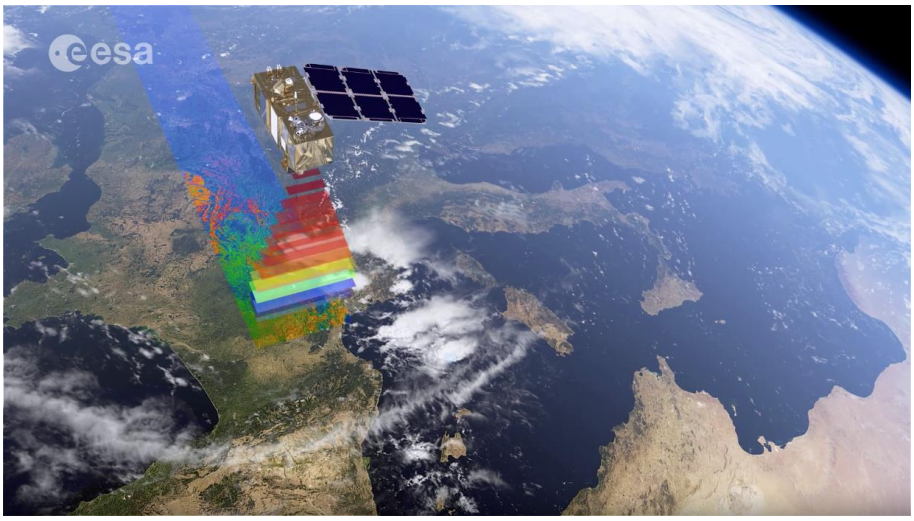

Water quality estimation using spaceborne platforms: A case study in Portuguese Dams

DIOGO JOSÉ MENDES DOMINGOS

Licenciado em Engenharia Informática, Redes e Telecomunicações

Dissertação para obtenção do Grau de Mestre
em Engenharia de Eletrónica e Telecomunicações

Orientador: Professor Doutor Paulo Alexandre Carapinha Marques

Júri:
Presidente: Professor Doutor Vítor Manuel de Oliveira Fialho
Vogal: Professor Doutor Andrea Radius

Julho de 2024

INSTITUTO SUPERIOR DE ENGENHARIA DE LISBOA

Departamento de Engenharia Eletrónica e Telecomunicações e Computadores

Water quality estimation using spaceborne platforms: A case study in Portuguese Dams

DIOGO JOSÉ MENDES DOMINGOS

Licenciado em Engenharia Informática, Redes e Telecomunicações

Dissertação para obtenção do Grau de Mestre
em Engenharia de Eletrónica e Telecomunicações

Orientador: Professor Doutor Paulo Alexandre Carapinha Marques, ISEL

Júri:
Presidente: Professor Doutor Vítor Manuel de Oliveira Fialho, ISEL
Vogal: Professor Doutor Andrea Radius, ICEYE

Julho de 2024

ACKNOWLEDGMENTS

Escrevo estes agradecimentos no fim de uma longa caminhada académica de quase 18 anos, já depois de ter tudo estudado, desenvolvido, testado e escrito.

Começo por agradecer ao meu orientador, o professor Paulo Marques, que aceitou, uma vez mais, embarcar noutra aventura académica comigo, repetindo a sua mentoria, previamente demonstrada no projeto final de curso. A si o meu grande obrigado, por me ter dado a mão quando estava indeciso e sem nenhum rumo definido, por me ter colocado os pés no chão quando foi preciso, e por ter demonstrado sempre o verdadeiro significado de professor.

De seguida agradeço a minha família, à minha mãe, Maria do Carmo, e ao meu pai, José, que me apoiaram desde o primeiro ao último momento, que me souberam acalmar quando tudo tinha desabado. Ao meu irmão, Tiago, que me ajudou das formas mais subtis, com apontamentos, com dicas sobre os assuntos que não dominava, por fazer sacrifícios que só agora me dou conta deles. O amor que sinto por vocês não se mede. À restante família, avós, tios, primos, e Marta, que me ajudaram nas minhas fases de crescimento, que me aturaram quando fazia asneira, obrigado por tudo. Em especial ao meu avô Antero, a minha Avó Deonilde, aos meus tios Manel, Fernando e Ilda, e ao meu padrinho Carlos, que me acompanharam neste processo desde o céu, obrigado por terem feito parte da minha vida, espero ter-vos feito orgulhoso.

Aos meus eternos colegas de faculdade Miguel Gama e Bernardo Balona, que me acompanharam praticamente desde o primeiro dia de faculdade, e estiveram comigo em tudo. Puxaram-me a terra quando necessário e enalteceram-me quando era tempo para isso. Nunca vos vou esquecer.

Aos meus amigos que me aturaram neste processo doloroso que é crescer, que me fizeram amadurecer, rir, chorar, cantar, tudo! Em especial ao Rodrigo Coutinho que está comigo desde a cresce, à Beatriz Bonnet que me acompanha desde o primeiro ano de escolaridade, ao Pedro Carvalho que se tornou das pessoas mais próximas, e ao Henrique Laureano e Rodrigo Mendes pelos anos de companheirismo desde o secundário.

Aos meus colegas de grupo da JAP, que são uma segunda família, João, Ricardo, Ana Margarida, Rafa, Maria e Inês, que são quem mais convivem comigo no momento. Tenho um orgulho imenso em ter decidido em ter apostado neste grupo e nesta maneira de viver. Em especial ao João e ao Ricardo que para além de problemas mais supérfluos, me ajudam com os meus problemas mais profundos e restritos.

À minha família e colegas de praxe, em especial à minha madrinha Ana Sofia Grácio, e as minhas irmãs de praxe, Claúdia Louro e Sandra Wang, que a nossa unidade não pare. Obrigado por fazerem parte deste percurso.

À minha querida terra, Fundada, que foi sempre o meu refúgio e porto seguro, em especial à Daniela Domingos e à Carla Silva, as primeiras pessoas de quem me tornei amigo de verdade num lugar tão perto e tão distante, que me ajudaram nas mais diversas situações, que me deram força e confiança para me tornar ainda mais parte da terra dos meus pais.

À minha querida Villa D'el Rei Tuna, que me deu a oportunidade de conhecer novas pessoas, fortalecer laços e sair da minha zona de conforto. Vai tuna!

A São Domingos de Rana e a São José, a todas as pessoas que fazem parte desta maravilhosa comunidade, em especial aos padres, JAP, comissões de festas e voluntários. É incrível o impacto que 2 anos têm numa pessoa. Obrigado por tornarem estes meros locais de passagem a casa.

Às instituições e respetivos membros que me ajudaram no desenvolvimento desta tese. À Associação Portuguesa do Ambiente, pela disponibilidade em facultar dados e/ou maneira de como obtê-los. À Celfinet, na pessoa do Miguel Pacheco, que sempre se mostraram disponíveis para me ajudar no que fosse preciso para que conseguisse conciliar o trabalho e a faculdade.

Às instituições de ensino que me formaram, escola EB1 Nº1 de São Domingos de Rana, Salesianos de Manique e Instituto Superior de Engenharia de Lisboa. Ao meu clube de coração, Grupo Sportivo de Carcavelos, que foi a minha segunda casa ao longo de 12 anos. Irão sempre permanecer dentro de mim.

Aos professores que passaram por mim nestes anos, em especial à professora Iva Pereira e professora Silvia Dias, que fizeram parte do meu percurso final nos Salesianos e que me marcaram das mais variadas formas. Ao professor Vítor Fialho, ao professor Paulo Marques e à professora Paula Louro, que fizeram parte do meu percurso no ISEL e que tornaram a vida universitária mais fácil, pela maneira de ser, pelo companheirismo e pelo ouvido interessado em resolver e esclarecer o problema dos alunos. Obrigado por me terem formado enquanto aluno e pessoa.

Por fim, agradeço a todos os que fizeram parte deste percurso académico, e que não foram mencionados de forma particular, professores, colegas de sala de aula, catequistas, colegas de equipa e amigos mais distantes. Obrigado por tudo.

A vida só faz sentido se for vivida em comunidade.

Statement of integrity

I declare that this dissertation / project work / internship report is the result of my personal and independent research. Its content is original, and all sources listed in the bibliographic references were consulted and are duly mentioned in the text. I further declare that all scientific and technical references relevant to the development of the work are duly cited and included in the bibliographic references.

The author

Assinado por: **Diogo José Mendes Domingos**
Num. de Identificação: 15826662
Data: 2024.07.19 20:12:15+01'00'

Lisbon, ……., ……

CHAVE MÓVEL

ABSTRACT

Monitoring the volume and quality of large bodies of water through *in situ* samples can be labour intensive, time consuming and expensive.

In order to increase the efficiency of these processes, there has been an investment, in recent years, in the use of spaceborne platforms that detect and store information from the energy reflected by the Earth.

This dissertation explores the various techniques proposed in recent literature for monitoring and estimating the quality and volume of water through remote sensing. A methodology is developed and tested to achieve these two objectives, using data obtained from the European Space Agency's (ESA) space missions.

The process uses data from the Sentinel-2 mission and the metrics needed to qualify the state of the water, such as the Chlorophyll-a indicator, the quantity of suspended particles and the concentration of coloured dissolved organic matter.

After validation of the methodology, a study of the last decade will be carried out on the evolution of water quantity and quality in some of Portugal's dams.

Keywords: Remote sensing, water quality, water volume, Chlorophyll-a, suspended particles, coloured dissolved organic matter.

RESUMO

O acompanhamento do volume e qualidade de grandes massas de água é dispendioso em termos logísticos, financeiros e temporais, desde a obtenção de amostras físicas até a análise laboratorial.

De forma a aumentar a eficiência destes processos, tem existido nos últimos anos um investimento na utilização de plataformas espaciais que detetam e guardam informação proveniente de energia refletida pela terra.

Esta dissertação explora as diversas técnicas propostas em bibliografia recente para monitorização e estimação da qualidade e volume de água em diversas barragens do território nacional. É desenvolvido e testado um processo para a obtenção destes dois objetivos, a partir dos dados obtidos pelas missões espaciais da Agência Espacial Europeia.

Este processo conta com o uso de dados adquiridos pela missão Sentinel-2 e de métricas necessárias para qualificar o estado da água, como o índice de Clorofila-a, a quantidade de partículas suspensas e a concentração de matéria orgânica colorida dissolvida.

Uma vez validada a metodologia, é feito um estudo da última década sobre a evolução da quantidade e qualidade de água em algumas das barragens portuguesas.

Palavras chave: Observação remota, qualidade da água, volume da água, Clorofila-a, partículas suspensas, matéria orgânica colorida dissolvida.

INDEX

1 INTRODUCTION 19

1.1 Motivation 19

1.2 Objectives 19

1.3 Document Organization 20

2 STATE OF THE ART 21

2.1 Optical remote sensing techniques 21

2.1.1 The Copernicus Programme 24

2.1.2 Sentinel-1 26

2.1.3 Sentinel-2 27

2.1.4 Sentinel-3 28

2.1.5 Satellites comparison 31

2.2 Metrics 32

2.2.1 Chlorophyll-a 33

2.2.2 Total Suspended Matter 34

2.2.3 Turbidity 34

2.2.4 Coloured Dissolved Organic Matter 35

2.2.5 Other metrics 36

2.2.6 Water Quality Indices 36

2.3 Training Courses 38

2.3.1 Tools 39

2.3.2 HYDR02 – Freshwater Quality Monitoring using Sentinel-2 41

2.3.3 Monitoring Water Quality of Inland Lakes using Remote Sensing 42

3 METHODOLOGY 43

3.1 Proposed solution 43

3.2 Portuguese Dams 43

3.2.1 Aguieira Dam 44

3.2.2 Castelo de Bode Dam 44
3.2.3 Alqueva Dam 45
3.2.4 Odelouca Dam 45
3.3 Process and Data Acquisition 46
3.3.1 Data Acquisition 46
3.3.2 Water quality monitoring process 47
3.3.3 Water quantity monitoring process 52
4 RESULTS 53
4.1 Training course replication 53
4.2 Results discussion 55
4.2.1 Pixel validation results comparison 55
4.2.2 Chlorophyll concentration results 57
4.2.3 TSM and CDOM concentration results 62
4.2.4 Water quantity evolution 72
5 CONCLUSIONS 75

FIGURES LIST

Figure 1 - Earth observation missions developed by ESA [11] 24
Figure 2 - Schematic View of the Deployed Sentinel-1 Spacecraft, extracted from [16] 26
Figure 3 - Twin-Satellite Sentinel-2 Orbital Configuration, extracted from[21] 27
Figure 4 - Whisk broom vs Push broom, extracted from [22] 28
Figure 5 - Sentinel-3 Satellite and Payloads, extracted from [30] 29
Figure 6 - GlobColour Chlorophyll Monthly Product from OLCI-A [31] 30
Figure 7 - Sentinel-2 layout of spectral bands, extracted from [34]. 31
Figure 8 - Visual verification of Chlorophyll [39] 33
Figure 9 - Example of different turbid water samples, extracted from [42] 35
Figure 10 - Absorption coefficients of water, CDOM, phytoplankton and non-algal particles, extracted from [41] 35
Figure 11 - Freshwater Quality Monitoring - Exercise workflow [35] 41
Figure 12 - Monitoring Water Quality of Inland Lakes using Remote Sensing 42
Figure 13 - Rivers and locations for the selected dams 43
Figure 14 – Aguieira Dam [62] 44
Figure 15 – Castelo de Bode Dam [63] 44
Figure 16 – Alqueva Dam [64] 45
Figure 17 – Odelouca Dam [65] 45
Figure 18 - Resample and Subset: (A): Before; (B): After 48
Figure 19 - (A) Chlorophyll concentration; (B) TSM concentration; (C) CDOM concentration. 49
Figure 20 - NDWI - water and vegetation reflectance's 50
Figure 21 – Side-by-side comparison between the default (A) and new (B) expression. 50
Figure 22 - *In Situ* locations for each dam 52
Figure 23 - Lago Trasimeno with the colour palettes for Chl-a (A), TSM (B) and CDOM (C) - Speaker version [55] 53
Figure 24 - Lago Trasimeno with the colour palettes for Chl-a (A), TSM (B) and CDOM (C) - Thesis version 54
Figure 25 – Aguieira dam on the 21-11-2017; (A) - NDWI (B) – Default 55
Figure 26 - Aguieira dam on the 30-01-2018; (A) - NDWI (B) - Default 55
Figure 27 – Castelo de Bode dam on the 02-09-2017; (A) - NDWI (B) – Default 56
Figure 28 - Alqueva dam on the 23-06-2021; (A) - NDWI (B) – Default 56
Figure 29 - Odelouca dam on the 22-11-2015; (A) - NDWI (B) – Default 56
Figure 30 - Linear regression for MCI in the Aguieira dam 57

Figure 31 - Linear regression for BandRatio in the Aguieira dam 57
Figure 32 - Linear regression for MCI in the Castelo de Bode dam..... 58
Figure 33 - Linear regression for BandRatio in the Castelo de Bode dam 58
Figure 34 - Linear regression for MCI in the Alqueva dam..... 58
Figure 35 - Linear regression for BandRatio in the Alqueva dam..... 59
Figure 36 - Linear regression for MCI in the Odelouca dam 59
Figure 37 - Linear regression for BandRatio in the Odelouca dam 59
Figure 38 - Empirical models for the Aguieira dam..... 60
Figure 39 - Empirical models for the Castelo de Bode dam 60
Figure 40 - Empirical models for the Alqueva dam 61
Figure 41 - Empirical models for the Odelouca dam..... 61
Figure 42 – Statistical analysis - TSM concentrations - Aguieira Dam..... 63
Figure 43 – Statistical analysis - TSM concentrations - Castelo de Bode Dam..... 63
Figure 44 – Statistical analysis - TSM concentrations - Alqueva Dam..... 64
Figure 45 – Statistical analysis - TSM concentrations - Odelouca Dam..... 64
Figure 46 – Visual analysis - TSM concentrations - Aguieira Dam..... 65
Figure 47 – Visual analysis - TSM concentrations - Castelo de Bode Dam..... 65
Figure 48 – Visual analysis - TSM concentrations - Alqueva Dam..... 66
Figure 49 – Visual analysis - TSM concentrations - Odelouca Dam..... 66
Figure 50 - Statistical analysis - CDOM absorption levels - Aguieiria Dam..... 68
Figure 51 - Statistical analysis - CDOM absorption levels – Castelo de Bode Dam 68
Figure 52 - Statistical analysis - CDOM absorption levels - Alqueva Dam..... 69
Figure 53 - Statistical analysis - CDOM absorption levels - Odelouca Dam..... 69
Figure 54 - Visual analysis - CDOM concentrations - Aguieira Dam..... 70
Figure 55 - Visual analysis - CDOM concentrations – Castelo de Bode Dam 70
Figure 56 - Visual analysis - CDOM concentrations - Alqueva Dam 71
Figure 57 - Visual analysis - CDOM concentrations - Odelouca Dam..... 71
Figure 58 - Volume evolution - Aguieira Dam 72
Figure 59 - Volume evolution - Castelo de Bode Dam 72
Figure 60 - Volume evolution - Alqueva Dam 73
Figure 61 - Volume evolution - Odelouca Dam 73

TABLES LIST

Table 1 - C2RCC bands description, extracted from [67]. 47
Table 2 - *In Situ* stations coordinates 51
Table 3 - Chlorophyl concentrations - speaker version 54
Table 4 - Chlorophyl concentrations - thesis version 54
Table 5 - TSM and CDOM mean concentrations for a selected season 62
Table 6 - Dates for the Aguieira Dam 83
Table 7 - Dates for the Castelo de Bode Dam 84
Table 8 - Dates for the Alqueva Dam 84
Table 9 - Dates for the Odelouca Dam 85
Table 10 - Chlorophyl concentrations for MCI and BandRatio - Aguieira Dam 86
Table 11 - Chlorophyl concentrations for MCI and BandRatio – Castelo de Bode dam 87
Table 12 - Chlorophyl concentrations for MCI and BandRatio – Alqueva dam 88
Table 13 - Chlorophyl concentrations for MCI and BandRatio – Odelouca dam 89
Table 14 - TSM concentrations – Agueira dam 90
Table 15 - TSM concentrations – Castelo de Bode dam 91
Table 16 - TSM concentrations – Alqueva dam 92
Table 17 - TSM concentrations – Odelouca dam 93
Table 18 - CDOM absorption values - Aguieira Dam 94
Table 19 - CDOM absorption values - Castelo de Bode Dam 95
Table 20 - CDOM absorption values - Alqueva Dam 96
Table 21 - CDOM absorption values - Odelouca Dam 97
Table 22 – Water volume – Aguieira Dam 98
Table 23 - Water volume – Castelo de Bode Dam 102
Table 24 - Water volume - Alqueva Dam 106
Table 25 - Water volume - Odelouca Dam 110

ACRONYM LIST

ESA European Space Agency
NASA National Aeronautics and Space Administration
UAV Unmanned Aerial Vehicles
Chl-a Chlorophyll-a
TSM Total Suspended Matter
CDOM Coloured Dissolved Organic Matter
SAR Synthetic Aperture Radar
MSI Multispectral Instrument
$\boldsymbol{\rho_w}$ Water-Leaving Reflectance
km kilometres
m metres
µm micrometres
nm nanometres
NIR Near Infrared
AC Atmospheric Correction
C2RCC Case 2 Coast Colour processor
WQIs Water Quality Indices
NDWI Normalized Difference Water Index
NDVI Normalized Differences Vegetation Index
gNDVI green Normalized Difference Vegetation Index
NSMI Normalized Soil Moisture Index
MCI Maximum Chlorophyll Index
RUS Copernicus Research and User Support
ARSET Applied Remote Sensing Training Program
SNAP The Sentinel Application Platform
QGIS The Quantum Geographic Information System
GEE Google Earth Engine
CyAN Cyanobacteria Assessment Network
EO Earth observation
EPA Environment Protection Agency
Dam^3 Cubic Decametres
APA Agência Portuguesa do Ambiente
SNIRH Sistema Nacional de Informação de Recursos Hídricos
IOP Inherent Optical Properties

1

INTRODUCTION

This thesis addresses the potential in using satellite imagery as way to monitor water quality, its advantages and held backs. It starts with a review of recent literature, followed by the process used and ends with results presentation, discussion and conclusions.

The satellite images selected were from the Sentinel-2 mission due to its resolution, revisiting cycle, applicability and previous work done. Being this a study about water quality, Sentinel-3 was taken into to account because of its OLCI[1] instrument but was ruled out due to its resolution and revisit time. Other solution was to use a synthetic aperture radar (SAR) instead a multispectral instrument (MSI) because of its all-weather capacity and non-necessity of a cloud-free sky. This was also ruled out due to the difficulty to distinguish between the multiple factors that can generate the same desired dark spots for a study region.

1.1 Motivation

The main motivation for this work is the impact that the climate changes have worldwide and, in particular, in Portugal. Changes in seasons, dry winters, extremely hot summers, droughts, floods, having the two opposite sides of weather in a week/week and half period, all of this motivates to try and help, even if it's in small ways.

With this in mind and with the interest in satellites, the idea of studying water quality via satellite images was born.

Monitoring the water quality of large water bodies through *in situ* samples is the most accurate way but also labour intensive, time consuming and expensive.

The main objective of this project is to have a way to help the decision-making in earlier stages of water quality problems using space borne platforms. By monitoring water bodies through satellite data, it is possible to have a good estimate of water health and direct resources to where those are needed.

1.2 Objectives

There are three objectives to this work: 1) verify the use and application of the water monitoring technique provided by one of the training courses studied in this thesis; 2) develop a study on the

[1] Ocean and Land Colour Instrument

evolution of the water quality, and 3) study the water quantity evolution. The last two objectives were applied in four main Portuguese dams, one to the north, one to the centre and two to the south.

1.3 Document Organization

This document is organised as follows. The first chapter is the introduction of this thesis theme, the motivations behind it and the objectives proposed to achieve it.

The second chapter reviews the state of the art, and is divided into three main categories, optical remote sensing techniques, metrics and training courses. The first sub-chapter gives an entry point for the comprehension of the remote sensing techniques and missions, having some literature where the three main missions were used. The second one leans in the metrics used for water quality assessment being supported by the recent literature and the last one focuses on the training courses related with the theme of this project, allowing a practical approach to the problem.

The third chapter presents the methodology and is composed by three sub-chapters. It begins with the proposed solution, followed by the dams presentation, and ends with data acquisition and process development. The process development is divided into two branches, water quality monitoring and water quantity monitoring.

The fourth chapter brings the results obtained throughout the last decade and his divided in to six categories. It starts with the replication of the training course, in order to validate the scripts developed, followed by the addition of a novel formula introduced in this work for pixel validation and its effects. Next there is the presentation and discussion of the results obtained for the chlorophyll, TSM and CDOM concentrations and it ends with the water quantity evolution.

The fifth chapter brings the conclusions and future work for this thesis.

2

STATE OF THE ART

This chapter explores the various techniques proposed in the literature, looking in depth at the three water quality assessment parameters that will be used to develop this work.

It will cover case studies for specific regions that have used *in situ* and remote sensing data, with a particular interest in those focusing on Portuguese waters, and the metrics utilized by said case studies. Two training courses containing recent literature and practical examples will also be covered, one was organized by Copernicus from the European Space Agency (ESA) and the other by ARSET from the National Aeronautics and Space Administration (NASA).

2.1 Optical remote sensing techniques

In terms of optical remote sensing, there are various approaches to obtain water quality values. In Yang H et al. [1], different techniques based on remote sensing are studied and presented, but for this project satellite imagery was the path chosen to work with.

In Yang H et al. it's summarized the progress on optical remote sensing water quality retrieval in terms of data sources, retrieval modes and several specific water quality parameters retrieval algorithms. The available data sources for remote sensing water quality retrieval can be split into two, satellite-borne and non-satellite remote sensing data, and the water quality parameters retrieval modes can be divided into four: empirical; analytical; semi-empirical; and artificial intelligence mode.

Satellite-Borne Remote Sensing Data

Satellite-borne remote sensing data is composed of multispectral and hyperspectral data. Multispectral data, contains around 10 bands, and it's available in several missions like MSS, TM, ETM+, OLI, ESA's Sentinel-2, ENVISAT MERIS, France's SPOT satellite data, and NOAA's AVHRR data. Hyperspectral data, contains hundreds to thousands of bands, and can be found in instruments like AVIRIS, Hyperion or CHRIS Proba [2]. While multispectral imaging measures more spaced out bands using a wider bandwidth, hyperspectral imaging measures continuous spectral bands with a narrower bandwidth.

Considering the spatial, temporal and spectral resolution and the accessibility, Landsat series data are the most commonly used for water quality monitoring, such as total suspended matter (TSM), chemical oxygen demand and total phosphorus. Generally, due to resolution limitations, multispectral remote sensing water quality retrieval models are mainly constructed with empirical methods, which are more suitable for a certain specified period or water region.

Hyperspectral satellites have multiple bands with about 0.01 micrometres (μm) spectral resolution. Higher spectral resolution data have plentiful bands, which can be selected precisely and optimally for establishing water quality retrieval methods to distinguish the spectral mixing differences in multispectral data, thus greatly improving the accuracy of water quality parameters retrieval algorithms and showing good application potential [1].

Non-Satellite Remote Sensing Data

Non-satellite remote sensing data has been used in recent years, and various airborne remote sensing data and ground measured spectral data can also be used as data sources for remote sensing water quality retrieval. With the rapid progress of unmanned aerial vehicles (UAV) technology, the light and small UAV system, equipped with multi-spectral camera, high spectrometer, infrared sensor and Lidar, is convenient and effective in water environment management. Airborne-based data has the limitations of high flight costs or uncertain risks such as internal system failures, pilot factors, external environmental impacts and UAV supervision issues [1], [3]. Except for the airborne-based spectrometer, portable spectrometers can be flexibly used on board to detect the water surface reflectance with adjustable spectral ranges.

Non-satellite spectrometers have the strength of having higher spectral and spatial resolution and they can provide continuous ground feature spectral curves. In addition, compared with satellite data, non-satellite remote sensing data are much less affected by the atmosphere. However, non-satellite remote sensing data sources based on aircraft measurement or ground measurement have a higher cost and are limited by their weak capacity for comprehensive observation of large areas of lakes and rivers.

Water quality parameters retrieval modes

The empirical mode is a kind of correlation statistical regression formula, which can be established by using a ground-measured water quality parameter value and reflectance of the optimal band or combination of bands. The advantage of the empirical mode is that it is simple and easy to operate and can be refined by selecting more precise spectral channels to increase the accuracy of water quality parameters retrieval. However, this mode has three obvious disadvantages. Firstly, it is hard for simple empirical models to meet the accuracy requirements of water quality parameters concentration estimation because the related spectral characteristics are mainly affected by the complex composition of water quality variables including phytoplankton pigments, suspended mater, and coloured dissolved mater, etc., which bring great uncertainty to the inversion of water quality concentration. Secondly, due to regional and temporal constraints, empirical models are difficult to preanalyse, and the established models in a certain water area may not be applicably used in other regions. Finally, the empirical model requires a lot of field water quality sampling data as the basis to assure a relatively higher accuracy.

The analytical mode uses bio-optical models and radiation transmission models to simulate the propagation of light in the atmosphere and water bodies to describe the relationship between water quality components and the radiance or reflection spectrum of off-water radiation. In 1975, Gordon et al. proposed the general relationship between the apparent optical reflectance and water properties in water bodies[4]. Based on the bio-optical inversion model, Gilerson calculated the

chlorophyll-a concentration of lakes in eastern Nebraska by using some sampling data. However, the composition of the water body and radiation transmission procedure is rather complex because many factors need to be measured for the model to be established, such as the inherent optical characteristics of water, surface tourism characteristics, and water quality variables. In addition, the spectral resolution of most satellite sensors and those measured near the ground are inconsistent, which leads to some difficulties in model research. Therefore, the quantitative remote sensing inversion based on the analytical mode is difficult to achieve and is limited in practical applications [5], [6].

The semi-empirical mode is a combination of the empirical mode and the analytical mode. By using a certain paradigm derived from rigorous analytical models, the semi-empirical mode has a good applicability to calculate the water quality variables by combining only a small amount of *in situ* data and reflectance or radiance values. Some scholars used this method to retrieve water quality components such as chlorophyll-a (Chl-a), total suspended matter (TSM), coloured dissolved organic matter (CDOM) and associated visibility and turbidity with higher accuracies[7], [8]. As for the study of suspended matter concentration retrieval, Lathrop, found that the SPOT–1 Red band and Near Infrared (NIR) band were more sensitive to the suspended matter concentration, so they calculated different suspended matter concentrations with Red-Green band ratio and NIR band based on this mode. The semi-empirical method considers the optical characteristics of water quality parameters and has better portability than the empirical method.

The Artificial Intelligence mode (AI) is a kind of implicit algorithm that is different from the previous modes and that can provide explicit equations. Due to complicated and various background effects from the water surface, a combination of water quality parameters and sediment deposits, AI mode can capture both linear and non-linear relationships compared with traditional statistical or physical modes. A large number of scholars have applied the AI mode such as neural networks and support vector machines in water quality retrieval and achieved relatively satisfactory result [1], [9], [10].

2.1.1 The Copernicus Programme

There are several space missions capable of providing high quality data for carrying out this or other environmental projects, such as the ERS, Envisat, CryoSat-2, GOCE and Copernicus from the European Space Agency; Landsat, Jason-3, Aqua, Aura from NASA; Chollian from KARI (South Korea) or COSMO from ASI (Italy), among others. These are some examples of Earth monitoring missions capable of helping in environmental monitoring and combat.

In this case, three Copernicus missions were taken into consideration, Sentinel-1, Sentinel-2 and Sentinel-3. In the end, the Sentinel-2 images were selected for the development of this work, due to its resolution and applicability to the problem at hand.

The Copernicus programme was created to provide accurate, timely and easily accessible information to improve the management of the environment, understand and mitigate the effects of climate change and ensure civil security [11].

It includes six core thematic services: atmosphere monitoring, land monitoring, marine environment monitoring, emergency management, security and climate change.

The atmosphere monitoring service includes monitoring for air quality and UV forecasts at global and European level, greenhouse gases, climate forcing and emissions.

The land monitoring service includes the monitoring for water management, agriculture and food security, land-use change, forest monitoring, soil quality, urban planning and natural protection services.

The marine environment monitoring service includes the monitoring for marine safety and transport, oil-spill detection, water quality, ocean forecasting and the polar environment.

The emergency management service supports mitigating the effects of natural and manmade disasters such as floods, forest fires and earthquakes and contribute to humanitarian aid exercises.

The security supports peacekeeping efforts, maritime surveillance and border control.

Finally, the climate change service cuts across all the above themes and is about providing authoritative quality assured information about the past, current and future states of the climate in Europe and worldwide [12].

Figure 1 - Earth observation missions developed by ESA [11]

To meet the operational needs of the Copernicus programme, ESA developed the family of Sentinel satellites, as seen in Figure 1. These missions are underpinned by the Copernicus Ground Segment, which oversees satellite operations, as well as data acquisition, production and dissemination.

The Sentinel constellation is made up of 7 missions, totalling 11 satellites, focusing on atmosphere, land and ocean monitoring.

Sentinel-1 is an imaging radar mission, equipped with a synthetic aperture radar (SAR) instrument, providing continuous all-weather, day-and-night imagery at C-band. It can be used, for example, for oil spillages, ice monitoring, forestry, among other applications [13].

Sentinel-2 is a wide-swath and high-resolution mission equipped with a multispectral instrument (MSI), that supports land monitoring studies, including vegetation, soil and water cover, as well as observation of inland waterways and coastal areas. It can be used for example, for forest fire scar mapping [14].

Sentinel-3 primary objective is marine observation, and it enables the study of the sea-surface topography, sea and land surface temperature and ocean and land colour. Composed of three satellites, the mission's primary instrument is a radar altimeter, but the polar-orbiting satellites will carry multiple instruments, including optical imagers.

Sentinel-4 is dedicated to air quality monitoring. The Sentinel-4 Ultraviolet-Visible-Near-Infrared instrument is a spectrometer carried aboard Meteosat Third Generation satellites, operated by EUMETSAT. The mission aims to provide continuous monitoring of the composition of the Earth's atmosphere at high temporal and spatial resolution and the data will be used to support monitoring and forecasting over Europe.

Sentinel-5 is dedicated to air quality monitoring. The Sentinel-5 Ultraviolet-Visible-Near-Infrared sounder instrument is a spectrometer carried aboard the MetOp Second Generation satellites. The mission aims to provide continuous monitoring of the composition of the Earth's atmosphere. It provides wide-swath, global coverage data to monitor air quality around the world.

Sentinel-5P, a precursor satellite mission, aims to fill in the data gap and provide data continuity between the retirement of the Envisat satellite and NASA's Aura mission and the launch of Sentinel-5. The main objective of the Sentinel-5P mission is to perform atmospheric measurements, with high spatio-temporal resolution, relating to air quality, climate forcing, ozone and ultraviolet radiation. The satellite was successfully launched on 13 October 2017 from the Plesetsk cosmodrome in Russia.

Sentinel-6 Michael Freilich is the next radar altimetry reference mission to extend the legacy of sea-surface height measurements, until at least 2030. It is an Earth Observation satellite mission developed to provide enhanced continuity to the very stable time series of mean sea level measurements and ocean sea state that started in 1992, with the TOPEX/Poseidon mission [15].

2.1.2 Sentinel-1

The Sentinel-1 mission comprises a constellation of two sun-synchronous polar-orbiting satellites, sharing the same orbital plane with 180° orbital phasing difference, operating day and night performing C-band synthetic aperture radar imaging, enabling them to acquire imagery regardless of the weather. It operates in four exclusive imaging modes with different resolutions, down to 5 metres (m), and coverages, up to 400 km (kilometres). It provides dual polarisation capability, short revisit times (12 days for one satellite and 6 days with two satellites) and rapid product delivery. Figure 2 shows the schematic view of the deployed Sentinel-1 spacecraft [16].

This mission has four acquisition modes resulting in several products for each one:

- Stripmap
- Interferometric Wide Swath
- Extra-Wide Swath
- Wave

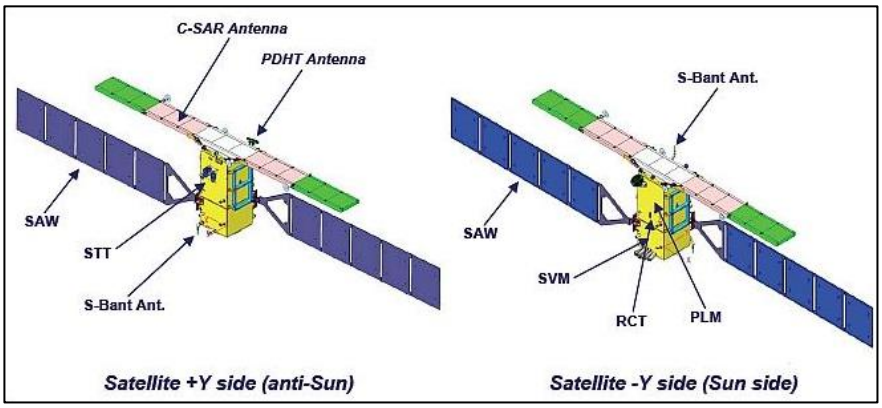

Figure 2 - Schematic View of the Deployed Sentinel-1 Spacecraft, extracted from [16]

In terms of literature, SAR based satellites applied to water monitoring are primarily used to evaluate wetlands, floods or oil spills [13], [17], [18].

In Westerhoff R et al. [19], an automated global water mapping based on wide-swath orbital synthetic aperture radar is purposed. To do so, they merged MODIS optical imagery with ASAR and came to the conclusion that where MODIS suffers from clouds, ASAR shows hydrologically correct results, as observed through the clouds and as verified by other knowledge from the ground.

In Wang G. et al [20], SAR images were used to detect and monitor algal blooms in the Taihu Lake in China but were facing issues to correctly identify algal bloom regions. Even though the dark spots captured by the satellite had a good correlation with *in situ* data, the same dark regions could be caused by other factors such as low winds or rain cells.

2.1.3 Sentinel-2

The Copernicus Sentinel-2 mission comprises a constellation of two polar-orbiting satellites placed in the same sun-synchronous orbit, phased at 180° to each other, as seen in Figure 3. It aims at monitoring variability in land surface conditions, and its wide swath width (290 km) and short revisit time (10 days at the equator with one satellite, and 5 days with 2 satellites under cloud-free conditions which results in 2-3 days at mid-latitudes) will support monitoring of Earth's surface changes.

This mission carries an optical instrument payload that samples 13 spectral bands at tree spatial resolutions:

- 4 bands at 10 m
- 6 bands at 20 m
- 3 bands at 60 m

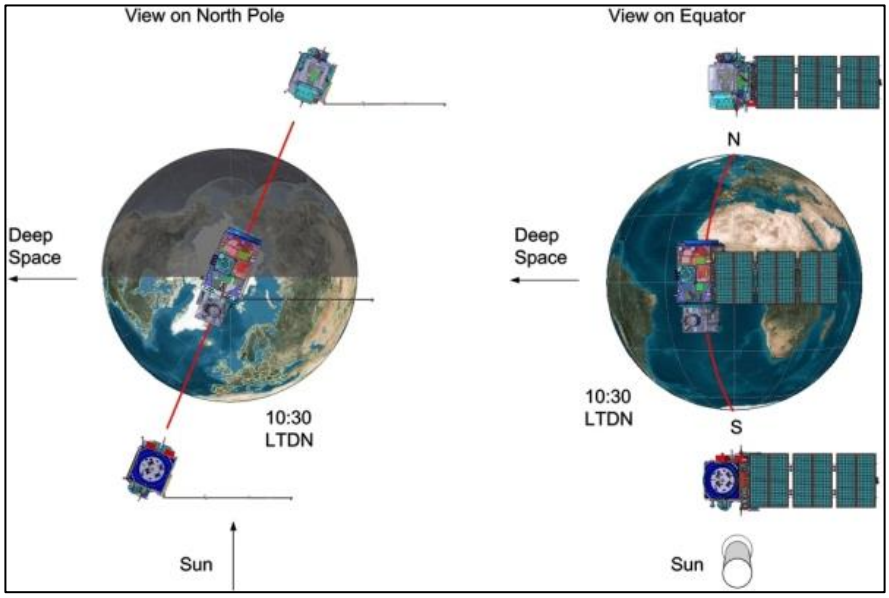

Figure 3 - Twin-Satellite Sentinel-2 Orbital Configuration, extracted from[21].

These satellites continue the legacy of SPOT and LANDSAT by continuing to provide similar types of image data and contributing to ongoing multispectral observations. These satellites are used to support a variety of services and applications offered by Copernicus, including land management, agriculture, forestry, disaster control, humanitarian relief operations, risk mapping, and security concerns [21].

On board of each one, there is a Multispectral Instrument (MSI) that uses a push-broom concept, Figure 4. It works by collecting rows of image data across the orbital swath and utilises the forward motion of the spacecraft along the path of the orbit to provide new rows for acquisition.

Earth is subdivided on a predefined set of tiles, defined in UTM/WGS84 projection and using a 100 km step. However, each tile has a surface of 110x110 km² in order to provide large overlap with the neighbouring.

The average period of observation over land and coastal areas is approximately 17 minutes and the maximum period of observation is 32 minutes [21].

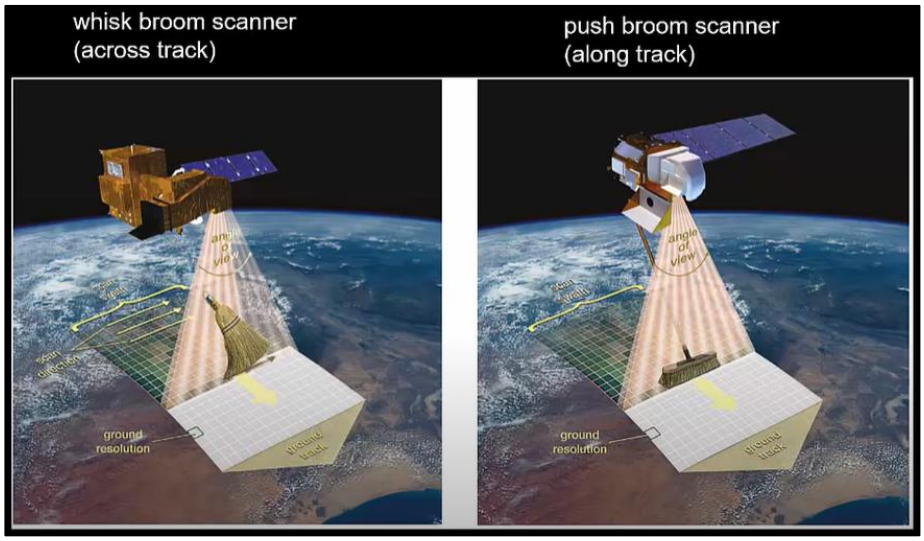

Figure 4 - Whisk broom vs Push broom, extracted from [22]

In most articles researched for this thesis, Sentinel-2 data was used for water quality assessment in large water bodies, such as estuaries, reservoirs and lakes. In Portugal it was used to study water quality parameters in the Sado estuary by Giulia Sent et al. [23] and in the Alqueva reservoir by Miguel Potes et al. [24]. In Argentina and Spain, was used in eutrophics reservoirs by German Alba et al.[25] and Manuel Viso-Vázquez et al. [26], respectively. For lakes it was used by Kaire Toming et al. [27] in Estonia, by Isabela Cabalero et al. [28] in the Philippines during the 2020 typhoon season and by Tadesse Mucheye et al. [29] in Ethiopia.

2.1.4 Sentinel-3

The Copernicus Sentinel-3 is a European Earth Observation satellite mission developed to support Copernicus applications related with ocean, land, atmospheric, emergency, security and cryospheric monitoring.

The main objective is to measure sea surface topography, sea and land surface temperature, and ocean and land surface colour with high accuracy and reliability to support ocean forecasting systems, environmental monitoring and climate monitoring.

The mission was also created by the need for continuity in provision of ERS, ENVISAT and SPOT vegetation data, with improvements in instrument performance and coverage [30].

The spacecraft, Figure 5 , carries four main instruments:

- OLCI: Ocean and Land Colour Instrument
- SLSTR: Sea and Land Surface Temperature Instrument
- SRAL: SAR Radar Altimeter
- MWR: Microwave Radiometer.

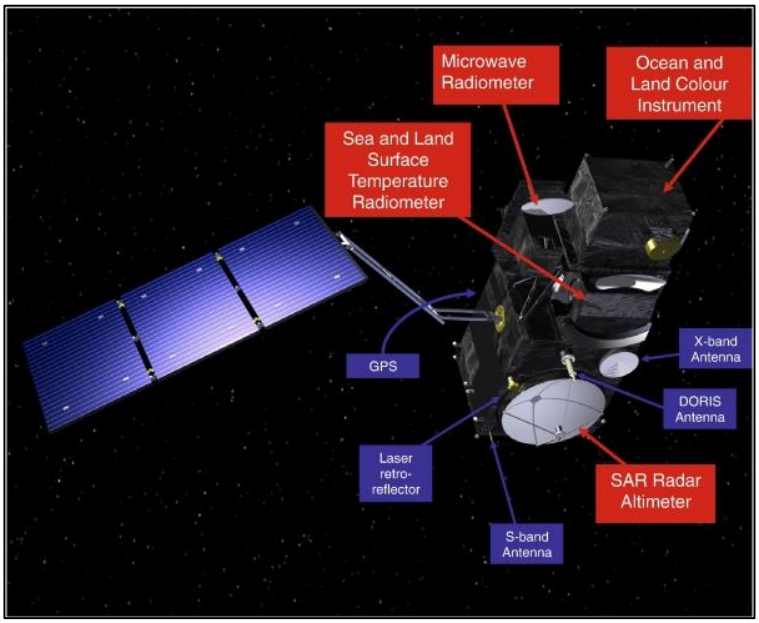

Figure 5 - Sentinel-3 Satellite and Payloads, extracted from [30]

The OLCI is of special interest because of its function and application. This is an optical instrument used to provide data continuity for ENVISAT's MERIS. Like the MSI from Sentinel-2, this instrument is a push-broom imaging spectrometer that measures solar radiation reflected by the Earth, at a ground spatial resolution of 300 m, in 21 spectral bands [30].

The primary objective of it is to screen the ocean and land surface to harvest information related to biology (e.g. phenology of marine and terrestrial biomass). OLCI also provides reliable information on the atmosphere, especially on the aerosol's characterization. All applications of OLCI including contributions to climate study are presented in this applications section. [30]

In terms of water monitoring, measuring ocean colour from space allows information to be gathered about marine biological constituents. This measurement relates to water colouration (visible spectrum), which is affected by elements present in the water and especially by population with phytoplankton biomass (as indexed by Chl-a, Figure 6) which constitutes the first element of the trophic chain and associated detrital material [31].

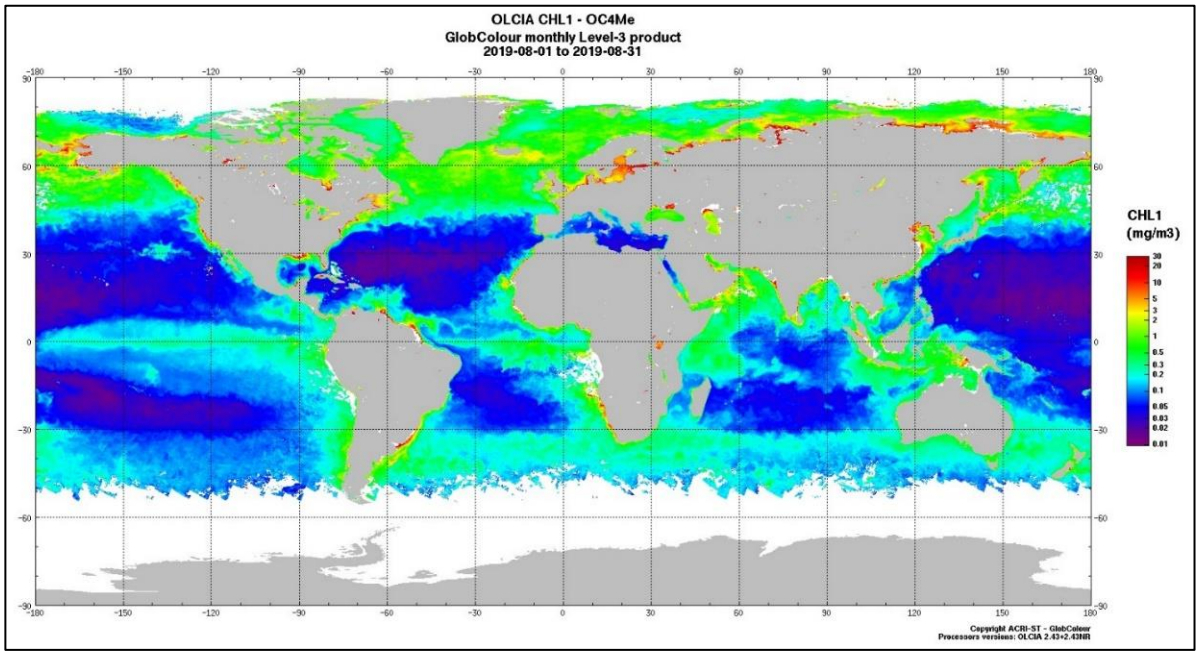

Figure 6 - GlobColour Chlorophyll Monthly Product from OLCI-A [31]

Similar to Sentinel-2, Sentinel-3 data was also used for water quality assessment in the Alqueva reservoir in Portugal. Although the instrument OLCI from Sentinel-3 has much lower spatial resolution (300 m) compared to Sentinel-2/MSI and Landsat data, it presents an adequate resolution to represent the spatial variations of water quality in the reservoir (the largest artificial lake in Western Europe).

Its measurements are taken at the top of the atmosphere (TOA). It is thus necessary to atmospherically correct the data to account for the absorption and scattering atmospheric effects and obtain the surface signal. After the atmospheric correction, the authors then proceed to categorize the period studied into four optical water types (OWT). In order to have qualitative and quantitative estimations of water quality in the period studied, the OWT classification was analysed together with the estimations of water quality parameters. With this Gonçalo Rodrigues et al, present two different methodologies to estimate the water quality in a large reservoir [32]: the water quality parameters using a quantitative analysis (empirical algorithms), and the assignment of an optical water type (qualitative analysis) and come to the conclusion that, because there are always some uncertainties when estimating water quality parameters using satellite remote sensing, using two different and independent methodologies to represent the water quality in the same day/area provides greater reliability in the results [32].

Another study was carried out in Hungary, on lake Balaton [33], that used machine learning gaussian process regression (GPR) for water quality estimation. In this paper the authors used an automatic model selection algorithm to determine the most suitable Chl-a retrieval GPR model for lake Balaton.

In order to evaluate the accuracy of the method, Katalin Blix et al. compared their results with *in situ* measurements. The overall findings for the S3 OLCI products showed the poorest performance for Chl-a content retrieval, which is the most important water quality parameter. Therefore, the authors studied the possibility of improving Chl-a content estimation in Lake Balaton by using an alternative approach.

A larger, more representative dataset suitable for evaluating a locally tuned model by extending the *in situ* measurements with a synthetic dataset for S3 OLCI, was generated by Katalin Blix et al. for complex waters. With this they used an automatic model selection algorithm (AMSA) approach to determine the most suitable number and combination of spectral bands to be used in the GPR model and obtained significant improvements in regression strength. Even though the four feature ranking methods currently implemented in AMSA are-derived from different mathematical principles, the ranking showed high consistency.

2.1.5 Satellites comparison

Having three types of instruments that retrieve water quality in different ways is very important because they can corroborate and support each other's results.

When comparing the three satellites between them, the Sentinel-3 has a lower resolution and a longer revisit time.

SAR could be a better option for water quality because of its cloud-free coverage and different acquisition modes but has its own problems such has region distinguishing difficulties between low winds, rain cells, algal blooms and other factors.

Sentinel-2 is the more balanced out of the three spacecrafts, having a spatial resolution ranging from 10 to 60 m, a temporal resolution ranging from 5 to 10 days and a spectral resolution of 13 bands, that goes from 443 nanometres (nm) up to 2190 nm, Figure 7.

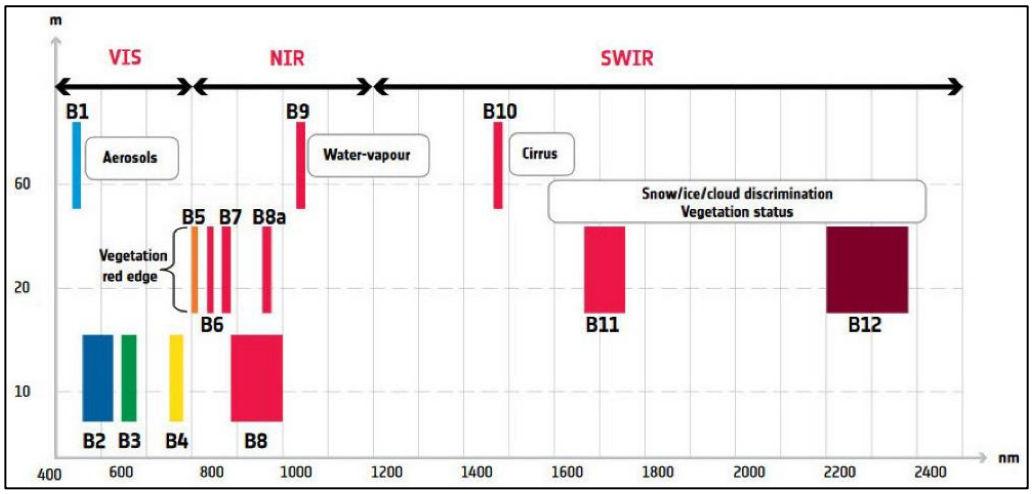

Figure 7 - Sentinel-2 layout of spectral bands, extracted from [34].

Chlorophyll can be easily monitored by optical remote sensing because the algal blooms and Chl-a have significantly different reflectivity on different wavelength bands. So, from the comparison between satellites, the mission that is more appropriate for this kind of work is Sentinel-2.

2.2 Metrics

Water quality can be measured in various ways, as was presented previously, from *in situ* samples to remote sensing data. But it all comes down to the parameters used. There are several metrics used for water quality assessment such as:

- Chlorophyll-a (Chl-a)
- Total Suspended Matter (TSM)
- Coloured Dissolved Organic Matter (CDOM)
- Turbidity
- Temperature
- Phosphorus
- Dissolved Oxygen
- pH

The basis of this thesis relies on the ESA training [35], so only three parameters will be considered: Chl-a, TSM and CDOM. Turbidity will also be highlighted due to its correlation with TSM and CDOM.

Before we dig through the specific metrics it's important to highlight that 90 to 98 percent of the signal derives from the atmosphere and water surface, so only 10 to 2 percent of it is used for water quality assessment.

With this, it's crucial to have a good atmospheric correction (AC) in order to remove the scattered signal of atmosphere and retrieve the signal from the water's surface, water-leaving reflectance (ρ_w) [36]. Not all water bodies can be treated with the same AC procedure. In Warren et al. [37], a study was done with six different AC processors to see the impact they had in the different water bodies.

Ansper and Alikas [36], refer that Case 1 waters are mostly dominated by phytoplankton, whereas Case 2 waters with different concentrations of optically active substances (Chl-a, CDOM, TSM) are more complex when deriving water quality parameters.

It is also important to take into account that different study areas will require different approaches in terms of bands or wavelengths used. What works for one case can have an inefficient impact on another, so testing different algorithms and different processors is crucial.

2.2.1 Chlorophyll-a

Chlorophyll, any member of the most important class of pigments involved in photosynthesis, the process by which light energy is converted to chemical energy through the synthesis of organic compounds.

It is found in virtually all photosynthetic organisms, including green plants, cyanobacteria, and algae, absorbing energy from light. This energy is then used to convert carbon dioxide to carbohydrates.

Chlorophyll, Figure 8, occurs in several distinct forms: chlorophylls a and b are the major types found in higher plants and green algae, chlorophylls c and d are found, in different algae, chlorophyll e is a rare type found in some golden algae and bacterio-chlorophyll occurs in certain bacteria [38].

Chlorophyll–a can indicate the distribution of plankton biomass and is the most basic indicator reflecting the primary productivity and eutrophication of water bodies, so it is commonly used for water quality purposes [1].

Figure 8 - Visual verification of Chlorophyll [39]

Ansper and Alikas [36], wrote that for Case 1 waters, AC algorithms assume that the water-leaving radiance is zero in the near infrared (NIR) part of the spectrum. This assumption is not valid in turbid Case 2 waters because of the scattering by particles that increase the ρ_w in the NIR part. It causes over-correction in the visible (VIS) part of the ρ_w spectrum. In small narrow lakes or in the vicinity of the coast, the adjacency effect also influences the reflected light field because pixels are affected by the signal originating from the surrounding land. Pixels from the coastline are brighter than water pixels, and the multiple scattering precludes accurate derivation of water quality parameters.

As Chl-a has absorption peaks in VIS part of the spectrum, it is possible to estimate Chl-a in remote sensing applications through model-based or empirical approaches. A model-based approach uses bio-optical models to simulate ρ_w or the top-of-atmosphere (TOA) radiance spectrum with specified water constituents. An empirical approach based on band ratios is also used, with the small disadvantage of a smaller sensitivity, but being easier to develop and apply.

For case 1 and 2 waters, Ansper and Alikas, developed two equations based on the chlorophyll absorption peaks, but used the reflectivity measured since they were working with optical sensors two. This is possible because the absorption and reflection are directly proportional, meaning that if one of them is high the other one will be low.

When combining the low and high reflection values, the accuracy of the measure increases, resulting in truer values.

For Case 1 oceanic waters, the Blue–Green two-band ratio model algorithms are the most successfully, because of the phytoplankton domination. The model uses blue and green wavelengths because the first absorption peak of Chl-a is around 440 nm (λ_{blue}) and minimal absorption is around 550 nm (λ_{green}):

$$Chl\ a\ \propto \frac{\rho(\lambda_{blue})}{\rho(\lambda_{green})}. \quad (1)$$

For Case 2 waters, algorithms at blue–green wavelengths fail because of absorption and scattering due to CDOM and TSM. Due to the second Chl-a absorption peak near 675 nm, the Two-Band NIR–Red Ratio Model is widely used. The red band is located in the range of maximum Chl-a absorption between 660 and 690 nm (λ_{red}) and the NIR band characterizes the range of wavelengths between 700 and 720 nm (λ_{NIR}):

$$Chl\ a\ \propto \frac{\rho(\lambda_{NIR})}{\rho(\lambda_{red})}. \quad (2)$$

Other authors based their work in other approaches, Potes et al. [24] adapted algorithms developed for MERIS to MSI, regulating the wavelengths for the Sentinel-2 instrument, Alban Germán et al. used a linear regression based on the Pearson analysis of the data used in their work [25]

For Sentinel-3 similar approaches to the Ansper and Alikas one, were followed by Gonçalo Rodrigues et al. [32], using bands in the green and NIR part of the spectrum.

2.2.2 Total Suspended Matter

Total Suspended Matter (TSM) is a measure of the concentration of particulate material in the surface water such as mud, silt, and other fine-scale debris, including both organic and inorganic fractions [40].

TSM concentration is one of the key parameters in main water quality components. The high concentration of suspended matter in estuaries and inland lakes will disturb the optical properties of water, such as the depth of the true light layer, and then influence the growth of aquatic plants and the primary productivity of water bodies. The reflectance in the 580–680 nm and 700–900 nm spectral range are most sensitive to TSM concentration changes and are the best choice for TSM concentration remote sensing [1].

Giardino et al. [41] also used similar bands for the concentration of TSM, using red-to-green and NIR-to-red band ratios, but concluded that, for their study, NIR is not affected much by TSM.

Like Giardino et al., in [23] NIR bands were used but better results were obtained.

2.2.3 Turbidity

Turbidity, which is caused by suspended chemical and biological particles, can have both water safety and aesthetic implications for drinking-water supplies, Figure 9. Turbidity itself does not always represent a direct risk to public health. However, it can indicate the presence of pathogenic microorganisms and be an effective indicator of hazardous events throughout the water supply system, from catchment to point of use.

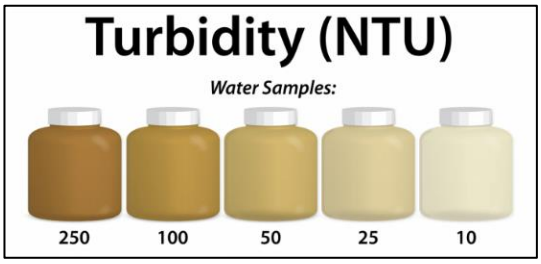

Figure 9 - Example of different turbid water samples, extracted from [42]

For example, high turbidity in source waters can harbour microbial pathogens, which can be attached to particles and impair disinfection, in filtered water can indicate poor removal of pathogens. An increase in turbidity in distribution systems can indicate sloughing of biofilms and oxide scales or ingress of contaminants through faults such as mains breaks [43].

Since turbidity isn't a measure strictly for water quality, it can be utilized for other purposes, for example, in [44] the authors made use of the Sentinel-2 derived turbidity product to monitor changes in the water transparency in the Venice lagoon before and after the first COVID-19 lockdown.

In terms of wavelengths used, turbidity relates with TSM, so bands in the red and NIR are commonly used. In [23], the authors came to the same conclusion, better results were obtained when NIR bands were used.

For Sentinel-3 OLCI, blue and red-to-NIR bands were used to monitor water turbidity [32].

2.2.4 Coloured Dissolved Organic Matter

In Giardino et al. [41] some historical names as gelbstoff or yellow matter are presented. It is also explained that most of its compounds are produced during the decay of plant matter and consist of various humic and fulvic acids. Their absorption is mainly caused by aromatic groups with various degrees and types of substitution, including monosubstituted and polysubstituted phenols and various aromatic acids.

The absorption of Coloured Dissolved Organic Matter (CDOM) depends on the water constituents and has a relatively complex composition. Has an important impact on water colour, underwater light field and chemical processes. CDOM can absorb part of ultraviolet and visible light. When the CDOM concentration increases, the absorption can extend to the blue band near 440 nm, Figure 10.

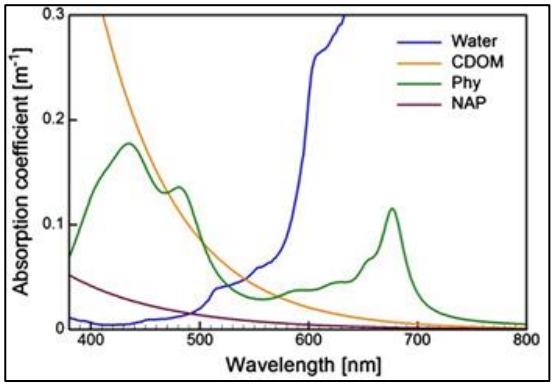

Figure 10 - Absorption coefficients of water, CDOM, phytoplankton and non-algal particles, extracted from [41]

In Yang et al. [1] various approaches used to obtain this concentration are presented, varying according to the water bodies studied. In both instruments studied in this work, MSI and OLCI, CDOM concentration is obtained and analysed [1], [23], [27], [33], [36], [41].

2.2.5 Other metrics

Other parameters obtained via remote sensing can be used as water quality metrics. Parameters like temperature, dissolved oxygen, phosphorus or pH are some examples of it.

Temperature is a key physical parameter to understand the prevailing water quality and the interaction among sea and atmosphere. Satellite sensors can measure the surface layer temperature of the sea by the thermal infrared region of the electromagnetic spectrum [23], [45], [46].

Dissolved oxygen is a critical parameter for water quality because it directly impacts the aquatic life. In [47], the authors studied dissolved oxygen in Owabi reservoir from satellite images.

Phosphorus is essential for plants and algae growth, but in excess can lead to the eutrophication of a water system [48]

The pH determines freshwater acidity and alkalinity. The volume and chemical composition of both organic and inorganic compounds contained in groundwater are primarily tracked [49].

In [50] The prediction of pH values to separate saline lakes from freshwater lakes at a broad scale was achieved by considering linear and non-linear regression methods. The filtered composition with a higher correlation between the auxiliary image bands and field-measured pH values among the five seasonal filters was selected using stepwise multiple linear regression. The spectral values of the lakes used for pH prediction were collected for the pixel (30 x 30 m) that overlaps the GeoReferred water pH sample collected in the field.

2.2.6 Water Quality Indices

We can use Water Quality Indices (WQIs) to study and analyse all the metrics and data contained within them. WQIs refers to a set of water quality parameter data that aggregate to produce a single value to the water quality, reducing the huge amount of data into a simple and easy expression. It also enables comparisons of water quality status for different locations and different times, which eventually will help inform water quality status to the management and the public in a simple manner [51].

In Viso-Vázquez et al. [26], the authors used a set of spectral indices, to assess the concentration of chlorophyll-a and cyanobacteria in their study area.

The spectral indices used were the Normalized Difference Water Index (NDWI), the Normalized Differences Vegetation Index (NDVI), the green Normalized Difference Vegetation Index (gNDVI), the Normalized Soil Moisture Index (NSMI), and Toming's Index.

The NDWI, proposed by McFeeters, is designed to: (1) maximize the reflectance of the water body in the green band; and (2) minimize the reflectance of water body in the NIR band,

$$\mathrm{NDWI} = \frac{\rho_{green} - \rho_{NIR}}{\rho_{green} + \rho_{NIR}} \tag{3}$$

The NDVI is a dimensionless index that describes the difference between visible and near-infrared reflectance of vegetation cover. It is used to detect vegetation in different environments; in our case, it was used only to evaluate the surface level of the lake,

$$\mathrm{NDVI} = \frac{\rho_{NIR} - \rho_{red}}{\rho_{NIR} + \rho_{red}} \tag{4}$$

The gNDVI is resistant to atmospheric effects, and it has a greater dynamic range than the NDVI and is five times more sensitive to Chl-a concentrations; this index avoids the saturation problem of the NDVI at relatively low chlorophyll concentrations.

$$\mathrm{gNDVI} = \frac{\rho_{NIR} - \rho_{green}}{\rho_{NIR} + \rho_{green}} \tag{5}$$

The index used to obtain the value model is a transformation of Total Suspended Solids (TSS) using NSMI. NSMI is a widely used universal transformation. The values generated vary between -1 and 1, where lower figures indicate the presence of clearer water. The height of the Chl-a reflectance peak between 700 and 720 nm was studied to estimate the concentration of Chl-a in the waters of lakes or reservoirs. Band 5 of Sentinel-2 analyses this spectral region (705 nm),

$$\mathrm{NSMI} = \frac{\rho_{red} + \rho_{green} - \rho_{blue}}{\rho_{red} + \rho_{green} + \rho_{blue}} \tag{6}$$

The logarithm studied in Toming et al. [52] calculates the height of the peak against the baselines of band 4 (665 nm) and band 6 (740 nm),

$$\text{Toming's Index} = \rho_{VRE5} - \frac{\left(\frac{\rho_{red}}{\rho_{VPRE6}}\right)}{2} \tag{7}$$

Ansper et Alikas [36], showed in their work the Maximum Chlorophyll Index (MCI) that has been used by the MERIS sensor, which is based on the height of the peak at 709 nm and is used with Chl-a over 10 mg/m^3,

$$MCI = L_{709} - L_{681} - 0.389(L_{753} - L_{681}) \tag{8}$$

In the MCI algorithm, L represents the Top-of-Atmosphere radiance at the specific wavelengths, and the index 0.389 represents the ratio of wavelengths (709 - 681)/(753 - 681).

The authors also showed the Fluorescence Line Height (FLH) algorithm. Fluorescence line height (FLH) is a relative measure of the amount of radiance leaving the sea surface in the chlorophyll fluorescence emission band. Satellite-derived FLH images provide information about the surface chlorophyll distribution which in turn can be used for monitoring surface phytoplankton blooms in coastal waters [53].

This is the most suitable for waters where Chl-a concentration is 1–20 mg/m^3 and it uses the Chl-a fluorescence peak maximum near 685 nm, that is located between the linear baseline of two adjacent bands,

$$FLH = L_{681} - L_{665} - 0.364(L_{709} - L_{665}) \quad (9)$$

In the FLH algorithm, $L_{681}$is the water-leaving radiance at the fluorescence maximum peak wavelength of MERIS band and the index 0.364 represents the ratio of wavelengths (681 - 665)/(709 - 665).

2.3 Training Courses

On a practical level, there are many courses that could be used as a start point for this kind of work. In this thesis two courses are covered, one organized by RUS Copernicus (ESA) [35] and one by ARSET (NASA) [54]:

- HYDR02 – Freshwater Quality Monitoring using Sentinel-2 by RUS Copernicus [55];
- Monitoring Water Quality of Inland Lakes using Remote Sensing by ARSET [56].

The HYDR02 training course was selected to be the basis of this thesis because of the higher spatial resolution of Sentinel-2, previous work with this satellite and familiarity with the tools used.

Copernicus Research and User Support

Running from 2017 to December 2021, the Copernicus Research and User Support (RUS) service aimed to develop an online free-access platform to promote the uptake of Copernicus data and support the scaling up of educational and R&D activities.

In particular, the service provided Copernicus data access, cloud computing resources, access to effective software tools and training services allowing users to develop their understanding and exploitation capabilities in relation to Copernicus.

The service was funded by the European Commission, managed by the European Space Agency and operated by CSSI and its partners.

There are 7 categories of training, Land, Ocean/Coasts, Risk Monitoring, Hydrology, Geology/Cryology, Atmosphere and Algorithms, with a total of 50 courses.

Applied Remote Sensing Training Program

Started in 2015, the Applied Remote Sensing Training Program (ARSET) is still up and running with new trainings appointed for February and March. It offers in-person and online trainings for beginners and advanced practitioners alike, across a breadth of topics including disaster management, ecological forecasting, agriculture, public health, and air quality and water resources management.

As ARSET expanded on its early success, it became part of NASA Applied Sciences' Capacity Building program area. The Capacity Building Program exists to build worldwide capacity in the ability to use NASA Earth Observations for decision making.

There are 7 categories of training, Fundamentals, Climate and Resilience, Disasters, Health and Air Quality, Ecological Conservation, Water Resources and Capacity Building, with a total of 106 courses.

2.3.1 Tools

The tools selected by both organizations for their training courses are free and available to everyone. This way, anyone can expand their theoretical and practical knowledge.

In this section only the tools used in both training courses will be exposed. The RUS Copernicus training uses one main application, The Sentinel Application Platform (SNAP), and proposes one for the statistical analysis, The Quantum Geographic Information System (QGIS). The ARSET training uses mainly Google Earth Engine (GEE) and Cyanobacteria Assessment Network Application (CyAN app) for exploratory purposes.

The Sentinel Application Platform

The Sentinel Application Platform (SNAP) is a common architecture for all sentinel toolboxes, being ideal for Earth observation (EO) processing and analysis due to the following technological innovations: extensibility, portability, modular rich client platform, generic EO data abstraction, tiled memory management, and a graph processing framework [57].

SNAP and the individual sentinel toolboxes support numerous sensors other than sentinel sensors. With it, it's possible to access all the data from the satellites and do data exploration, heavy processing and mathematical expressions applications.

The Quantum Geographic Information System

The Quantum Geographic Information System (QGIS) is a friendly user Open-Source Geographic Information System licensed under the GNU General Public License. This application is used to visualize, manage, edit and analyse data. It also allows the user to compose printable maps and see, for example, a placement of a wildfire and its area or to perform statistical analysis[58].

Google Earth Engine

Google Earth Engine (GEE) is a platform for scientific analysis and visualization of geospatial datasets, for academic, non-profit, business and government users.

It hosts satellite imagery and stores it in a public data archive that includes historical earth images going back more than forty years. The images, ingested on a daily basis, are then made available for global-scale data mining. It also provides APIs and other tools that enable the analysis of large datasets.

One of Earth Engine missions is to organize geospatial information and make it available for analysis and for that it has worked in close collaboration with Google Cloud to bring the Landsat and Sentinel-2 collections to Google Cloud Storage as part of the Google Cloud public data program [59].

Cyanobacteria Assessment Network Application

The Cyanobacteria Assessment Network (CyAN) is a multi-agency project promoted by the Environment Protection Agency (EPA) to develop an early warning indicator system to detect algal blooms in United States freshwater systems. This research supports federal, state, tribal, and local partners in their monitoring efforts to assess water quality to protect aquatic and human health.

Objectives include: (1) create a standard approach for early identification of algal blooms; (2) develop an information dissemination system for expedient public health advisory postings; and (3) understand connections between health, economic, and environmental conditions to cyanobacterial and phytoplankton blooms.

EPA's CyAN mobile application provides access to cyanobacterial bloom satellite data for over 2,000 of the largest lakes and reservoirs across the United States. EPA scientists developed the app to help local and state water quality managers make faster and better-informed management decisions related to cyanobacterial blooms [60].

Virtual Machines

When the RUS Copernicus programme was active, virtual machines were available directly from the RUS web page. Since it was terminated, their virtual machines were move to TerraScope, a Belgium project that provides access the open-source satellite data of the Copernicus programme [61].

It is possible to use virtual machines to analyse and process satellite data, being available both in GEE and in TerraScope.

2.3.2 HYDR02 – Freshwater Quality Monitoring using Sentinel-2

The HYDR02 – Freshwater Quality Monitoring using Sentinel-2 training studies the Trasimeno Lake, Italy, in 2018 and starts by introducing the RUS service, followed by the water quality monitoring using optical data, finishing with a Sentinel-2 review. After a quick overview of those topics, it moves to the proposed exercise and ends with a question and answers session [55].

In terms of water quality, the course talks about optically active constituents as chlorophyl-a, total suspended mater and coloured dissolved mater, about optically deep and shallow waters effects and the atmosphere signal contributions.

The training highlights the impact of the atmospheric correction (AC), the types of water, case 1 or 2 waters, and some AC processors as Case 2 Coast Colour processor (C2RCC) or Sen2Cor.

It talks about the water quality metrics, their properties, the bands used, and the equations considered for those metrics. After this introduction it moves on to the exercise.

For the exercise, a training kit is given with a report containing all the steps and auxiliary data, as pressure values and *in situ* data for a statistical analyses and comparison. The exercise follows the steps presented in Figure 11.

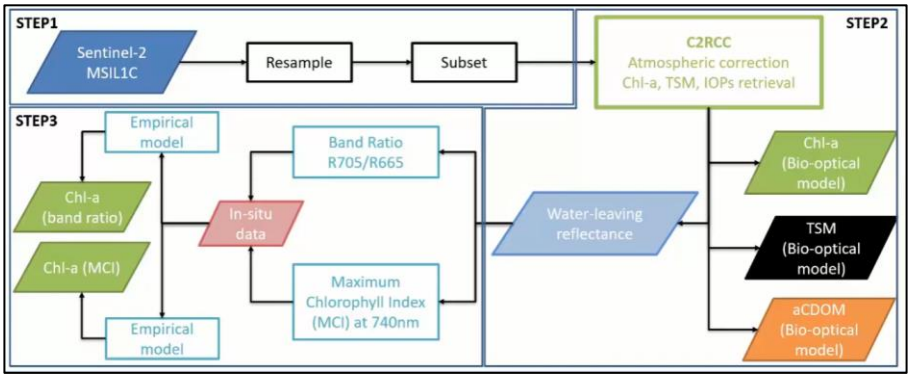

Figure 11 - Freshwater Quality Monitoring - Exercise workflow [35]

The workflow can be divided into three main steps, resampling and subset, C2RCC algorithm application and the development of the empirical models.

Before any application of equations or indices, a resample and subset process is performed, this helps transform a multi-sized product into a single-sized one, reduce the amount of data being processed each time and focus the data only on the study area.

The next step implements the use of the C2RCC algorithm, which allows the user to perform the atmospheric correction and apply the optical active constituent's retrieval. The atmospheric correction is essential because it will remove the scattered signal of the atmosphere and retrieve the signal from the water surface as the water leaving reflectance.

Afterwards, the water leaving reflectance's, resulting from the previous step, is applied in two empirical models, the band ratio of red-to-NIR and the MCI at 740 nm.

In the end *in situ* data will be used to calibrate the models in order to extract the chlorophyll-a concentration.

It is possible to do all these steps by hand and is doable when working with fewer samples, but it is not advised when working with larger quantities. So, for the application of these steps, a series of scripts were created. This ensured that the same procedure is applied to all the selected products and prevents minor mistakes.

2.3.3 Monitoring Water Quality of Inland Lakes using Remote Sensing

The Monitoring Water Quality of Inland Lakes using Remote Sensing training focus on using remote sensing observations from Landsat 8 and 9, Sentinel-2, and Sentinel-3 for assessing water quality parameters, including Chl-a concentration, turbidity, and TSM in inland lakes, Figure 12. It also highlights the importance of *in situ* measurements of these parameters, coincident with satellite observations, in developing methodologies for operational water quality monitoring [56].

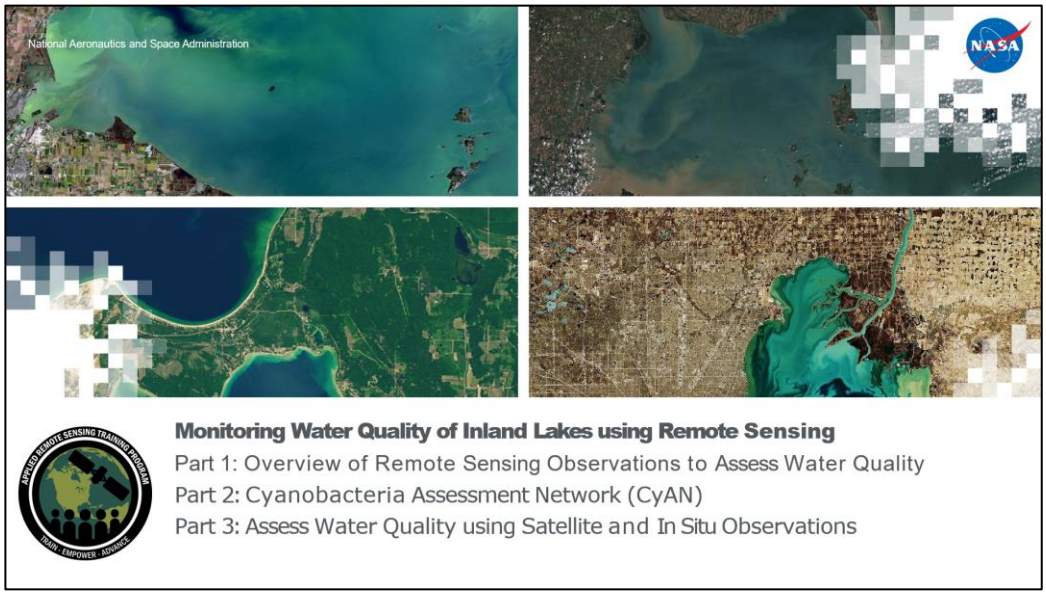

Figure 12 - Monitoring Water Quality of Inland Lakes using Remote Sensing

The training is divided into three parts, each with a brief theorical description, a practical exercise and finalizes with a question and answers session.

The first part gives an overview of remote sensing to assess water quality. Here it's described the state-of-the art, high spatial and spectral resolution observations, and the *in situ* measurements of water quality parameters. This parts exercise introduces GEE, and the way to access Landsat 8 and Sentinel-2 surface reflectance data and Sentinel-3 top of the atmosphere reflectance data.

The second part gives an overview on the Cyanobacteria Assessment Network and finalizes with a demonstration of the CyAN website and application.

The third and last part gives a brief review of methodologies to assess water quality from remote sensing and the benefits and limitations of various satellite sensors for water quality monitoring. The final exercise consists of calculating the spectral indices as indicators of water quality from Landsat, Sentinel-2, and Sentinel-3 observations, and in the development of statistical coefficients to derive water quality parameters based on remote sensing and *in situ* data.

3

METHODOLOGY

Considering the requirements listed in chapter 1 and the technologies described and selected in chapter 2, here the system proposed and developed is presented.

This chapter describes the entire methodology used to develop and implement the study of the water quality and quantity evolution in the Portuguese dams.

3.1 Proposed solution

This thesis will have two different approaches for the two objectives proposed in the first chapter. For water quality assessment, the training course developed by ESA and shown in chapter 2, is implemented, however we proposed a novel approach for pixel validation to improve obtained results.

For the water quantity, the study will be done purely based on simple mathematics without image processing.

As this is a study carried out in Portugal, and knowing the climate problems the country faces, four dams were selected across the country, one in the central northwest, one in the centre, one in the central southeast and one in the southwest.

3.2 Portuguese Dams

To select the dams for this study, some criteria had to be followed, cloud-free images and *in situ* stations for air and water quality parameters. Many didn't have air quality stations, or they would be too far, other had clouds all around the year, mostly the north ones.

After analysing several candidates that complied to the rules established, the dams for this study were selected, as shown in Figure 13:

- The Aguieira dam
- The Castelo de Bode dam
- The Alqueva dam
- Odelouca

Figure 13 - Rivers and locations for the selected dams

3.2.1 Aguieira Dam

Located in the municipality of Mórtagua, in the district of Viseu, is fed by the Mondego River and started operating on 1st of January 1981, Figure 14. It has a maximum capacity of 423030 cubic decametres (dam^3) and is used to produce hydroelectric energy, flood prevention, irrigation and water supply.

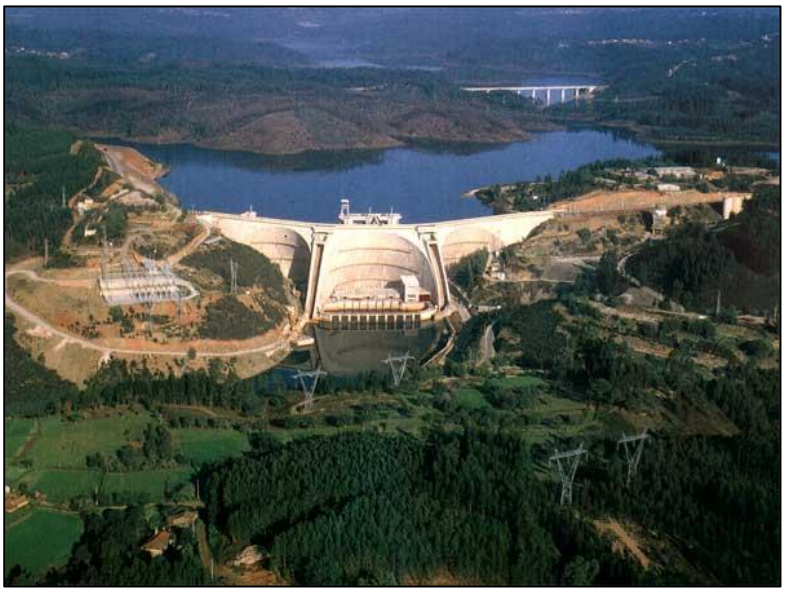

Figure 14 – Aguieira Dam [62]

3.2.2 Castelo de Bode Dam

Located in the municipality of Tomar, in the district of Santarém, is fed by the Zêzere River and started operating on 1st of January 1951, Figure 15. It has a maximum capacity of 1095000 dam^3 and is used to produce hydroelectric energy, flood prevention, recreation and water supply.

Figure 15 – Castelo de Bode Dam [63]

3.2.3 Alqueva Dam

Located in the municipality of Moura, in the district of Beja, is fed by the Guadiana River and started operating on 7th of February 2002, Figure 16. It has a maximum capacity of 4150000 dam^3 and is used to produce hydroelectric energy, irrigation and water supply.

Figure 16 – Alqueva Dam [64]

3.2.4 Odelouca Dam

Located in the municipality of Monchique, in the district of Faro, is fed by the Odelouca stream and started operating on 1st of January 2008, Figure 17. It has a maximum capacity of 157000 dam^3 and is used for water supply.

Figure 17 – Odelouca Dam [65]

3.3 Process and Data Acquisition

As said in the introduction of this chapter, there will be two different approaches for the water quality and water quantity assessment.

For water quality, the main approach will be divided in to two processes. For chlorophyll concentration acquisition the study will consist in image processing, empirical model application and statistical analysis based on *in situ* and satellite data. For TSM and CDOM, the study will consist of image processing and statistical analysis based on satellite data.

Water quantity, will have a more direct approach, taking advantage of the recorded volume provided by SNIHR and correlating it with the maximum volume of each dam.

Since we will be working with hundreds of satellite products and *in situ* data, several scripts were developed. This way human error can be kept at the minimum possible and the workflow can be optimized.

3.3.1 Data Acquisition

As previously presented, the data required for this study is acquired from four databases, being them:

- SNIHR[2]
- Copernicus browser[3]
- Visual Crossing[4]
- QualAR[5]

The *Sistema Nacional de Informação de Recursos Hídricos* (SNIHR) processes, validates and publicises all the information collected by the APA's monitoring networks and other entities (local and regional - Azores and Madeira) regarding water resources.

Copernicus browser provides access to a wide range of Earth observation data from the Copernicus Sentinel missions and more. The Copernicus Data Space Ecosystem provides tools for easy discovery, visualization and download.

Visual Crossing is a weather data and enterprise analysis tools provider. It has a database containing historical weather data, forecasts and climate summaries information.

QualAR is an online information system developed by *Agência Portuguesa do Ambiente* (APA) with the aim of centralising all the information on air quality monitoring and forecasting. It is an indispensable tool for assessing and managing air quality in Portugal.

For the data acquired there were three factors that can limit the amount of data available for this study, chlorophyll measurements, satellite images taken with few days from the water sample retrieval and cloud-free satellite images.

[2] https://snirh.apambiente.pt/index.php?idMain=2&idItem=1
[3] https://browser.dataspace.copernicus.eu/
[4] https://www.visualcrossing.com/weather-data
[5] https://qualar.apambiente.pt/

With these three factors as rules, data from each dam was acquired. Appendix A contain the selected days for in situ and satellite data, as well as the difference between the two acquisition dates, for each dam.

It's important to note that the chlorophyl concentration retrieved from SNIHR is in µg/L and the concentration retrieved from SNAP is in mg/m^3. These two measures are equivalent, but the most common used in water samples is µg/L.

3.3.2 Water quality monitoring process

In order to obtain the metrics to evaluate the water quality, this thesis will follow the training course presented in chapter 2, the HYDR02 – Freshwater Quality Monitoring using Sentinel-2.

This course takes advantage of SNAP and its applications. The key factor of this course, and this thesis, is the use of the C2RCC processor.

This processor relies on a large database of simulated water leaving reflectance's, and related top-of-atmosphere radiances. Neural networks are trained in order to perform the inversion of spectrum for the atmospheric correction, i.e. the determination of the water leaving radiance from the top of atmosphere radiances, as well as the retrieval of inherent optical properties (IOP) of the water body [66].

The processor only accepts satellite data without AC, so in this case the selected products will be Sentinel-2 Level 1-C products that have top of atmosphere reflectance images.

The resulting bands that will be of interest for this study are presented in Table 1.

Table 1 - C2RCC bands description, extracted from [67].

C2RCC bands (units)	Description	Metric
rhown	Normalized Water Leaving Reflectance	Chlorophyll
conc_tsm ($g.m^{-3}$)	Total suspended matter dry weight concentration	TSM
iop_bpart (m^{-1})	Scattering coefficient of marine particles at 443 nm	TSM
iop_bwit (m^{-1})	Scattering coefficient of white particles at 443 nm	TSM
iop_btot (m^{-1})	Total particle scattering at 443 nm	TSM
iop_agelb (m^{-1})	Absorption coefficient of gelbstoff at 443 nm	CDOM
c2rcc_flags	CR2CC Quality flags	TSM; CDOM

3.3.2.1 Chlorophyll process

The first thing needed, is the *in situ* data for each dam. This data can be obtained by going to the SNIRH database[6] and select the chlorophyll parameter from the desired dam stations. Appendix B contains all this information. After knowing which days have water samples analysed, we can proceed to extract the satellite products.

The satellite data extraction is a bit more complicated because there are two factors that impact the decision to select the day in question: (1) if is cloud-free on top of the dam; (2) how many

[6] https://snirh.apambiente.pt/index.php?idMain=2&idItem=1

days apart from the water sample retrieval. Since the concentration of chlorophyll varies greatly across the days, it's not appropriate to have to many days from *in situ* and satellite data retrieval. This data can be obtained by going to the Copernicus browser page[7].

After we have the satellite days, we can proceed to obtain the air quality factors for each dam, ozone concentration (O_3), air temperature and atmospheric pressure. The O_3 can be acquired in the QualAR database[8], and the temperature and atmospheric pressure in the Visual Crossing website[9].

Lastly, we need the elevation for each dam. This data can be obtained in SNIRH data base and can be found in the characteristics of each dam.

These last four factors will be used as input parameters in the C2RCC processor.

After we have all the products and factors, we can start running the scripts. The scripts are divided into four main ones:

1. Resample and Subset
2. C2RCC processor
3. Band Maths
4. Empirical Model

The first script will resample and subset all the products to a single-size and smaller area of interest. The resample process is important because not all instances support multi-size products. In this case we will resample with a reference band (band 2), which has a spatial resolution of 10 m, and subset with an area that contemplates only the selected dam. Figure 18 shows the before and after of the application of this script.

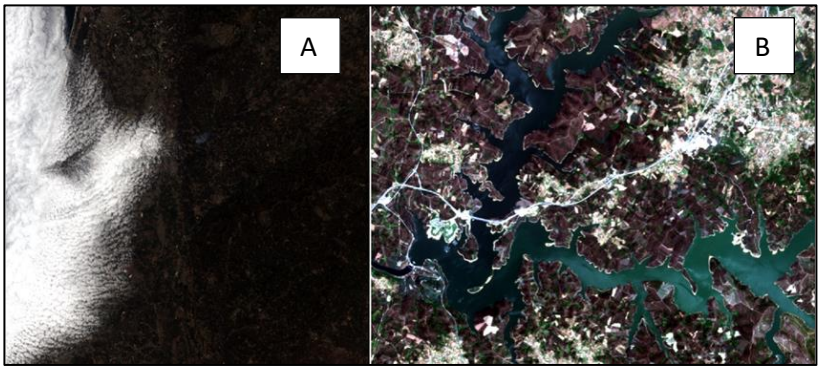

Figure 18 - Resample and Subset: (A): Before; (B): After

The second script uses the C2RCC processor along with the previous obtained factors. In this step we pre-define the pixel validation expression, dam elevation and salinity, for each dam.

For the pixel validation a new approach was tested and implemented. Subchapter 3.3.2.2 explains this novel expression.

[7] https://browser.dataspace.copernicus.eu/
[8] https://qualar.apambiente.pt/
[9] https://www.visualcrossing.com/weather-data

The salinity will have a value of 1E-4 across all dams because we are working with fresh water and the processor don't accept 0 values in this input. The other factors, O_3, temperature and atmospheric pressure, are defined at each iteration.

From this script we will obtain new products that contain the chlorophyll, TSM and CDOM concentrations. Figure 19 shows the different metric concentrations for the same day in the same dam (the colours presented are a mere colour palette application and don't have real impact on the actual concentrations).

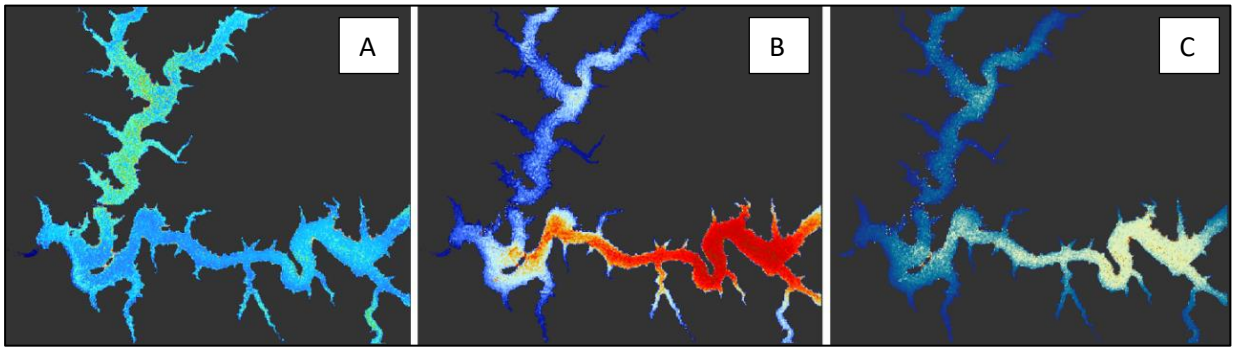

Figure 19 - (A) Chlorophyll concentration; (B) TSM concentration; (C) CDOM concentration.

The third script applies the MCI and BandRatio equations, using the band maths instances, as well as exporting the products to a GeoTIFF format so that they can be used in QGIS. The MCI and Band ratio expressions are as follows:

$$MCI = rhownB5 - rhownB4 - 0.53(rhownB6 - rhownB4) \quad (11)$$

$$BandRatio \rightarrow R705\_R655 = \frac{B5}{B4} \quad (12)$$

After the third script, the first round of statistical analysis is performed, by applying a linear regression between the satellite and the *in situ* data. With the resulting linear equation, we combine it with MCI and Band Ratio equations, and obtain the empirical models for each index.

The fourth script is equivalent to the third one, with the difference that will have the empirical models instead of the normal indices. With the results from this script, we perform the last round of statistical analysis by extracting the new chlorophyll concentration for each model in each station.

After this we can compare the statistical and visual results between non model and model results, shown in sub-chapter 4.2.2.

3.3.2.2 Novel pixel validation condition

Different from the training course, the pixel validation expression was changed. The default expression only considers band 8, in the NIR part of the spectrum, which lead to some products having more than only the water body presented.

With that in mind a new approach was developed. The new pixel condition is based on the NDWI and helps to clean out the remaining shadows of the products.

The NDWI was proposed by McFeeters, and it is designed to maximize the reflectance of the water body in the green band and minimize the reflectance of water body in the NIR band. Figure 20 presents the water and green vegetation reflectance's throughout the visible spectrum [55].

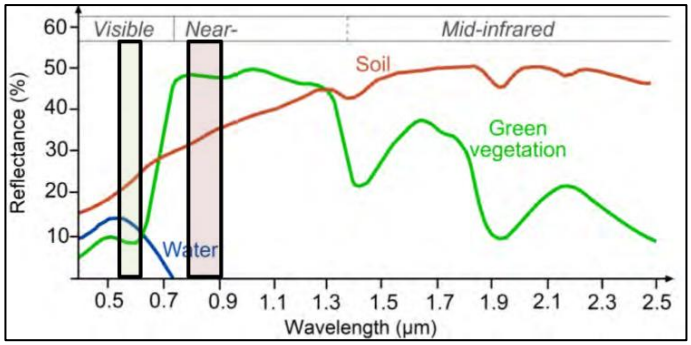

Figure 20 - NDWI - water and vegetation reflectance's

The new pixel validation expression his as follow:

$$Pixel\ Validation = B3 - B8 > 0\ \&\&\ B3 + B8 < 0.2 \quad (10)$$

We use B3-B8 > 0 to obtain the pixels values that mainly refer to water bodies and the B3+B8 < 0.2, to clean out the false water body pixels. In this case, these pixels are shadows produced by the top of cliffs or by recently burned ground. Figure 21 shows difference between using the default and the new expression. As we can see the image is much clearer and easier to analyse visually.

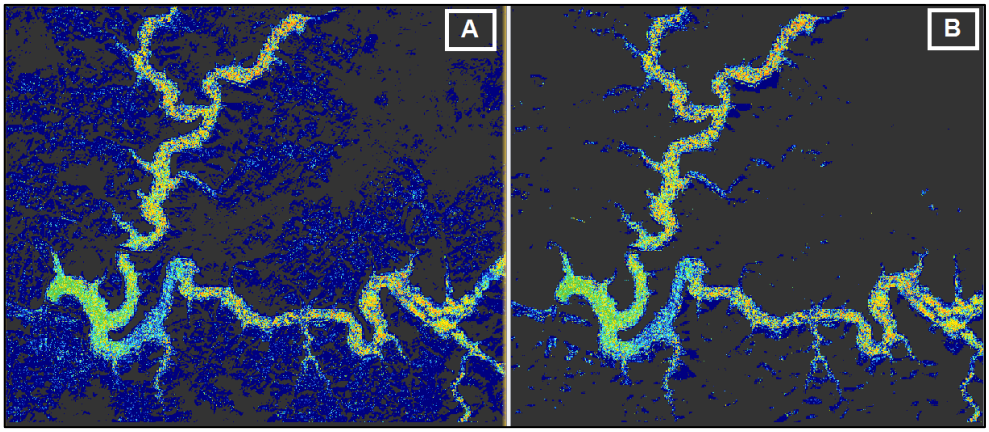

Figure 21 – Side-by-side comparison between the default (A) and new (B) expression.

3.3.2.3 TSM and CDOM process

Like the chlorophyll concentration process, we need *in situ* and satellite data, but because we already have this data from the previous process, we don't need to extract it again.

The only difference between the TSM and CDOM process and the Chlorophyll process is that we won't have *in situ* measures for TSM and CDOM, we will only work with satellite data. This means that we won't have empirical models to do comparisons. This data can be found in appendix C and D for TSM and CDOM values, respectively.

So, for the TSM and CDOM process, we will only have three scripts:

1. Resample and subset
2. C2RCC processor
3. Band Subset

Since the products are the same, the first and second script will perform same work.

The third script will perform band subsets. Different from the first, that performs a geographical subset, this one will subset the product with the bands of interest.

For the TSM, the bands of interest are as follows:

- conc_tsm
- iop_bpart
- iop_bwit
- iop_btot

And for the CDOM, the band of interest will be:

- iop_agelb

For TSM and CDOM we will also use the *in situ* stations locations for their concentrations retrieval. After this we can perform the statistical analysis, as shown in sub-chapter 4.2.3.

3.3.2.4 Statistical analysis

For the statistical analysis, we will use the QGIS platform which will help extract the values situated in the same coordinates as the *in situ* stations. For this precise data extraction SNAP will be used to create the shapefile with the location of *in situ* stations. Table 2 presents the coordinates for each station and Figure 22 have their location in each dam.

Table 2 - *In Situ* stations coordinates

	Stations Name	**Coordinates**
Aguieira dam (A)	est 1 meio - CCHE	40°20'37.4"N 8°11'38.7"W
	est 2 meio - CCHE	40°20'14.8"N 8°11'04.0"W
Castelo de Bode dam (B)	est 1meio - CCHE	39°32'38.6"N 8°18'54.1"W
	est 2meio - CCHE	39°32'46.5"N 8°18'14.0"W
Alqueva dam (C)	MONTANTE - CCHA (C)	38°13'05.2"N 7°27'55.9"W
Odelouca dam (D)	(S)	37°17'23.5"N 8°27'55.5"W
	INT	37°17'59.7"N 8°27'37.1"W

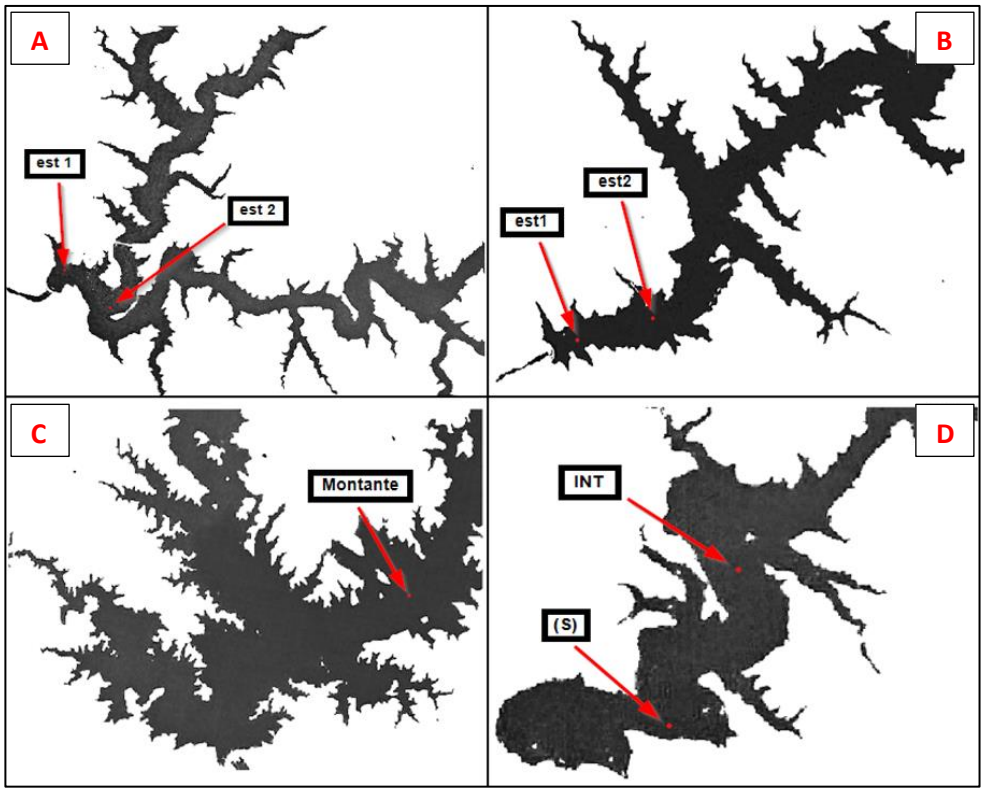

Figure 22 - *In Situ* locations for each dam

3.3.3 Water quantity monitoring process

For the water quantity monitoring, we will only have a mathematical view over the last 10 years. In the SNIRH data base it's possible to obtain the maximum volume and the registered volume for a defined period. The data for this process can be found in appendix E.

With the data obtained, we can obtain the percentage equation for each day selected, as followed:

$$Volume = \frac{Volume_{current} * 100}{Volume_{max}} \quad (13)$$

With the results, we can analyse and draw a conclusion on evolution of the water quantity throughout years, which is shown in sub-chapter 4.2.4

4

RESULTS

This section gives an insight into the results and obstacles surpassed during the development of this study. It begins with the training course replication, followed by the addition of the new pixel validation formula, and ends with the results for chlorophyll, TSM and CDOM concentrations and the evolution of the water quantity throughout the years.

4.1 Training course replication

The first thing to do before we start evaluating the water quality in the Portuguese dams, is to test and verify that the training course, presented in February of 2020, is still valid and working. The first tests were done manually with the same products that had written results in the step-by-step paper supplied by the speaker, this way if the course were no longer viable, other solutions could start to be taken into account.

The first tests were successful and presented similar results to the ones presented in the course. The slight difference between results happened because the formula utilised by the processor for the calculation of TSM had been updated since the time the course took place.

With this, the scripts for the process were developed and tested with all the products used in the course. Figure 23 and Figure 24 show the application of the colour palettes for each metric and the impact that the formula update had, particularly in the TSM concentration.

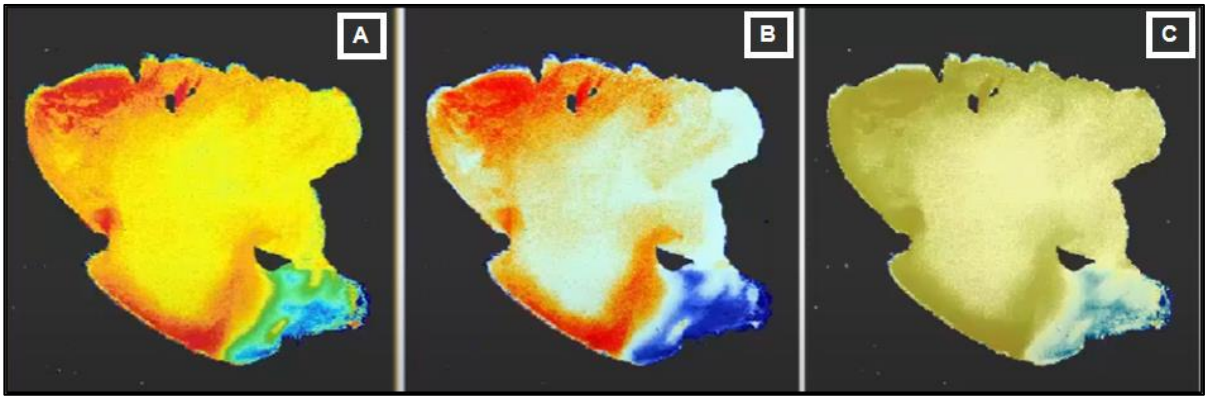

Figure 23 - Lago Trasimeno with the colour palettes for Chl-a (A), TSM (B) and CDOM (C) - Speaker version [55]

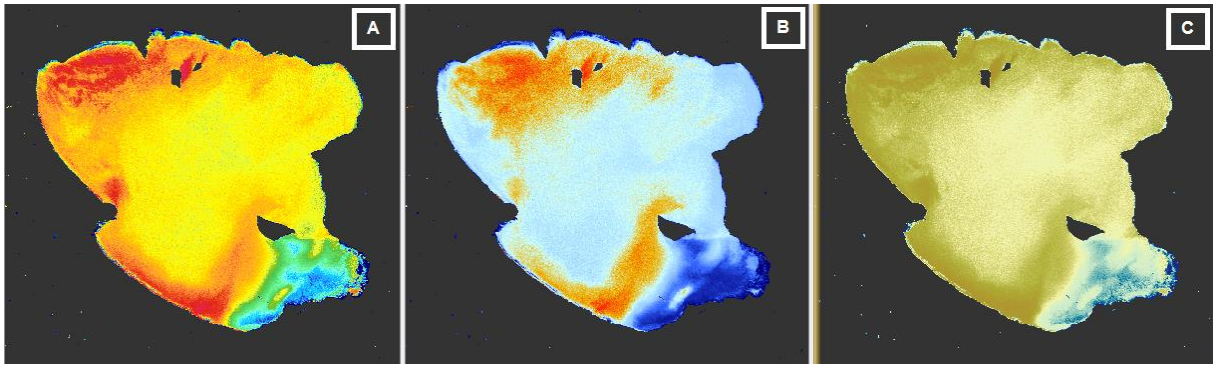

Figure 24 - Lago Trasimeno with the colour palettes for Chl-a (A), TSM (B) and CDOM (C) - Thesis version

It is important to emphasize that the training course also had scripts but for a different operating system and only for chlorophyl, so new scripts had to be created and the older ones had to be translated.

With the statistical analysis that the step-by-step had, it was not possible to see the difference between TSM and CDOM values, because the training course didn't evaluate these metrics statistically, only the chlorophyll one.

For the chlorophyll concentrations the values are aligned with the ones provided by the speaker, having differences only at the millionth of unit Table 3 and Table 4 show the alignment between versions.

Table 3 - Chlorophyl concentrations - speaker version

Data	Station code	MCI	R705/R665	Chl-a (mg/m3)
16-05-18	TRS30	0,00196	0,67388	2,9
16-05-18	TRS35	0,00247	0,68835	9,4
09-07-18	TRS30	0,00199	0,67142	6,5
09-07-18	TRS35	0,00342	0,70807	3,6
04-09-18	TRS30	0,00425	0,80622	39,4
04-09-18	TRS35	0,00349	0,77898	24,3
21-11-18	TRS30	0,00551	0,81416	22,7
21-11-18	TRS35	0,00865	0,85987	13,6

Table 4 - Chlorophyl concentrations - thesis version

Data	Station code	MCI	R705/R665	Chl-a (mg/m3)
16-05-18	TRS30	0,001962	0,673878	2,9
16-05-18	TRS35	0,002467	0,688352	9,4
09-07-18	TRS30	0,00199	0,67142	6,5
09-07-18	TRS35	0,003421	0,708068	3,6
04-09-18	TRS30	0,004251	0,806224	39,4
04-09-18	TRS35	0,003489	0,778978	24,3
21-11-18	TRS30	0,005513	0,814157	22,7
21-11-18	TRS35	0,008653	0,859865	13,6

4.2 Results discussion

Now that we have the scripts developed and tested, they were applied to each dam, for each metric (chlorophyl, TSM and CDOM). This sub-chapter will present the results in the form of graphs and show the evolution throughout the acquisition years.

The first round of tests was successful, but some days were not as clean as the other ones. This happened for all the dams. After some investigation we found that: the problem was caused by shadows or burnt land, since the pixel validation formula wasn't capable to deal with this issues.

4.2.1 Pixel validation results comparison

The default version of the formula only uses the band 8, in the NIR part of the spectrum. This band is regularly used to obtain the vegetation reflectance because it has higher reflectance value at this wavelength, as we can see in Figure 20 in sub-chapter 3.3.2.2.

Having detected the root of the problem, we replaced the default formula with the one adapted from NDWI, as explained before in sub-chapter 3.3.2.2. With this we saw increased results for the days that had some problems, as we can see in figures 25, 26, 27, 28 and 29. Even though this work and correct most of the products, there were some that still needed manual attention and refinement. For example, Figure 28 needed the values for equation 11, term B3+B8, to be adjusted to 0.5 to recover part of the lost dam.

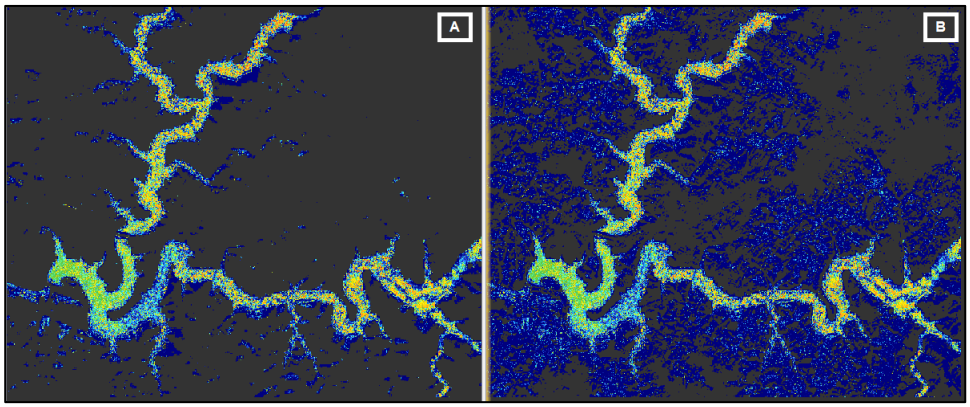

Figure 25 – Aguieira dam on the 21-11-2017; (A) - NDWI (B) – Default

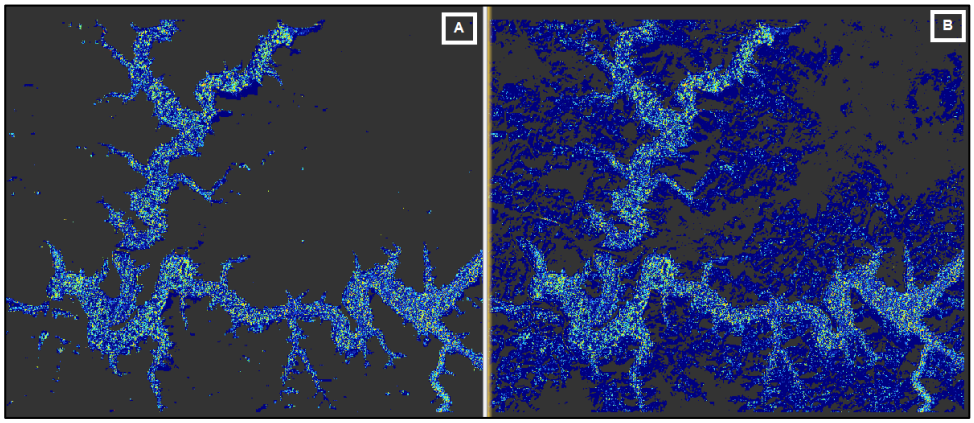

Figure 26 - Aguieira dam on the 30-01-2018; (A) - NDWI (B) - Default

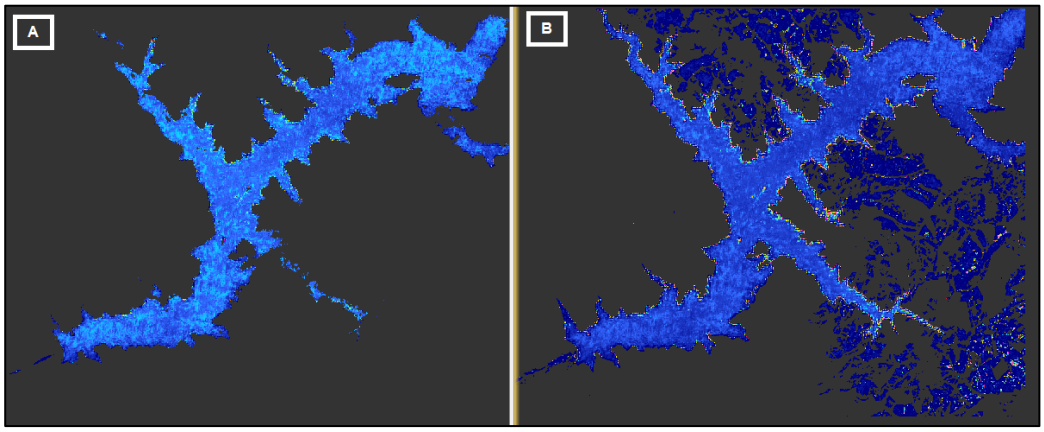

Figure 27 – Castelo de Bode dam on the 02-09-2017; (A) - NDWI (B) – Default

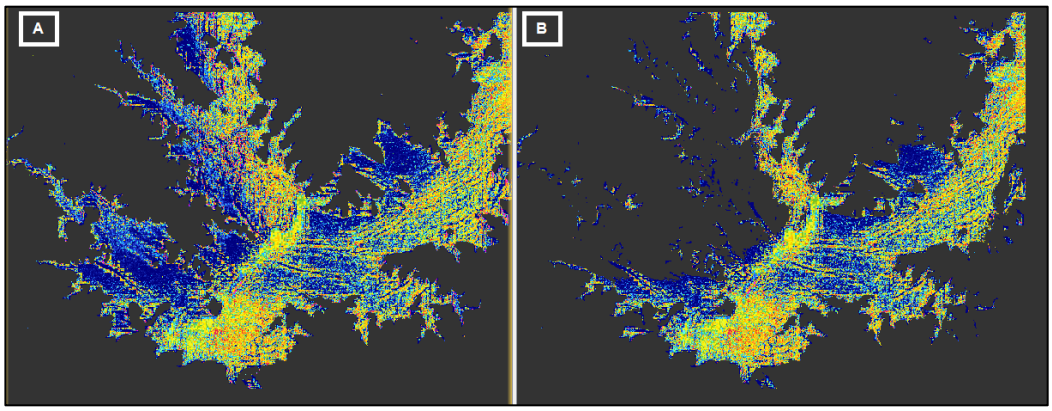

Figure 28 - Alqueva dam on the 23-06-2021; (A) - NDWI (B) – Default

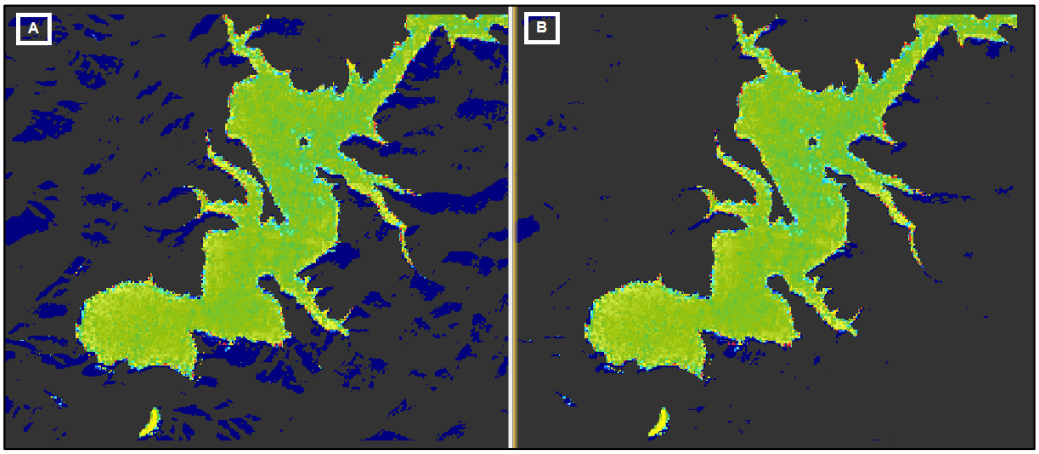

Figure 29 - Odelouca dam on the 22-11-2015; (A) - NDWI (B) – Default

4.2.2 Chlorophyll concentration results

For this metric, the concentrations were obtained using empirical models. To retrieve the empirical models, a linear regression was performed between the satellite and the *in situ* data. Figures 30, 31, 32, 33, 34, 35, 36 and 37 show the linear regressions applied for MCI and BandRatio, for each dam.

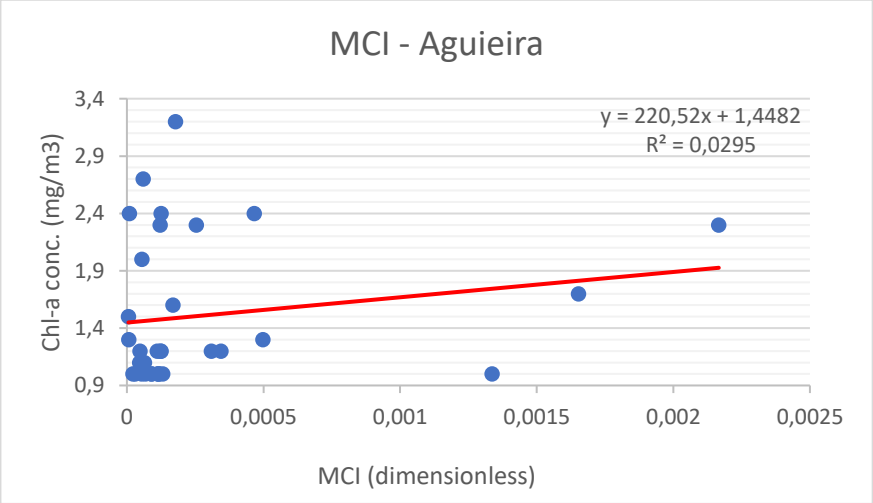

Figure 30 - Linear regression for MCI in the Aguieira dam

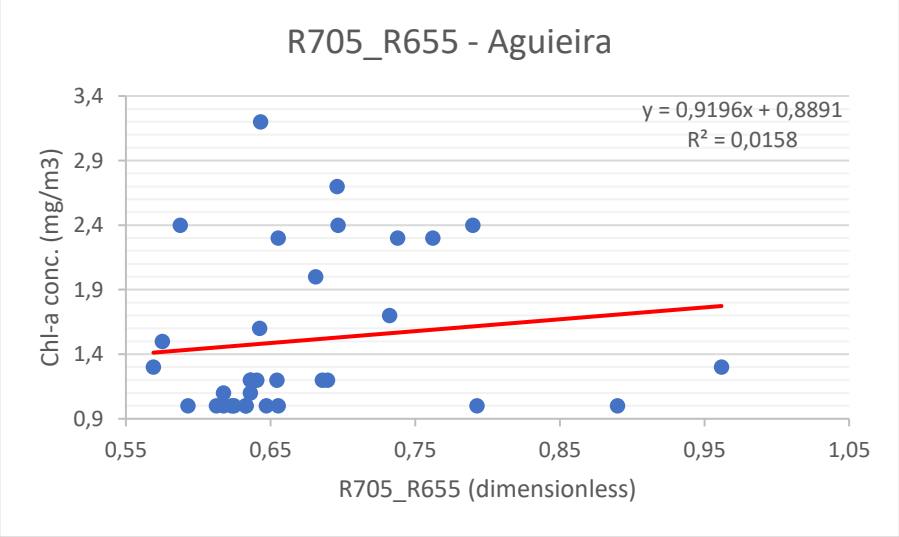

Figure 31 - Linear regression for BandRatio in the Aguieira dam

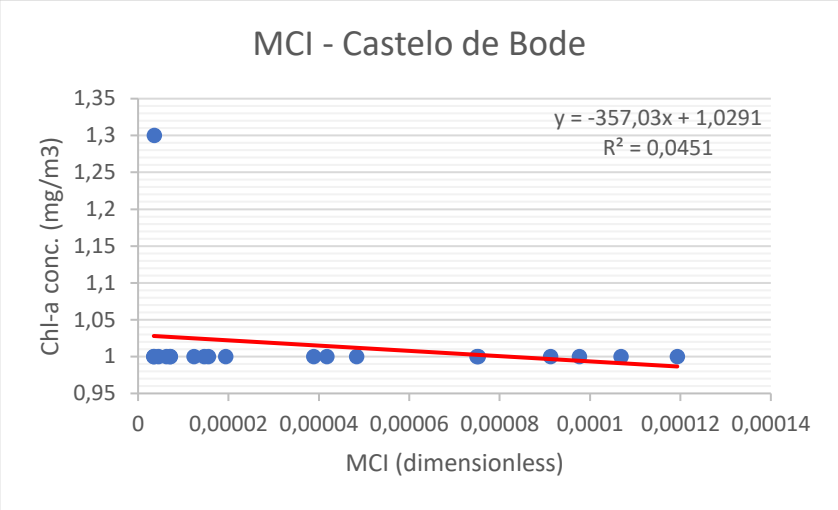

Figure 32 - Linear regression for MCI in the Castelo de Bode dam

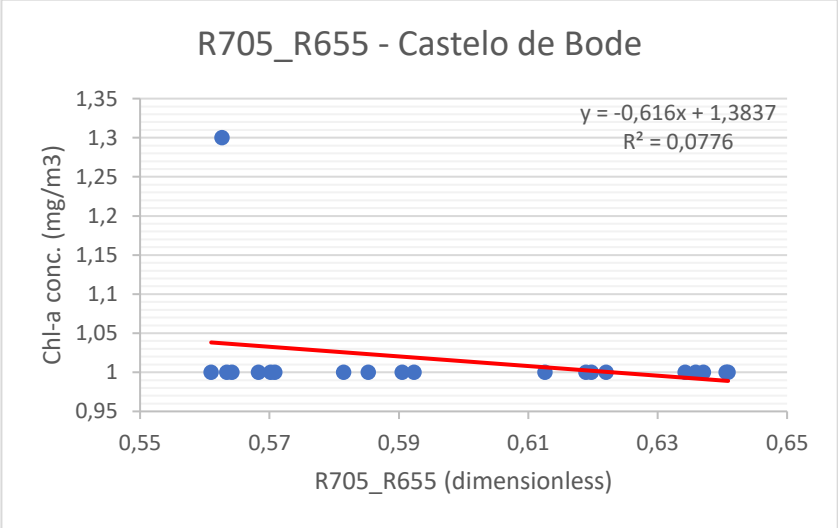

Figure 33 - Linear regression for BandRatio in the Castelo de Bode dam

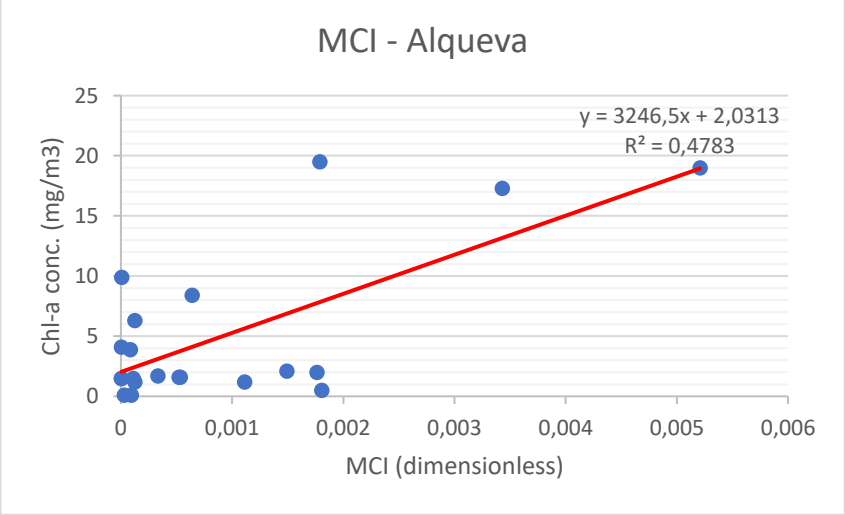

Figure 34 - Linear regression for MCI in the Alqueva dam

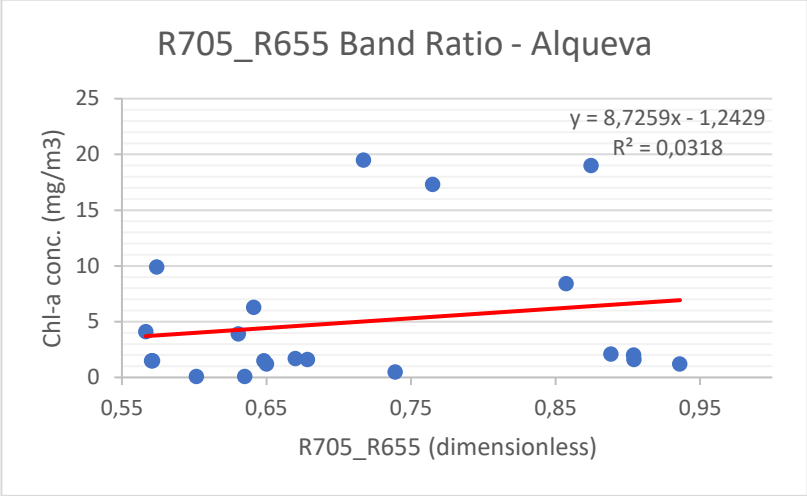

Figure 35 - Linear regression for BandRatio in the Alqueva dam

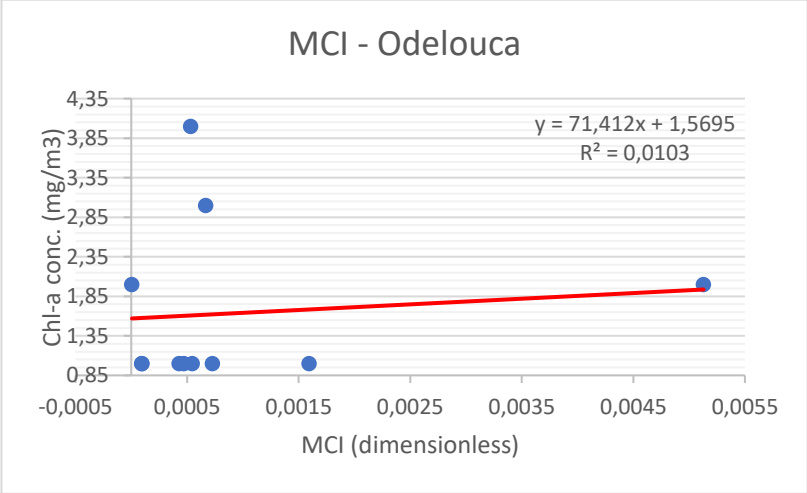

Figure 36 - Linear regression for MCI in the Odelouca dam

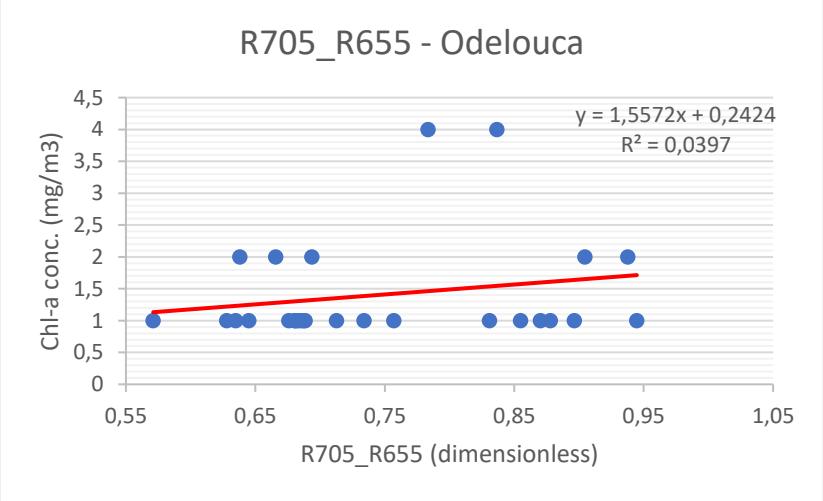

Figure 37 - Linear regression for BandRatio in the Odelouca dam

After the linear regression calculations, they are applied with the indices. To apply the linear regression equation with the indices, we simply substitute the x value in the linear regression equation for the index.

So, if the linear regression equation is $y = mx + a$, then the empirical models will be:

$$y = m * \left(rhownB5 - rhownB4 - 0.53(rhownB6 - rhownB4)\right) + a \quad (14)$$

$$y = m * \left(\frac{B5}{B4}\right) + a \quad (15)$$

Equation 14 refers to the MCI and equation 15 to the BandRatio, where m is the slope of the line and a is the value of y when x is zero. Once the empirical models are applied and the last set of scripts run, the new and corrected chlorophyll concentrations are obtained.

For each dam the chlorophyll concentration was plotted throughout the years that have satellite and *in situ* data. This way is possible to see the variance that occur for the *in situ* stations.

The following graphics in figures 38, 39, 40 and 41 are the results obtain with the empirical model application for each dam.

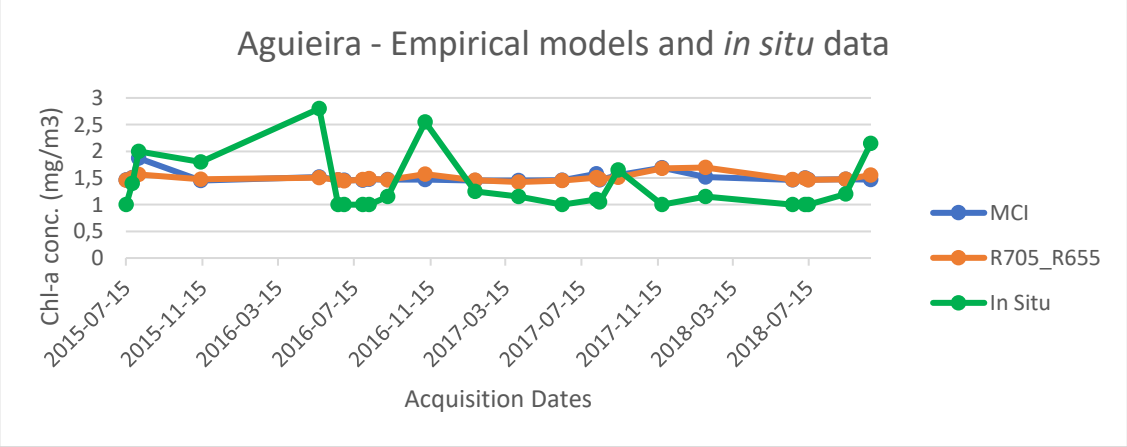

Figure 38 - Empirical models for the Aguieira dam

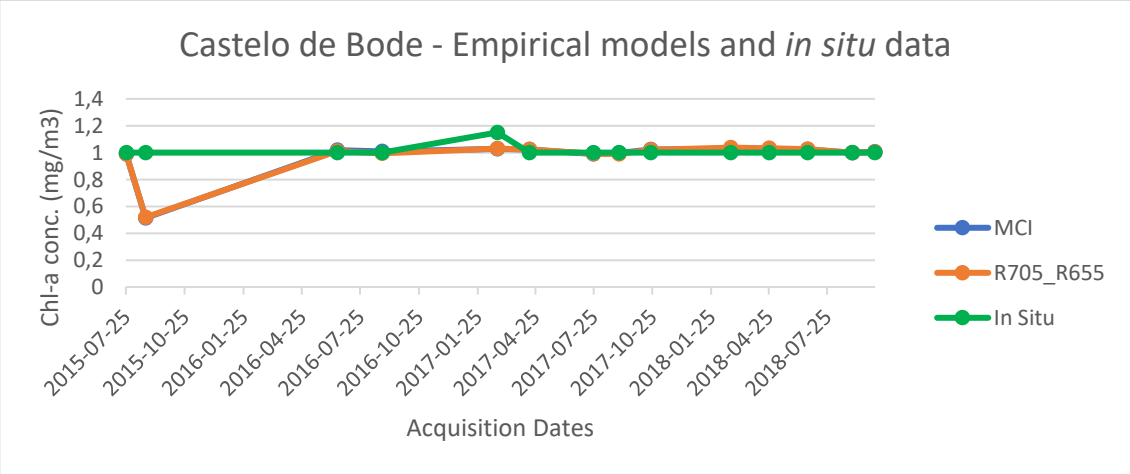

Figure 39 - Empirical models for the Castelo de Bode dam

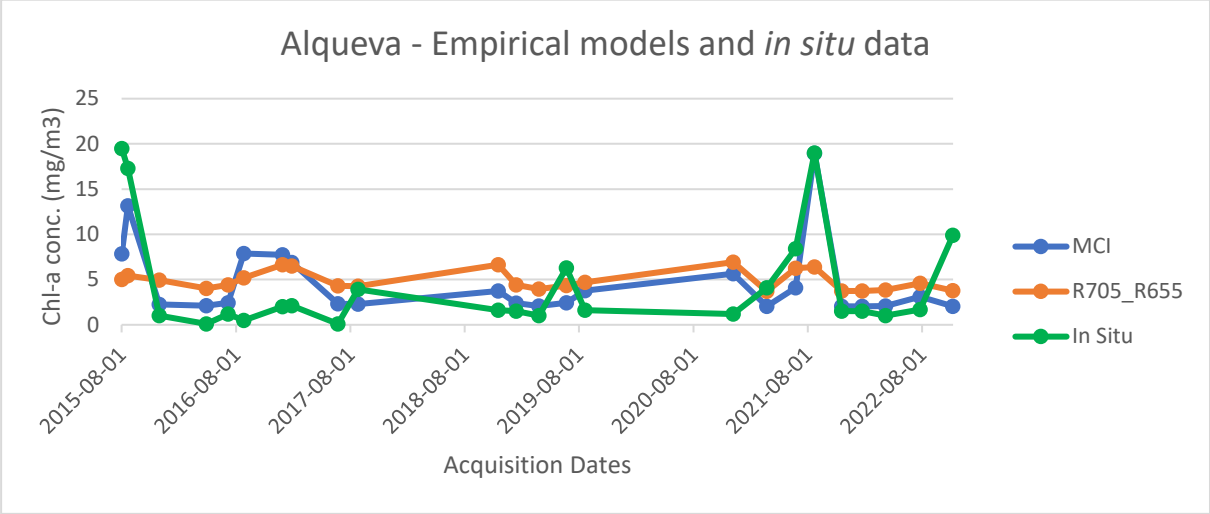

Figure 40 - Empirical models for the Alqueva dam

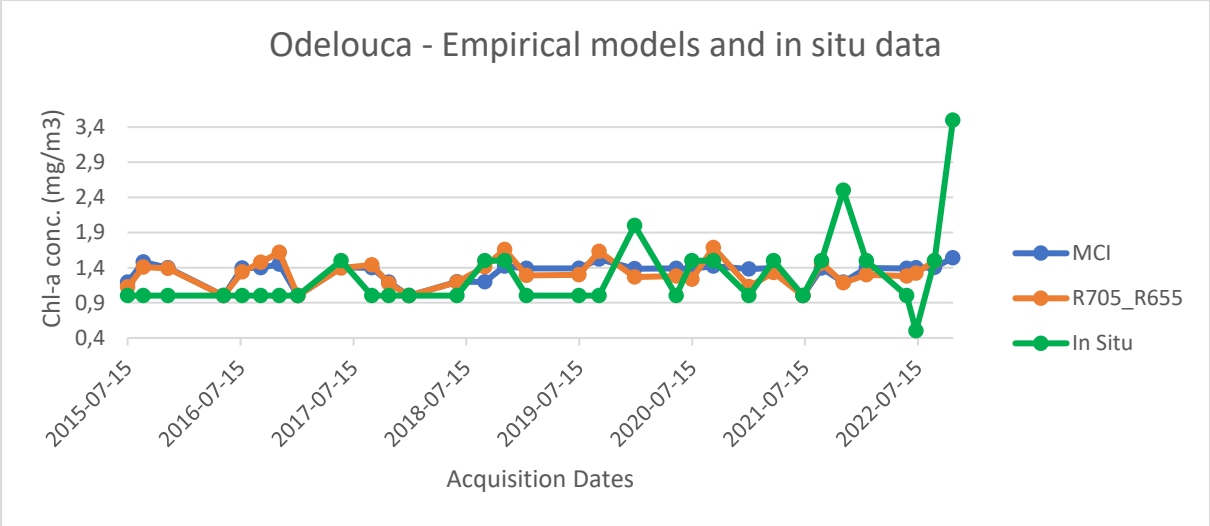

Figure 41 - Empirical models for the Odelouca dam

In all the dams we see that the empirical models follow the same or similar lines, i.e, have similar behaviours, with one or other value that runs from the normal pattern. When comparing with the *in situ* measures, we see some discrepancies, which is normal because some satellite acquisition dates are a bit far from the water sample retrieval days, especially in Alqueva and Odelouca dams, where some *in situ* measures are much higher than the satellite ones.

The results shown in the images have, in most of the cases, values closer to 1. These are very positive results because it means that Portugal presents a high-water quality.

From the four dams, the one that shows higher chlorophyll concentration values in satellite data is the Alqueva Dam, averaging around 5 mg/m^3. Even though the value is 5 times higher than the ones from the other dams, it's still considered a low value, because chlorophyll concentrations are considered harmful from 10 µg/L, which is the typical value considered for algal blooms.[68]

4.2.3 TSM and CDOM concentration results

For TSM and CDOM concentrations, the only results considered were the ones produced by the C2RCC processor. There were no *in situ* measures obtained for this two metrics since there was no 100% guarantee that the measures present in SNIHR where, in fact, TSM and CDOM measures.

Being these two metrics also very prune to a visual analysis, they will have their concentrations presented throughout the acquisition years along with some visual examples. Table 5 lists the days selected from each dam for the visual analysis. The season that presents the higher concentration value when compared to the mean value throughout the years, for each metric, is the summer. The Odelouca dam is the exception to the rule, having the autumn season as the one selected.

Table 5 - TSM and CDOM mean concentrations for a selected season

Aguieira	**Summer Season**	
Days	**TSM (mg/m^3)**	**CDOM (m^{-1})**
Mean Value	**0,557263911**	**0,163655001**
04-08-15	2,772912	0,502743
08-08-16	0,300227	0,096179
08-08-17	1,957476	0,402902
14-07-18	0,638053	0,131111
Castelo de Bode	**Summer Season**	
Days	**TSM (mg/m^3)**	**CDOM (m^{-1})**
Mean Value	**0,160139481**	**0,039919035**
25-07-15	0,4007	0,046204
28-08-16	0,179014	0,032393
24-07-17	0,465238	0,062774
24-06-18	0,052153	0,012532
Alqueva	**Summer Season**	
Days	**TSM (mg/m^3)**	**CDOM (m^{-1})**
Mean Value	**0,623393062**	**0,162236765**
01-08-15	2,789646	0,414354
25-08-16	1,443196	0,408268
25-08-17	0,440193	0,10719
20-08-19	1,263538	0,147572
22-08-21	2,207712	0,792728
25-07-22	0,704638	0,119482
Odelouca	**Autumn Season**	
Days	**TSM (mg/m^3)**	**CDOM (m^{-1})**
Mean Value	**0,854944413**	**0,258993654**
22-11-15	2,636177	0,518807
16-11-16	0,815041	0,437022
06-11-17	0,543048	0,311997
16-11-18	0,316178	0,108569
15-11-21	0,918223	0,455602
05-11-22	0,797973	0,540803

4.2.3.1 TSM concentration results

Similar to the chlorophyl concentrations, the values for TSM in both stations follow the same trend, and present lower values throughout the year. For the selected seasons, presented in Table 5, we can see in the images below, that those days have a higher TSM concentration. This can be explained by the higher temperatures that promote a higher organic matter concentration due to the algal blooms.

Figures 42, 43, 44 and 45 present a statistical analysis of TSM concentrations throughout the years and figures 46, 47, 48 and 49, the visual representation of the selected season.

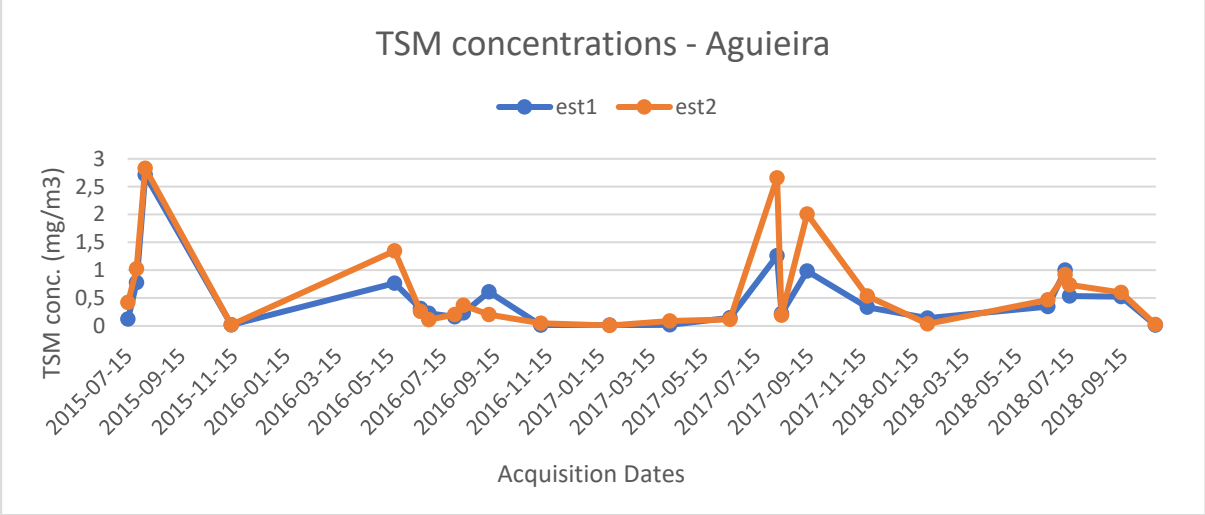

Figure 42 – Statistical analysis - TSM concentrations - Aguieira Dam

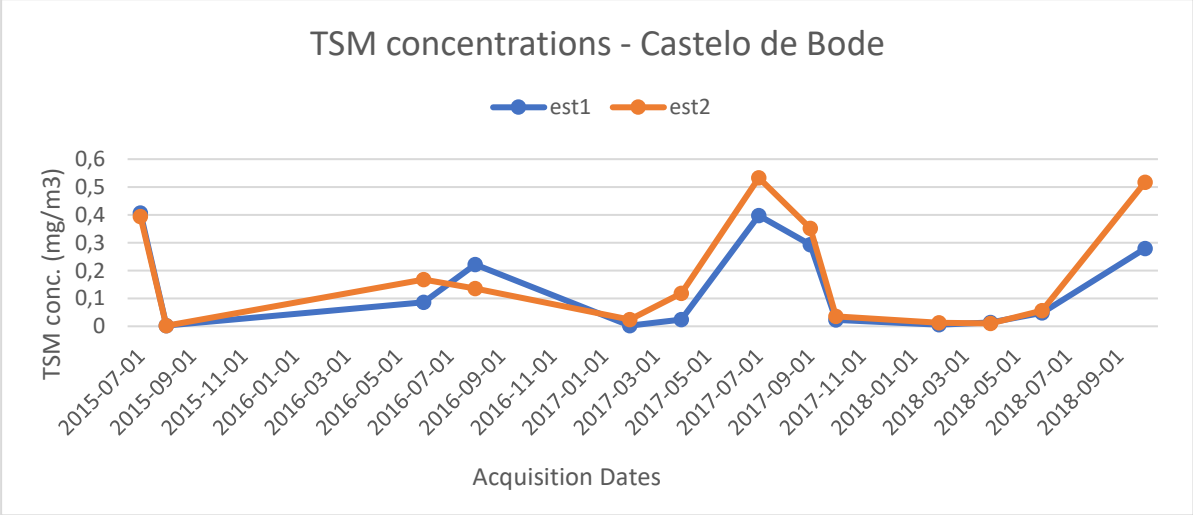

Figure 43 – Statistical analysis - TSM concentrations - Castelo de Bode Dam

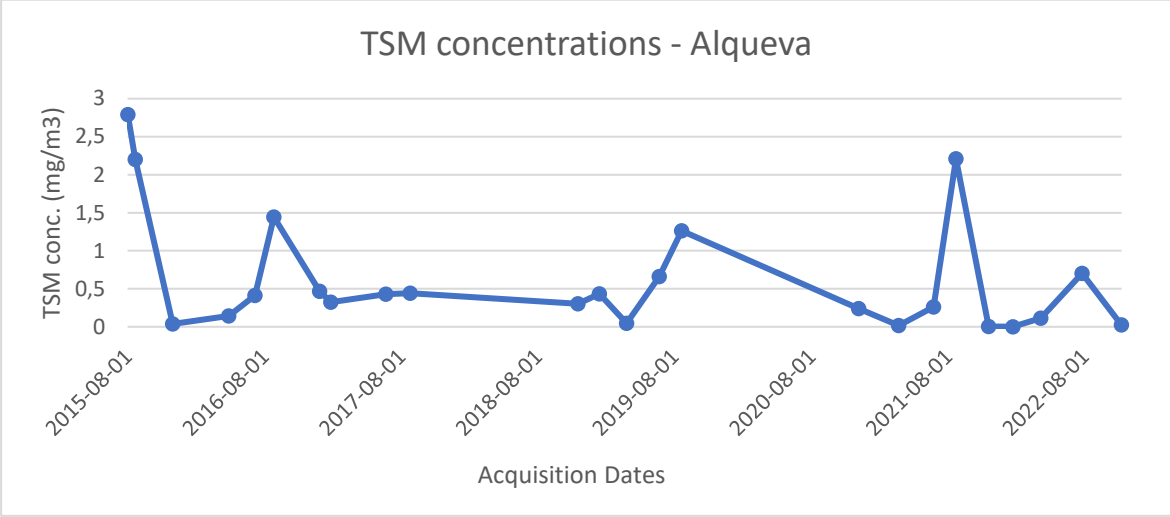

Figure 44 – Statistical analysis - TSM concentrations - Alqueva Dam

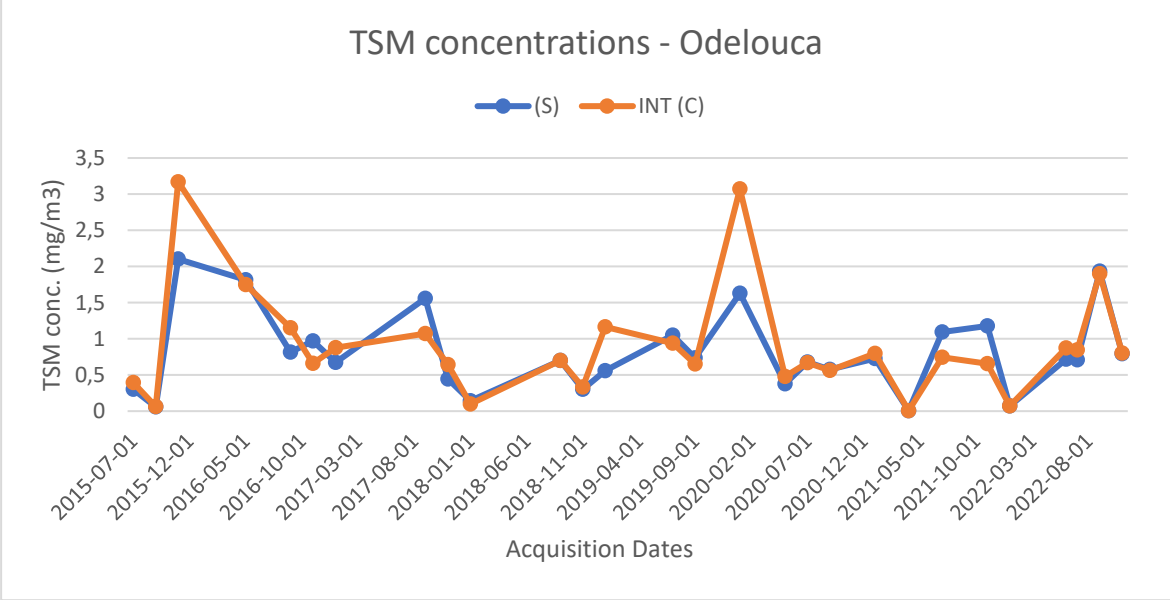

Figure 45 – Statistical analysis - TSM concentrations - Odelouca Dam

As we can see from the images above, the TSM measures for both *in situ* stations are very similar between each other, showing a low discrepancy. It's also important to refer that similar to the chlorophyl values, the TSM concentrations are low throughout the year, showing peaks around the summer for the Aguieira, Castelo de Bode and Alqueva dam, and around autumn for the Odelouca dam.

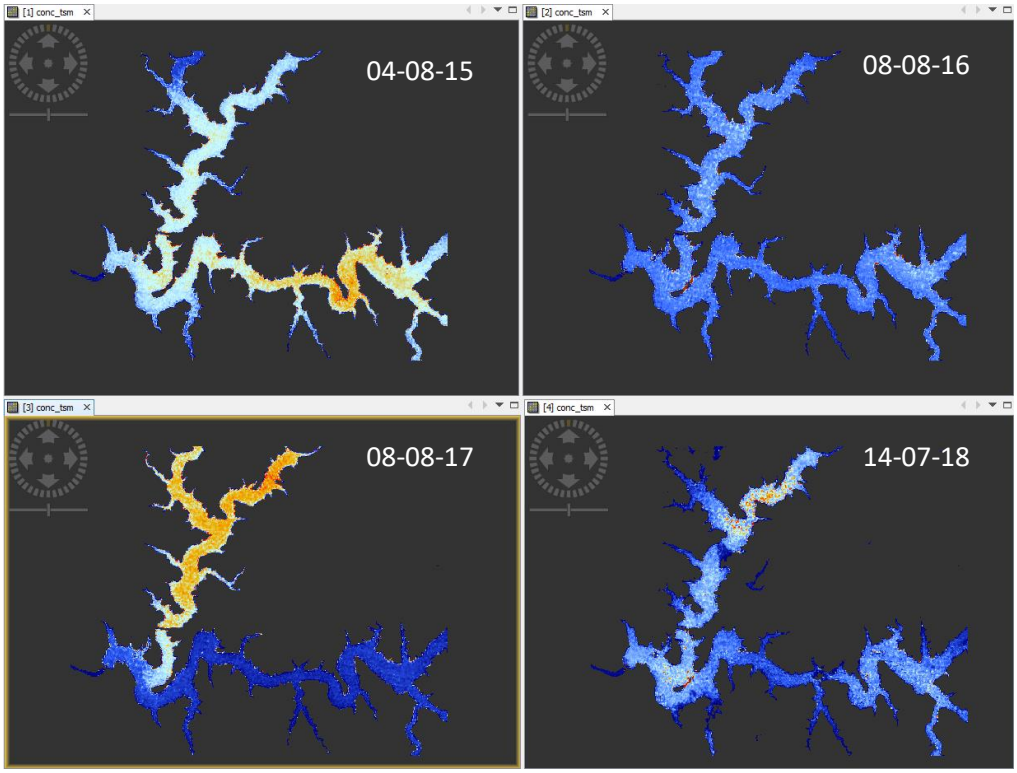

Figure 46 – Visual analysis - TSM concentrations - Aguieira Dam

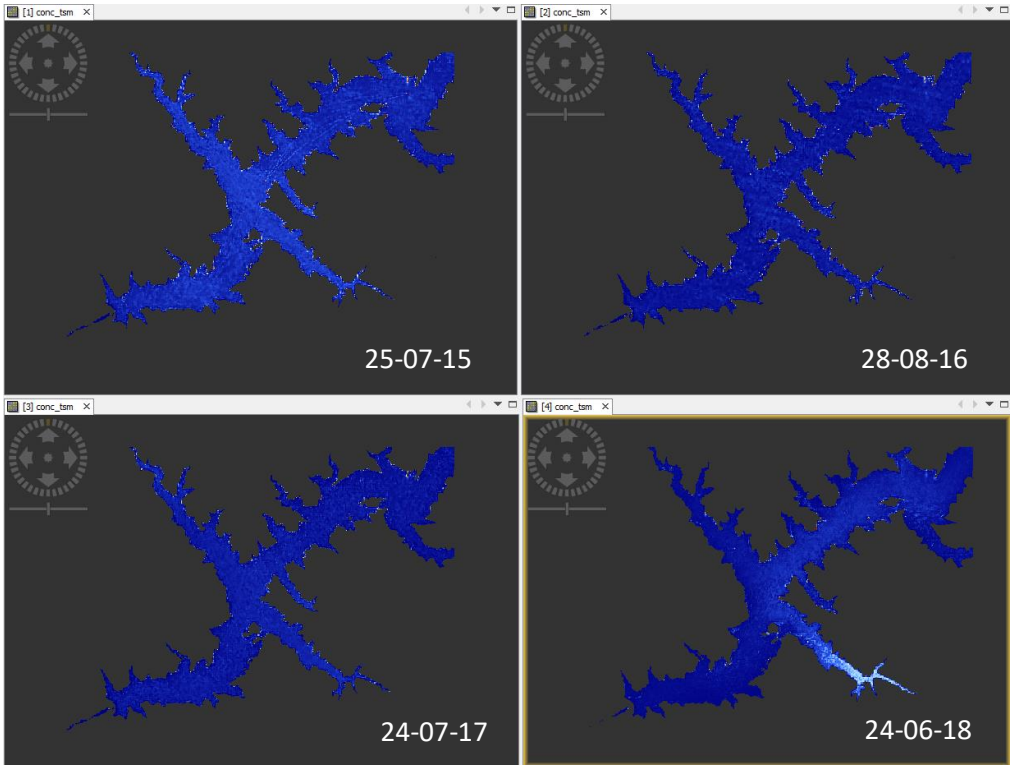

Figure 47 – Visual analysis - TSM concentrations - Castelo de Bode Dam

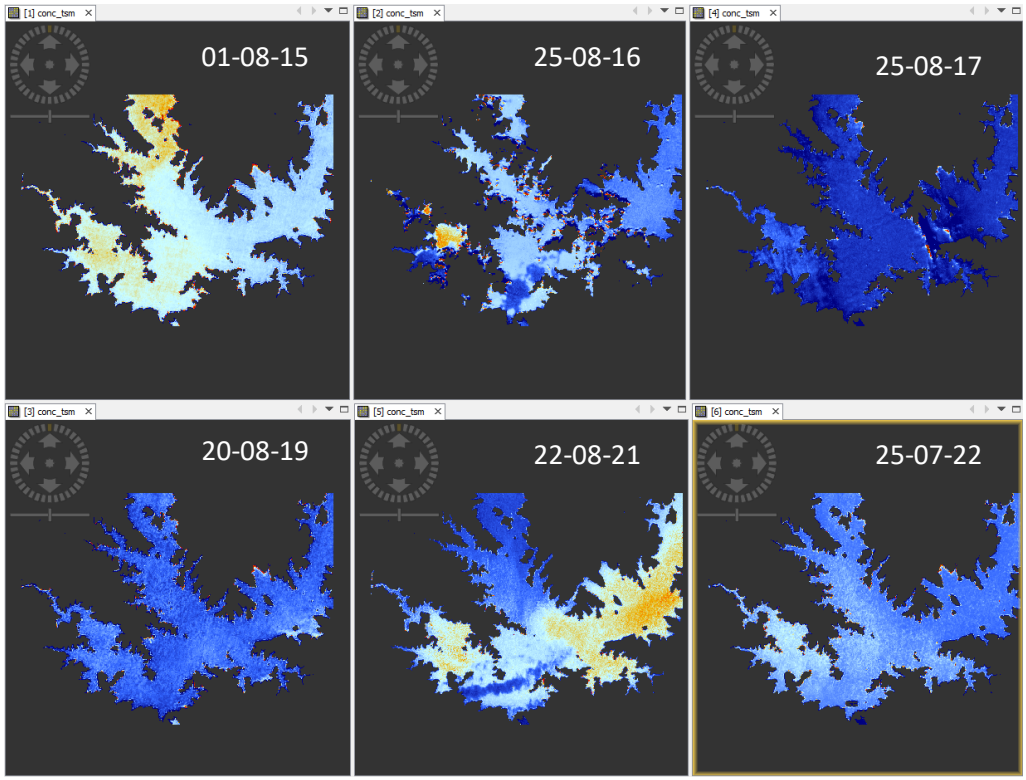

Figure 48 – Visual analysis - TSM concentrations - Alqueva Dam

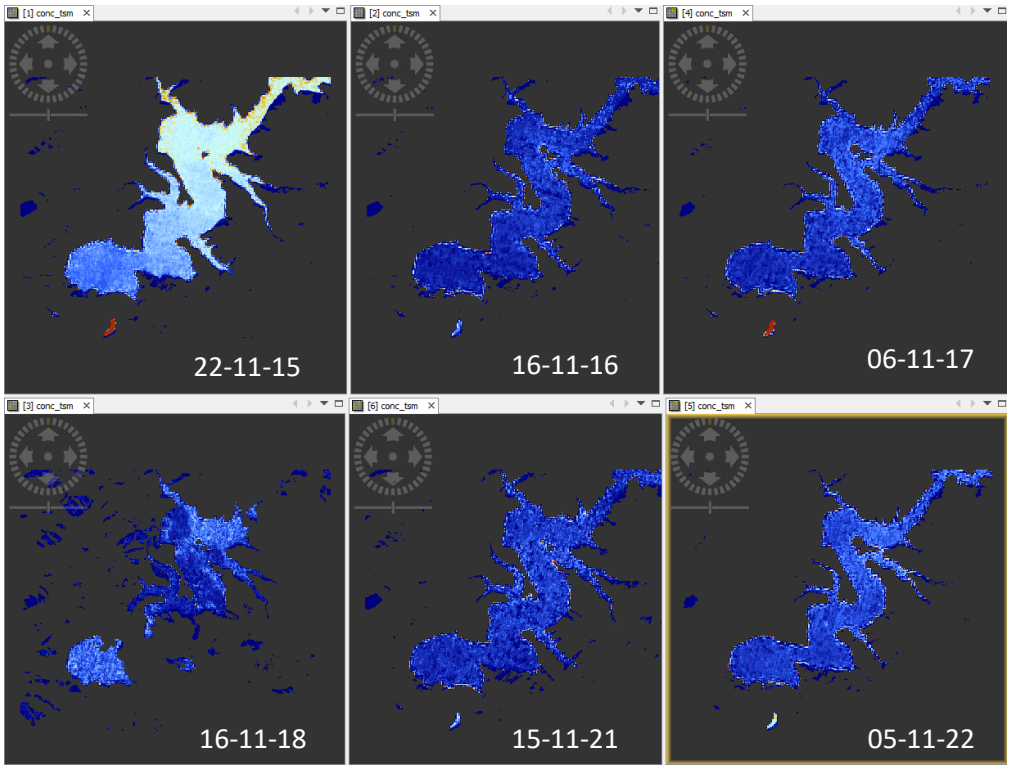

Figure 49 – Visual analysis - TSM concentrations - Odelouca Dam

Visually we see that across the water bodies the TSM concentration is very low, even though the images selected are from the dates with higher TSM values. In Figure 46 and Figure 48 is possible to see zones with higher values, coloured as orange and yellow, but this are from regions with staller water and without *in situ* stations, so they won't show up in the statistical results.

4.2.3.2 CDOM concentration results

For CDOM concentrations, the processor only produces the absorption and scattering levels for the CDOM flags. Even though the concentration is not measured, a high absorption means a high concentration.

With this said, even if high absorption means high concentration, the only way to correctly evaluate CDOM concentrations would be performing a linear regression between *in situ* concentration data and satellite absorption data. This way it would be possible to better estimate concentration levels for days that didn't have *in situ* data.

The absorption values vary between 0 and 1, and for the four dams, Aguieira and Alqueva dam show a great variance between low and medium/high absorption values, meaning that the CDOM concentrations have a great variance according to the season. If we take a look at the figures 50, 52, 54 and 56, from the Aguieira and Alqueva dams, it's possible to see that the high values occur during the summer season in both cases.

Another way to confirm this estimate, is to take a look at the Alqueva data in figures 40 and 52, we can see a peak at 01/08/2021, which also correspond to a high chlorophyll and TSM concentration, and CDOM absorption.

The Castelo de Bode dam, from the four dams, is the one that have lower absorption values, which leads to low concentration values. This is also confirmed by the visual analysis in Figure 55.

The Odelouca dam is the one that have higher CDOM absorption levels and when compared with the visual analysis, from Figure 57, we see that the possibility of a high CDOM concentration is very likely.

Figures 50, 51, 52 and 53 present a statistical analysis of CDOM concentration throughout the years, and figures 54, 55, 56 and 57, the visual representation of the selected season.

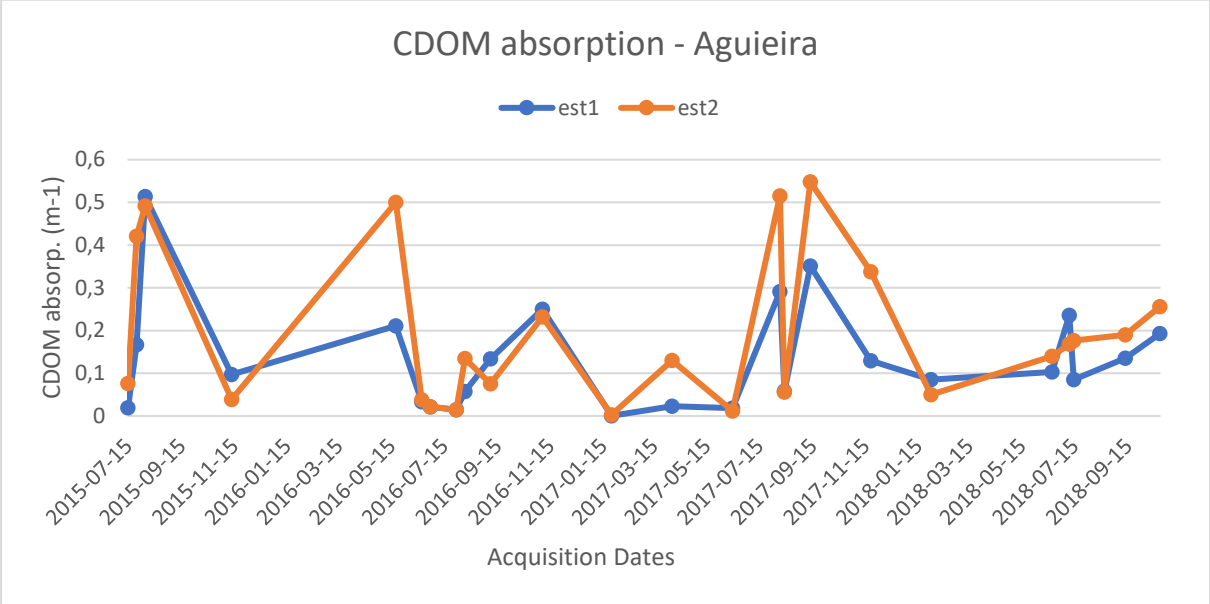

Figure 50 - Statistical analysis - CDOM absorption levels - Aguieiria Dam

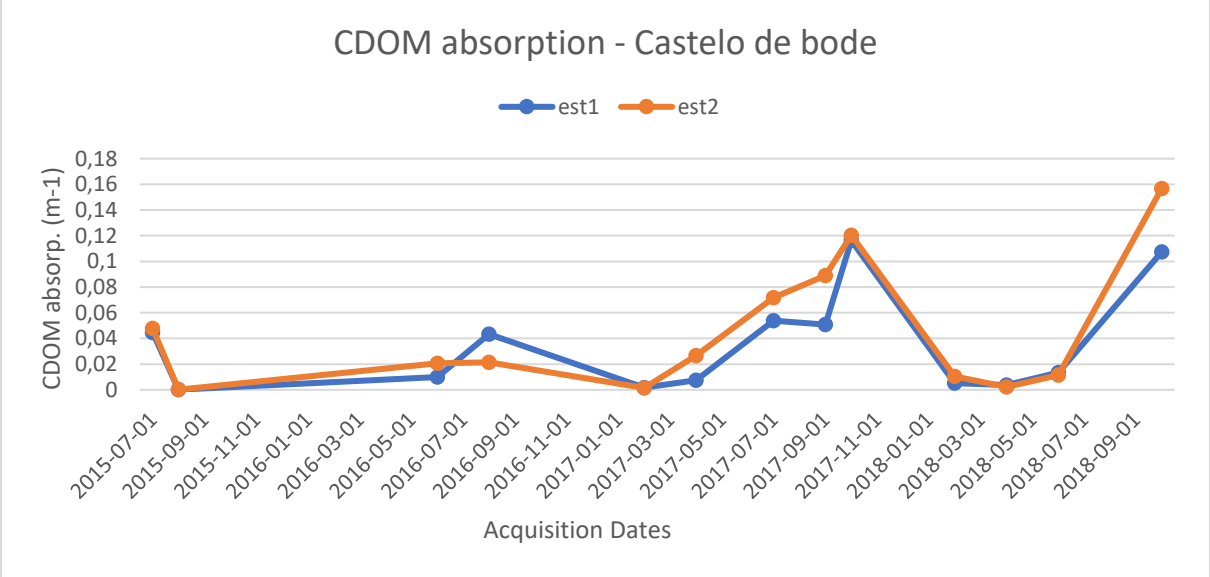

Figure 51 - Statistical analysis - CDOM absorption levels – Castelo de Bode Dam

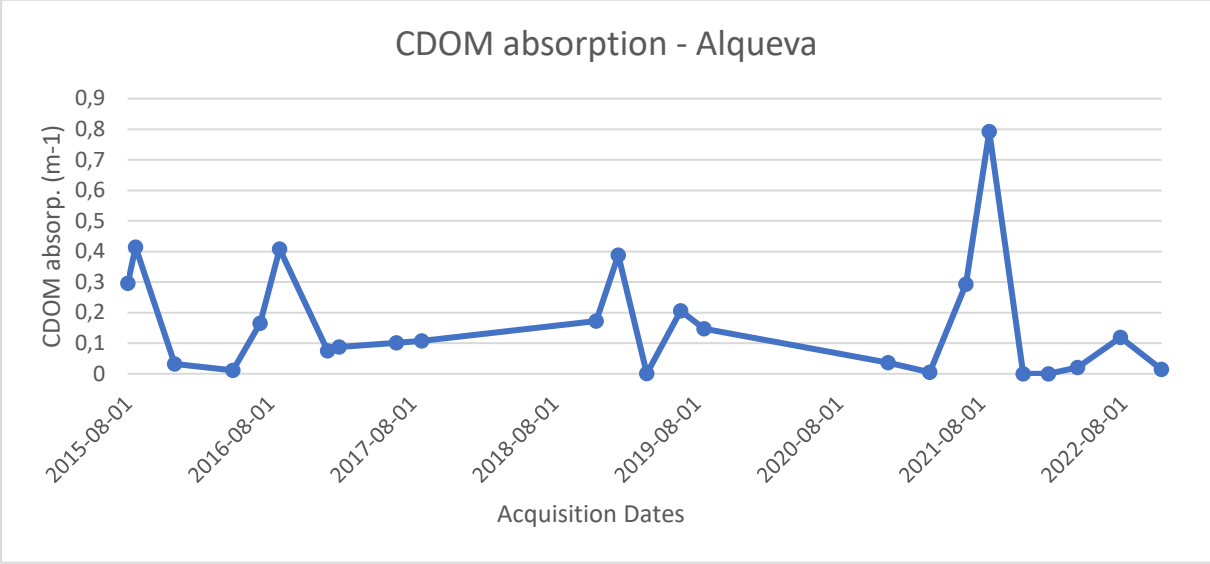

Figure 52 - Statistical analysis - CDOM absorption levels - Alqueva Dam

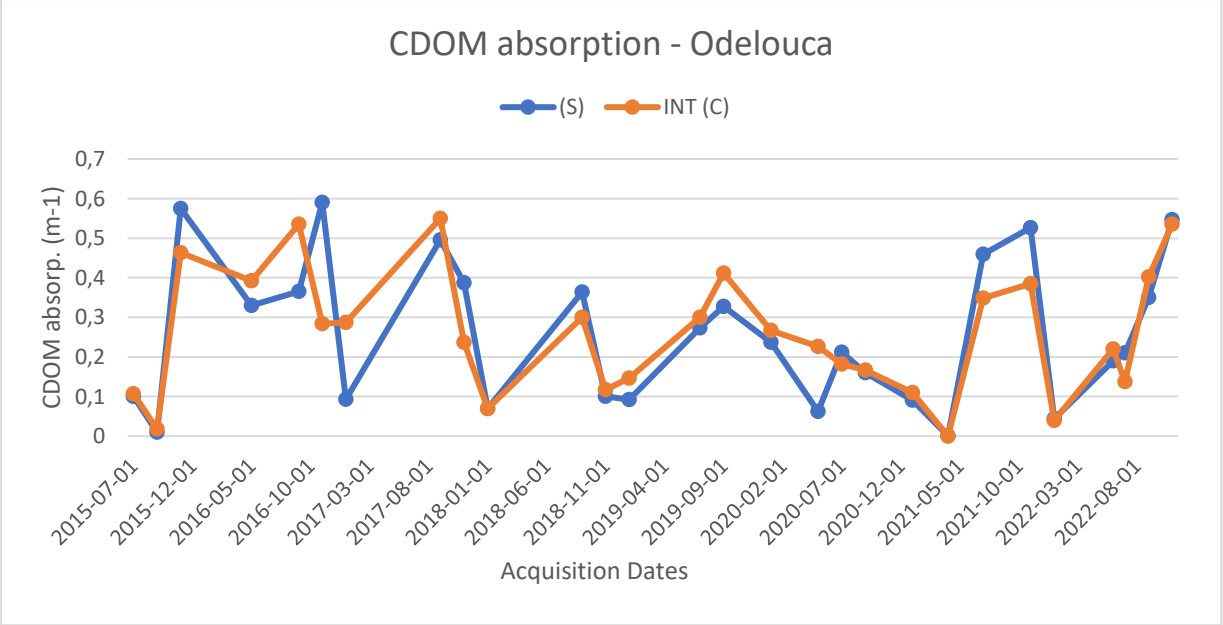

Figure 53 - Statistical analysis - CDOM absorption levels - Odelouca Dam

Similar to the chlorophyl and TSM concentrations, the CDOM absorption values are similar between *in situ* stations, following similar lines. In terms of values, as explained in the begin of sub-chapter 4.2.3.2, they present a similar trend as the previous metrics, having a higher value in the summer for the Aguieira, Castelo de Bode and Alqueva dam. For the Odelouca dam, we see a CDOM decrease between 2019 and 2020, and a comeback to typical values from 2021 onwards.

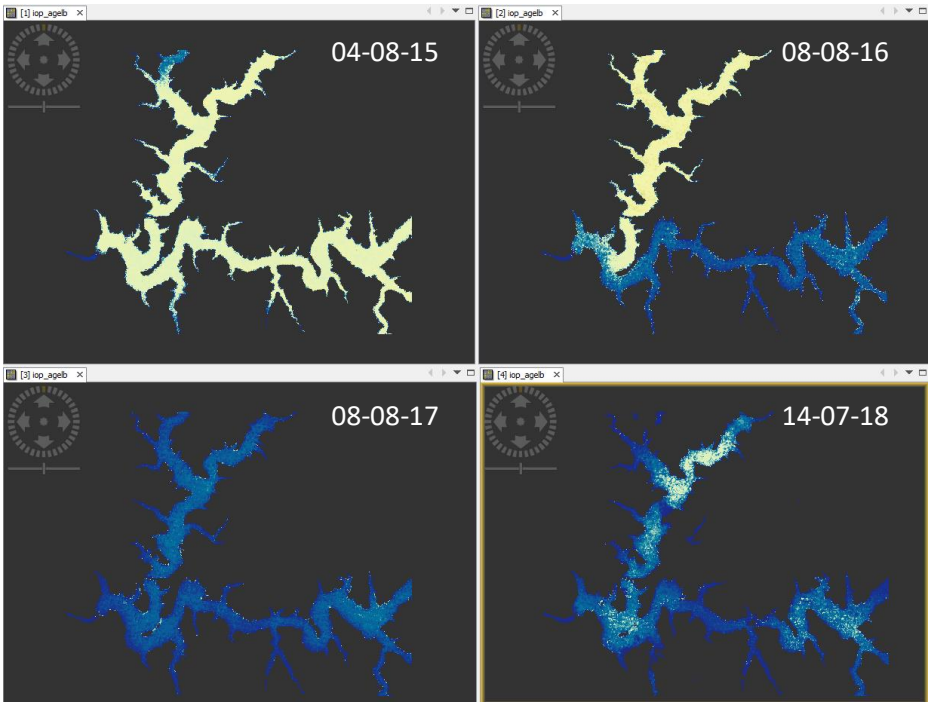

Figure 54 - Visual analysis - CDOM concentrations - Aguieira Dam

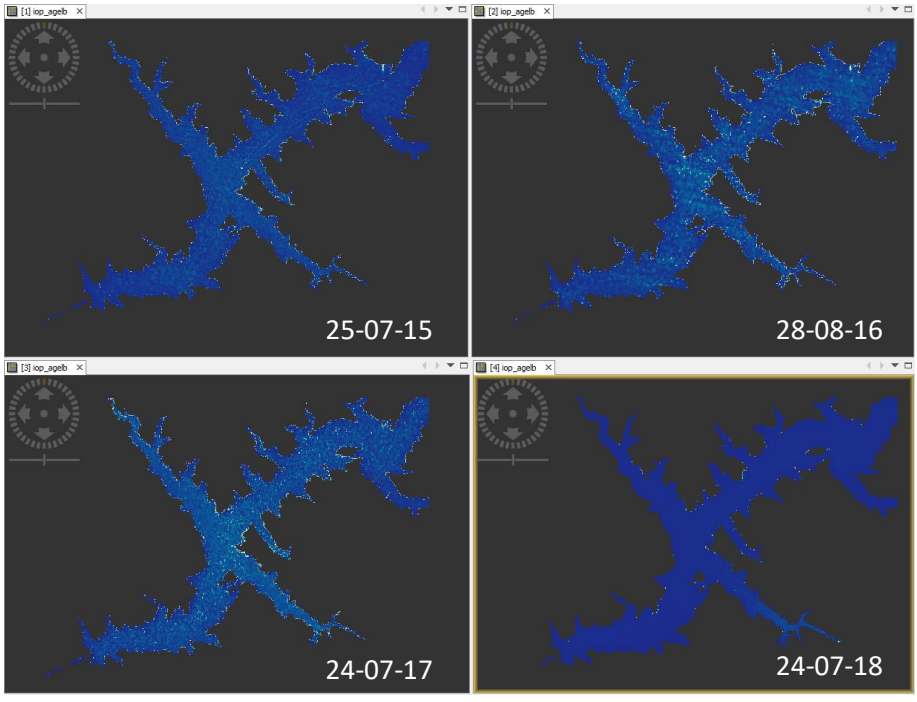

Figure 55 - Visual analysis - CDOM concentrations – Castelo de Bode Dam

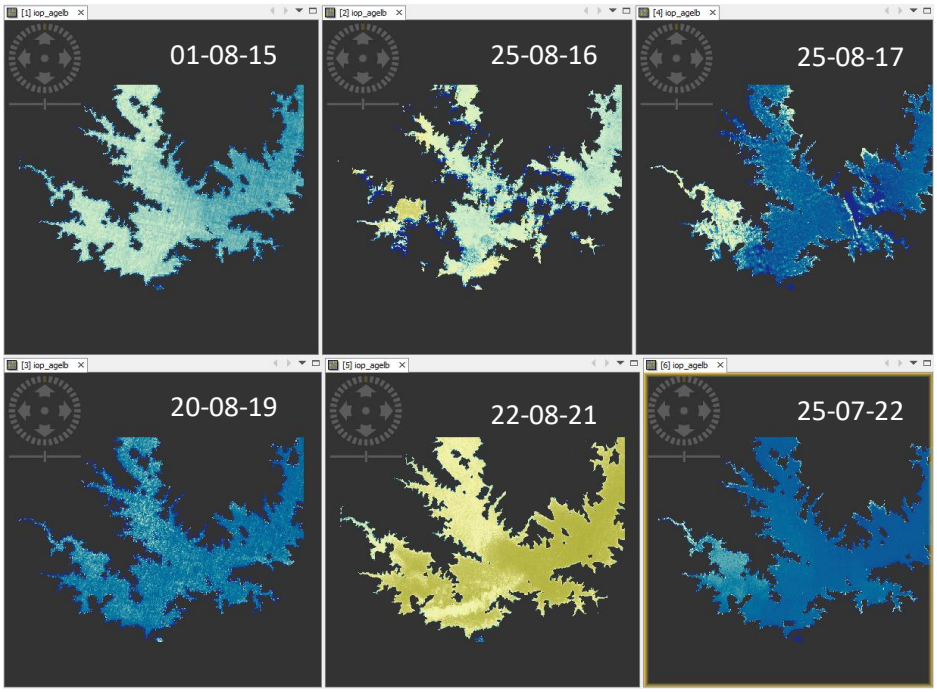

Figure 56 - Visual analysis - CDOM concentrations - Alqueva Dam

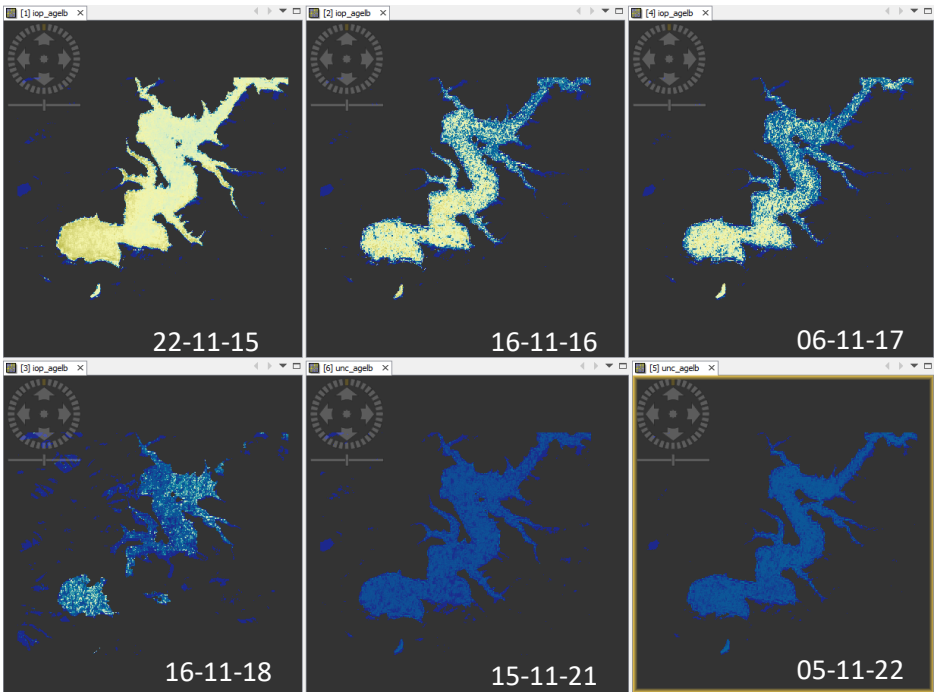

Figure 57 - Visual analysis - CDOM concentrations - Odelouca Dam

Visually, the only dam that doesn't present high CDOM absorption values is the Castelo de bode dam, having a measured maximum of 0.16, as seen in Figure 51. The others three dams have oscillating CDOM absorption values for the same period, as seen in the statistical analysis, and checked in the images above.

4.2.4 Water quantity evolution

The water quantity follows a simple mathematic approach and the results produced present its volume evolution throughout the last 12 years. Images 58, 59, 60 and 61 have the volume variance throughout the year.

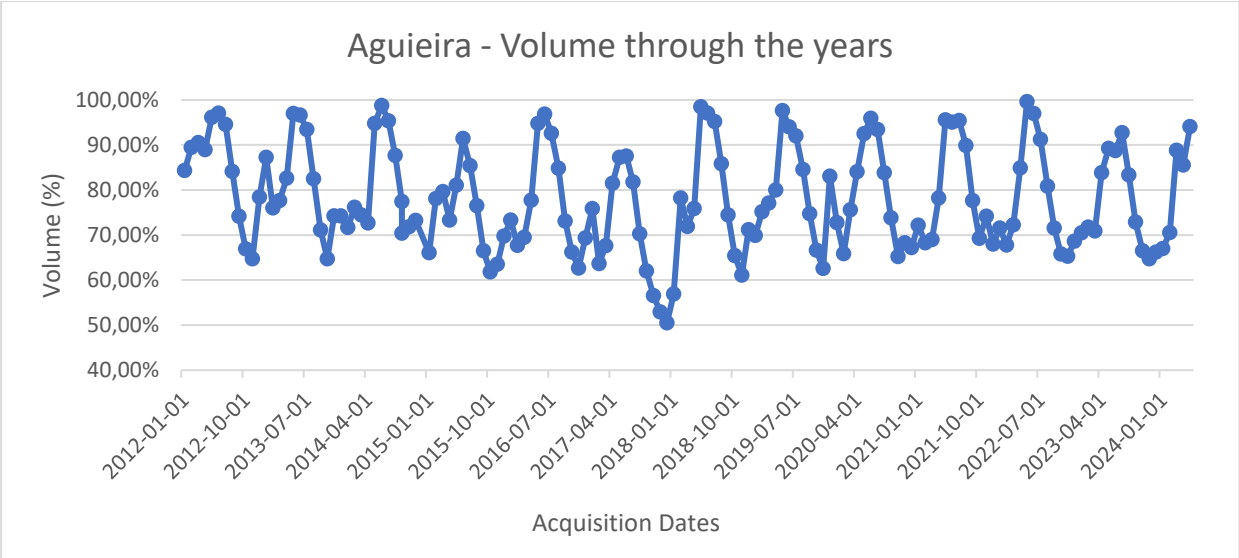

Figure 58 - Volume evolution - Aguieira Dam

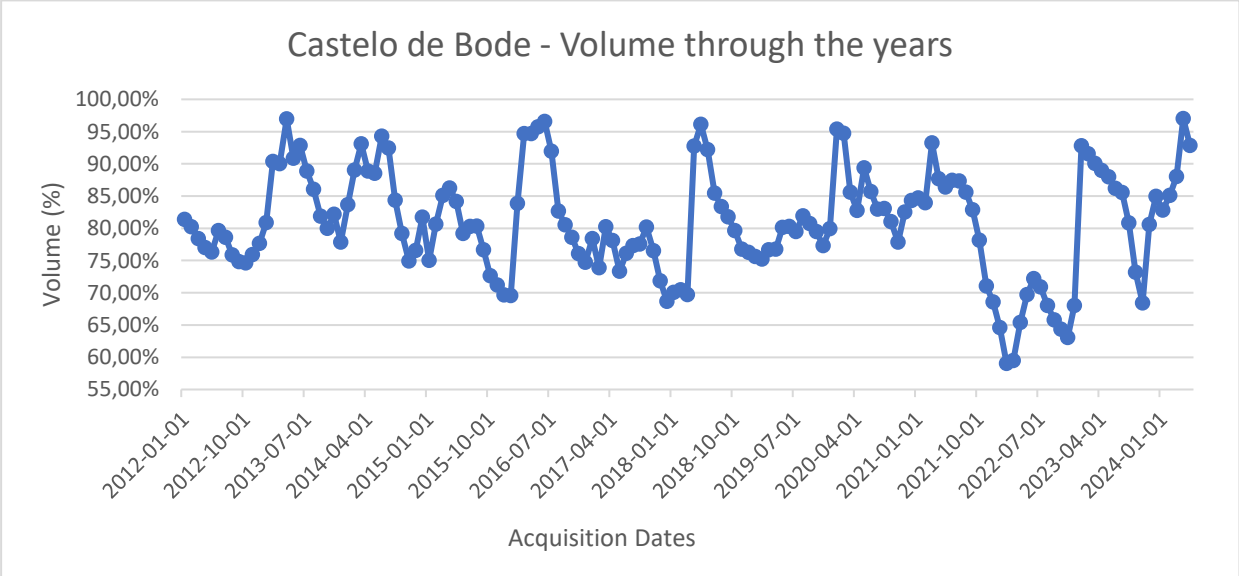

Figure 59 - Volume evolution - Castelo de Bode Dam

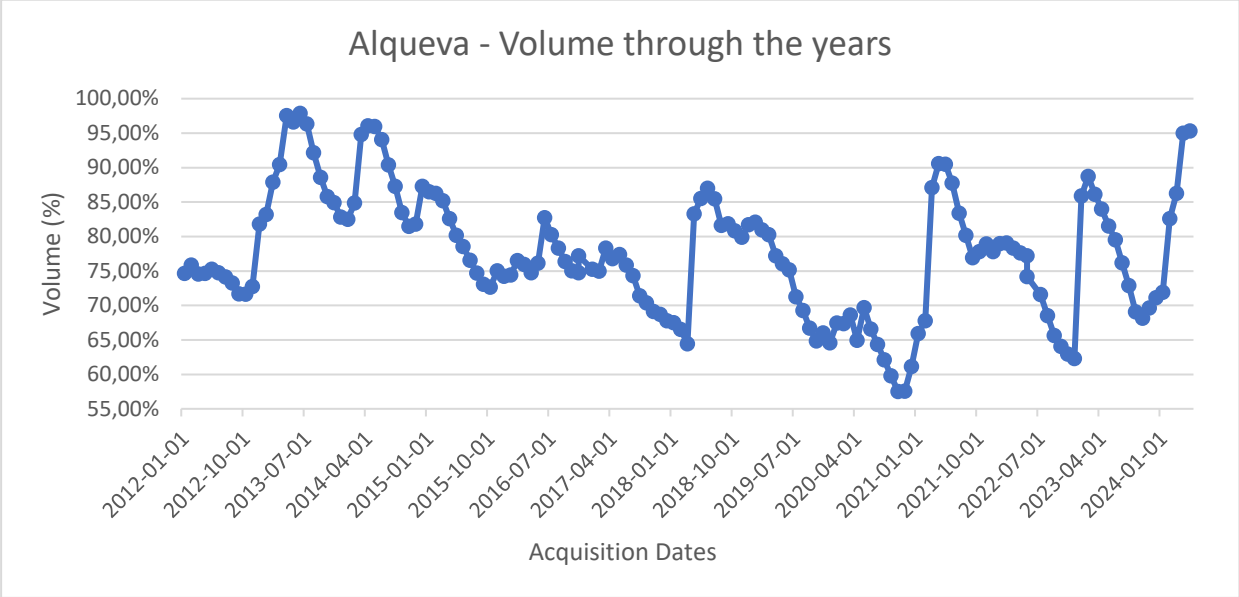

Figure 60 - Volume evolution - Alqueva Dam

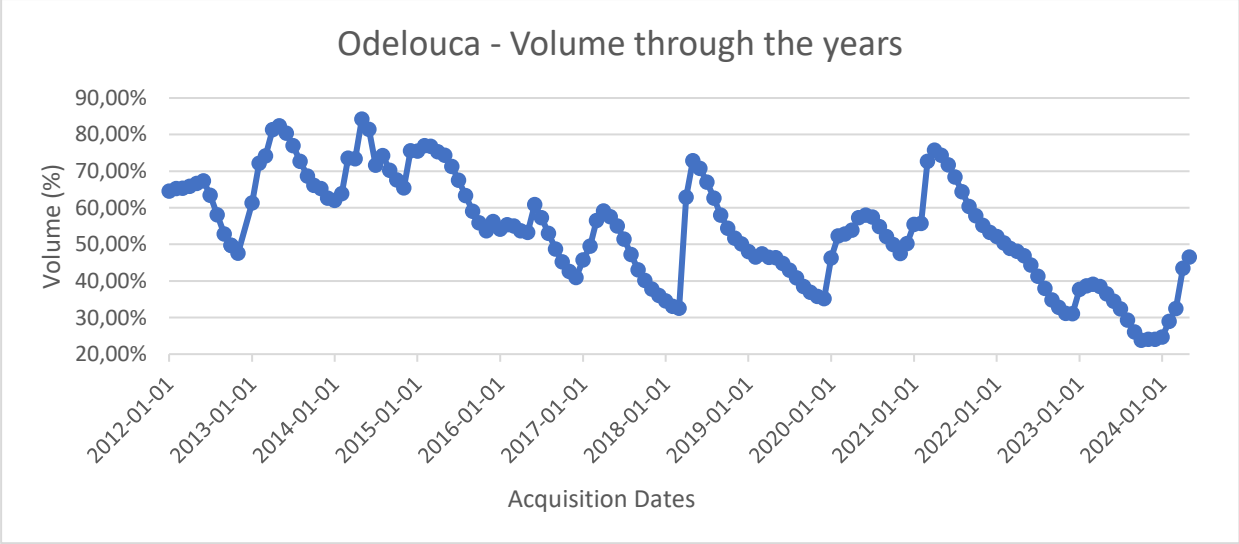

Figure 61 - Volume evolution - Odelouca Dam

As we can see from the images above the water volumes for the dams located at centre and north of Portugal are the ones that show a healthier volume through the years, even with some discrepancies. In the Aguieira dam, is possible to see a low value in January of 2018, which can be a result of the severe fire that occurred in October of 2017 and due to a drier winter. In the Castelo de Bode dam, a low value appears in January of 2022 corresponding to another drier winter combined with no water discharges from Spain.

At south of Portugal the drought is more severe, even though the Alqueva dam, currently, is at an all-time high, it shows a pattern of low values in the winter, due to dryer conditions and water

consumption needed by the local people for their own use, such as, self-consumption and use, garden irrigation, personal pools, or by local business such as local animal farms, golf courses and hotels.

The Odelouca dam shows the worse volume of the four dams, being in hotter region, its water resources are of extreme importance to the local population and local agriculture. The Algarve agriculture is mainly based on fruit crops, which need a lot of water. These factors combined with low precipitation, led to extreme drought scenarios and water limitations by the local authorities.

5

CONCLUSIONS

The main objectives of this work were the use of spaceborne sensors to estimate, chlorophyll, TSM and CDOM concentrations and water quantity evolution study.

The basic methodology was based on a training course from ESA. The only problem encountered was the difference between C2RCC versions, but showed to be irrelevant for the metrics concentrations, with low variability between versions.

An improvement was proposed in this thesis and applied to the four water dams, with a novel pixel validation formula that allowed to clean out shadow and burnt areas left by the default procedure. For its application five scripts were developed, 2 main ones, and two specifics for chlorophyll concentration extraction and one for TSM and CDOM concentrations extraction.

This new approach takes advantage of the chlorophyl absorption peaks. Using the band 3 and 8, instead of only the band 8 as set by default in the C2RCC processor, it increases the images quality, cleaning false water body pixels, such as shadows and burnt ground. This image quality improvement helps in the visual analysis, since the water body is better highlighted.

After the scripts ran, the statistical analysis for each metric were produced.

It's possible to conclude that the Portuguese water in these four dams is of a high quality, having low chlorophyll, TSM and CDOM concentrations throughout the years accessible to study.

In terms of water quantity, the analysis consisted in *in situ* data and showed that the dams in the north and centre showed a healthy volume, and the south dams, showed the impact of the last years droughts and extreme weather.

With this analysis, it's possible to retrieve other conclusions as well.

In terms of data continuity and availability, the *in situ* measures vary to much from dam to dam and year to year, having year with many samples and other with very few.

The satellite images have a major disadvantage, since we were working with optical sensors, days that are not cloud free on top of the dam, were not viable and lead to data loss.

These factors can lead to errors in the linear regressions performed for the empirical models, and models with a higher error rate.

The chlorophyl variability can also cause errors. If the *in situ* time measures differ to much from the satellite images retrieval, will also impact the linear regression and lead to less accurate predicaments.

Another factor that can impact is the distance between *in situ* stations for air quality and the water dams. This can lead to incorrect values used for the C2RCC processor, and result in incorrect metric values.

For future work different approaches could be implemented, such as the use of SAR, process automation and increase in *in situ* stations or the re-location of existing ones.

The use of SAR and neural networks to help the metric retrieval under bad weather, such as seen in [19] and [20], where the use of SAR is proposed and implemented but with both papers arriving to the conclusion that in order for this solution to work, optical imagery would still be need to train the neural network and to complement the data, or to find a better way to distinguish between the several factors that cause the same dark spots on the region of interest.

Even though the process is automated, visual analysis is still needed and manual refinement is still necessary. One possible solution is to have a control zone that would mitigate the need of visual analysis and would adjust the margin for the pixel validation expression, if necessary.

Another way to implement and automated process could be via neural networks, trained to filter only the water body and dispose land pixel values.

For TSM and CDOM measures, with *in situ* stations close to the middle of the water body the obtained results will be less accurate than the ones close to the edge. This happens because TSM and CDOM are more prone to develop in still water with low depth. To extract more accurate values from the satellite images, a perimeter shape file or a sections shapefile around the dam should be considered. This way the edge values could be extracted and compared with *in situ* and centre values.

Lastly, there could be a physical improvement, with the addition of new in situ stations or the re-location of existing ones to more troubled areas that needed extra oversight.

BIBLIOGRAPHY

[1] H. Yang, J. Kong, H. Hu, Y. Du, M. Gao, and F. Chen, 'A Review of Remote Sensing for Water Quality Retrieval: Progress and Challenges', *Remote Sens (Basel)*, vol. 14, no. 8, 2022, doi: 10.3390/rs14081770.

[2] D. R. Green, J. J. Hagon, C. Gómez, and B. J. Gregory, 'Chapter 21 - Using Low-Cost UAVs for Environmental Monitoring, Mapping, and Modelling: Examples From the Coastal Zone', in *Coastal Management*, R. R. Krishnamurthy, M. P. Jonathan, S. Srinivasalu, and B. Glaeser, Eds., Academic Press, 2019, pp. 465–501. doi: https://doi.org/10.1016/B978-0-12-810473-6.00022-4.

[3] Q. Xiao, Y. Li, F. Luo, and H. Liu, 'Analysis and assessment of risks to public safety from unmanned aerial vehicles using fault tree analysis and Bayesian network', *Technol Soc*, vol. 73, p. 102229, 2023, doi: https://doi.org/10.1016/j.techsoc.2023.102229.

[4] H. R. Gordon, O. B. Brown, and M. M. Jacobs, 'Computed relationships between the inherent and apparent optical properties of a flat homogeneous ocean.', *Appl Opt*, vol. 14 2, pp. 417–27, 1975, [Online]. Available: https://api.semanticscholar.org/CorpusID:36400967

[5] S. C. J. Palmer, T. Kutser, and P. D. Hunter, 'Remote sensing of inland waters: Challenges, progress and future directions', *Remote Sens Environ*, vol. 157, pp. 1–8, 2015, doi: https://doi.org/10.1016/j.rse.2014.09.021.

[6] C. F. Le, Y. M. Li, Y. Zha, D. Sun, and B. Yin, 'Validation of a Quasi-Analytical Algorithm for Highly Turbid Eutrophic Water of Meiliang Bay in Taihu Lake, China', *IEEE Transactions on Geoscience and Remote Sensing*, vol. 47, no. 8, pp. 2492–2500, 2009, doi: 10.1109/TGRS.2009.2015658.

[7] P. D. Hunter, A. N. Tyler, L. Carvalho, G. A. Codd, and S. C. Maberly, 'Hyperspectral remote sensing of cyanobacterial pigments as indicators for cell populations and toxins in eutrophic lakes', *Remote Sens Environ*, vol. 114, no. 11, pp. 2705–2718, 2010, doi: https://doi.org/10.1016/j.rse.2010.06.006.

[8] L. Zhou, D. A. Roberts, W. Ma, H. Zhang, and L. Tang, 'Estimation of higher chlorophylla concentrations using field spectral measurement and HJ-1A hyperspectral satellite data in Dianshan Lake, China', *ISPRS Journal of Photogrammetry and Remote Sensing*, vol. 88, pp. 41–47, 2014, doi: https://doi.org/10.1016/j.isprsjprs.2013.11.016.

[9] R. H. Becker *et al.*, 'Unmanned aerial system based spectroradiometer for monitoring harmful algal blooms: A new paradigm in water quality monitoring', *J Great Lakes Res*, vol. 45, no. 3, pp. 444–453, Jun. 2019, doi: 10.1016/J.JGLR.2019.03.006.

[10] Y. Chebud, G. M. Naja, R. G. Rivero, and A. M. Melesse, 'Water Quality Monitoring Using Remote Sensing and an Artificial Neural Network', *Water Air Soil Pollut*, vol. 223, no. 8, pp. 4875–4887, 2012, doi: 10.1007/s11270-012-1243-0.

[11] ESA, 'Europe's eyes on Earth: the EU's Copernicus Programme', Sentiwiki copernicus. Accessed: Jan. 22, 2024. [Online]. Available: https://sentiwiki.copernicus.eu/web/copernicus-programme

[12] J.-N. Thépaut, D. Dee, R. Engelen, and B. Pinty, 'The Copernicus Programme and its Climate Change Service', in *IGARSS 2018 - 2018 IEEE International Geoscience and Remote Sensing Symposium*, 2018, pp. 1591–1593. doi: 10.1109/IGARSS.2018.8518067.

[13] T. Rodrigues and P. Marques, 'Oil slick monitoring using Sentinel-I SAR images', Jan. 2021, pp. 1–8. doi: 10.23919/IRS51887.2021.9466231.

[14] D. Domingos, M. Gama, and P. Marques, 'Wildfire monitoring in Portugal using Sentinel-2', in *2023 3rd International Conference on Electrical, Computer, Communications and Mechatronics Engineering (ICECCME)*, 2023, pp. 1–4. doi: 10.1109/ICECCME57830.2023.10252320.

[15] ESA, 'Sentinel Missions Overview', Sentinel Copernincus. Accessed: Jan. 22, 2024. [Online]. Available: https://sentinels.copernicus.eu/web/sentinel/missions

[16] ESA, 'Overview of Sentinel-1 Mission', Sentinel Copernincus. Accessed: May 26, 2024. [Online]. Available: https://sentiwiki.copernicus.eu/web/s1-mission

[17] S. Maleki, V. Rahdari, and A. Soffianain, 'Drought impact detection on wetlands in the arid area using Synthetic Aperture Radar data', *Arabian Journal of Geosciences*, vol. 15, no. 9, p. 919, 2022, doi: 10.1007/s12517-022-10171-w.

[18] T. Berezowski, T. Bieliński, and J. Osowicki, 'Flooding Extent Mapping for Synthetic Aperture Radar Time Series Using River Gauge Observations', *IEEE J Sel Top Appl Earth Obs Remote Sens*, vol. 13, pp. 2626–2638, 2020, doi: 10.1109/JSTARS.2020.2995888.

[19] R. Westerhoff, M. Kleuskens, H. Winsemius, H. Huizinga, and R. Brakenridge, 'Automated global water mapping based on wide-swath orbital synthetic aperture radar', *Hydrology and Earth System Sciences Discussions*, vol. 9, May 2012, doi: 10.5194/hessd-9-7801-2012.

[20] G. Wang, J. Li, B. Zhang, Q. Shen, and F. Zhang, 'Monitoring cyanobacteria-dominant algal blooms in eutrophicated Taihu Lake in China with synthetic aperture radar images', *Chinese Journal of Oceanology and Limnology*, vol. 33, no. 1, pp. 139–148, 2015, doi: 10.1007/s00343-015-4019-8.

[21] ESA, 'SENTINEL-2 MISSION GUIDE', Sentinel Copernincus. Accessed: Jan. 22, 2024. [Online]. Available: https://sentinel.esa.int/web/sentinel/missions/sentinel-2

[22] A. Van Dijk, 'RS1.3 - Remote sensing: how does it work?', Water and Landscape Dynamics group, The Australian National University. Accessed: Jan. 23, 2024. [Online]. Available: https://www.youtube.com/watch?app=desktop&v=eFJs_edUWKs&ab_channel=ANUCentreforWaterandLandscapeDynamics

[23] G. Sent *et al.*, 'Deriving Water Quality Parameters Using Sentinel-2 Imagery: A Case Study in the Sado Estuary, Portugal', *Remote Sens (Basel)*, vol. 13, no. 5, 2021, doi: 10.3390/rs13051043.

[24] M. Potes *et al.*, 'Use of Sentinel 2 – MSI for water quality monitoring at Alqueva reservoir, Portugal', *Proceedings of the International Association of Hydrological Sciences*, vol. 380, pp. 73–79, 2018, doi: 10.5194/piahs-380-73-2018.

[25] A. Germán *et al.*, 'Space-time monitoring of water quality in an eutrophic reservoir using SENTINEL-2 data - A case study of San Roque, Argentina', *Remote Sens Appl*, vol. 24, p. 100614, 2021, doi: https://doi.org/10.1016/j.rsase.2021.100614.

[26] M. Viso-Vázquez, C. Acuña-Alonso, J. L. Rodríguez, and X. Álvarez, 'Remote Detection of Cyanobacterial Blooms and Chlorophyll-a Analysis in a Eutrophic Reservoir Using Sentinel-2', *Sustainability*, vol. 13, no. 15, 2021, doi: 10.3390/su13158570.

[27] K. Toming, T. Kutser, A. Laas, M. Sepp, B. Paavel, and T. Nõges, 'First Experiences in Mapping Lake Water Quality Parameters with Sentinel-2 MSI Imagery', *Remote Sens (Basel)*, vol. 8, no. 8, 2016, doi: 10.3390/rs8080640.

[28] I. Caballero and G. Navarro, 'Monitoring cyanoHABs and water quality in Laguna Lake (Philippines) with Sentinel-2 satellites during the 2020 Pacific typhoon season', *Science of The Total Environment*, vol. 788, p. 147700, 2021, doi: https://doi.org/10.1016/j.scitotenv.2021.147700.

[29] T. Mucheye, S. Haro, S. Papaspyrou, and I. Caballero, 'Water Quality and Water Hyacinth Monitoring with the Sentinel-2A/B Satellites in Lake Tana (Ethiopia)', *Remote Sens (Basel)*, vol. 14, no. 19, 2022, doi: 10.3390/rs14194921.

[30] ESA, 'Sentinel-3 Overview', Sentinel Copernincus. Accessed: Jan. 22, 2024. [Online]. Available: https://sentinel.esa.int/web/sentinel/missions/sentinel-3/overview

[31] ESA, 'Sentinel 3 - Maritime Monitoring', Sentinel Copernicus. Accessed: Jan. 22, 2024. [Online]. Available: https://sentinels.copernicus.eu/web/sentinel/user-guides/sentinel-3-olci/applications/maritime-monitoring

[32] G. Rodrigues, M. Potes, A. M. Penha, M. J. Costa, and M. M. Morais, 'The Use of Sentinel-3/OLCI for Monitoring the Water Quality and Optical Water Types in the Largest Portuguese Reservoir', *Remote Sens (Basel)*, vol. 14, no. 9, 2022, doi: 10.3390/rs14092172.

[33] K. Blix, K. Pálffy, V. R. Tóth, and T. Eltoft, 'Remote Sensing of Water Quality Parameters over Lake Balaton by Using Sentinel-3 OLCI', *Water (Basel)*, vol. 10, no. 10, 2018, doi: 10.3390/w10101428.

[34] L. Alparone, A. Arienzo, and A. Garzelli, 'Spatial Resolution Enhancement of Vegetation Indexes via Fusion of Hyperspectral and Multispectral Satellite Data', *Remote Sens (Basel)*, vol. 16, no. 5, 2024, doi: 10.3390/rs16050875.

[35] ESA, 'Copernicus RUS Training Materials: Videos, Theory and Practical materials', eo science for society, ESA. Accessed: Jan. 24, 2024. [Online]. Available: https://eo4society.esa.int/resources/copernicus-rus-training-materials/

[36] A. Ansper and K. Alikas, 'Retrieval of Chlorophyll a from Sentinel-2 MSI Data for the European Union Water Framework Directive Reporting Purposes', *Remote Sens (Basel)*, vol. 11, no. 1, 2019, doi: 10.3390/rs11010064.

[37] M. A. Warren *et al.*, 'Assessment of atmospheric correction algorithms for the Sentinel-2A MultiSpectral Imager over coastal and inland waters', *Remote Sens Environ*, vol. 225, pp. 267–289, May 2019, doi: 10.1016/J.RSE.2019.03.018.

[38] Britannica and The Editors of Encyclopaedia, 'chlorophyll', Encyclopedia Britannica. Accessed: Jan. 22, 2024. [Online]. Available: https://www.britannica.com/science/chlorophyll

[39] J. Van Deusen, 'SDG 14 and Life Below Water: What Space Can Tell Us about the Slimy Stuff at the Beach', Esri. Accessed: Jan. 23, 2024. [Online]. Available: https://www.esri.com/en-us/industries/blog/articles/sdg-14-and-life-below-water-what-space-can-tell-us-about-the-slimy-stuff-at-the-beach/

[40] NOOA CoastWatch East Coast Regional Node, 'OLCI Total Suspended Matter (TSM)', NOOA CoastWatch. Accessed: Jan. 23, 2024. [Online]. Available: https://eastcoast.coastwatch.noaa.gov/cw_olci_tsmnn.php

[41] C. Giardino *et al.*, 'Imaging Spectrometry of Inland and Coastal Waters: State of the Art, Achievements and Perspectives', *Surv Geophys*, vol. 40, no. 3, pp. 401–429, 2019, doi: 10.1007/s10712-018-9476-0.

[42] E. Atkin, 'How can I measure Turbidity?', Camlab, Cambridge, United Kingdom. Accessed: Jan. 23, 2024. [Online]. Available: https://camblab.info/how-can-i-measure-turbidity/

[43] World Health Organization, 'Water quality and health: Review of turbidity: Information for Regulators and Water Suppliers', Feb. 2017. Accessed: Jan. 23, 2024. [Online]. Available: https://www.who.int/publications/i/item/WHO-FWC-WSH-17.01

[44] F. Braga, G. M. Scarpa, V. E. Brando, G. Manfè, and L. Zaggia, 'COVID-19 lockdown measures reveal human impact on water transparency in the Venice Lagoon', *Science of The Total Environment*, vol. 736, p. 139612, 2020, doi: https://doi.org/10.1016/j.scitotenv.2020.139612.

[45] A. Tuzcu Kokal, I. Ismailoglu, N. Musaoglu, and A. Tanik, 'Detection of surface temperature anomaly of the Sea of Marmara', *Advances in Space Research*, vol. 71, no. 7, pp. 2996–3004, 2023, doi: https://doi.org/10.1016/j.asr.2022.10.055.

[46] R. Handcock *et al.*, 'Thermal Infrared Remote Sensing of Water Temperature in Riverine Landscapes', in *Fluvial Remote Sensing for Science and Management*, 2012, pp. 85–113. doi: 10.1002/9781119940791.ch5.

[47] Y. Y. Adusei, J. Quaye-Ballard, A. A. Adjaottor, and A. A. Mensah, 'Spatial prediction and mapping of water quality of Owabi reservoir from satellite imageries and machine learning

models', *The Egyptian Journal of Remote Sensing and Space Science*, vol. 24, no. 3, Part 2, pp. 825–833, 2021, doi: https://doi.org/10.1016/j.ejrs.2021.06.006.

[48] J. Li, J. Wang, Y. Wu, Y. Cui, and S. Yan, 'Remote sensing monitoring of total nitrogen and total phosphorus concentrations in the water around Chaohu Lake based on geographical division', *Front Environ Sci*, vol. 10, p. 1014155, Jan. 2022, doi: 10.3389/fenvs.2022.1014155.

[49] K. P. Dandge and S. S. Patil, 'Spatial distribution of ground water quality index using remote sensing and GIS techniques', *Appl Water Sci*, vol. 12, no. 1, p. 7, 2021, doi: 10.1007/s13201-021-01546-7.

[50] O. J. R. Pereira *et al.*, 'Estimating Water pH Using Cloud-Based Landsat Images for a New Classification of the Nhecolândia Lakes (Brazilian Pantanal)', *Remote Sens (Basel)*, vol. 12, no. 7, 2020, doi: 10.3390/rs12071090.

[51] Z. Al-Janabi, A. H. Al Obaidy, and F. Hassan, 'A brief review of water quality indices and their applications', in *IOP Conference Series: Earth and Environmental Science*, Jan. 2021. doi: 10.1088/1755-1315/779/1/012088.

[52] T. Kutser *et al.*, 'Remote Sensing of Black Lakes and Using 810 nm Reflectance Peak for Retrieving Water Quality Parameters of Optically Complex Waters', *Remote Sens (Basel)*, vol. 8, no. 6, 2016, doi: 10.3390/rs8060497.

[53] Y. Umamaheswara Rao, P. V Nagamani, N. K. Baranval, P. Rama Rao, T. D. V Prasada Rao, and S. B. Choudury, 'Detection of Phytoplankton Blooms in the Turbid Coastal Waters Using Satellite-Derived Fluorescence Line Height off Kakinada Coast', *Journal of the Indian Society of Remote Sensing*, vol. 47, no. 11, pp. 1857–1864, 2019, doi: 10.1007/s12524-019-01022-5.

[54] ARSET, 'LEARN TO USE EARTH OBSERVATIONS: Training', NASA Applied Sciences. Accessed: Jan. 24, 2024. [Online]. Available: https://appliedsciences.nasa.gov/get-involved/training

[55] T. Šmejkalová, 'RUS webinar: Freshwater Quality Monitoring with Sentinel-2', eo science for society.

[56] A. Mehta, S. McCartney, B. Seegers, and B. Schaeffer, 'ARSET - Monitoring Water Quality of Inland Lakes using Remote Sensing', ARSET. Accessed: Jan. 24, 2024. [Online]. Available: https://appliedsciences.nasa.gov/get-involved/training/english/arset-monitoring-water-quality-inland-lakes-using-remote-sensing

[57] ESA, 'SNAP', STEP - Scientific Toolbox Exploitation Platform. Accessed: Jan. 24, 2024. [Online]. Available: https://step.esa.int/main/toolboxes/snap/

[58] QGIS, 'QGIS - The Leading Open Source Desktop GIS', QGIS. Accessed: Jan. 24, 2024. [Online]. Available: https://qgis.org/en/site/about/index.html

[59] Google, 'A planetary-scale platform for Earth science data & analysis', Google Earth Engine. Accessed: Jan. 24, 2024. [Online]. Available: https://earthengine.google.com/faq/

[60] Earth Science Applied Sciences, ‘CyAN: Cyanobacteria Assessment Network’, NASA. Accessed: Jan. 24, 2024. [Online]. Available: https://appliedsciences.nasa.gov/what-we-do/projects/cyan-cyanobacteria-assessment-network

[61] J. Everaerts, H. Erdem, and J. Dries, ‘Accessing EO Data Using Terrascope Platform’, eo4geo. Accessed: Jan. 24, 2024. [Online]. Available: http://www.eo4geo.eu/training/accessing-eo-data-using-terrascope-platform/

[62] Agência Portuguesa do Ambiente, ‘Barragem da Aguieira’. Accessed: May 27, 2024. [Online]. Available: https://cnpgb.apambiente.pt/gr_barragens/gbportugal/Aguieira.htm

[63] EDP, ‘Barragem de Castelo de Bode’. Accessed: May 27, 2024. [Online]. Available: https://portugal.edp.com/pt-pt/edp-portugal/central-hidroeletrica-de-castelo-de-bode

[64] LUSA, ‘Barragem de Alqueva a menos de um metro de atingir a cota máxima’, 2024. Accessed: May 27, 2024. [Online]. Available: https://expresso.pt/sociedade/2024-04-01-Barragem-de-Alqueva-a-menos-de-um-metro-de-atingir-a-cota-maxima-dfdaa9f9

[65] Águas de Portugal, ‘Barragem da Odelouca’. Accessed: May 27, 2024. [Online]. Available: https://www.adp.pt/pt//?id=61&img=3&bl=2

[66] C. Brockmann *et al.*, ‘Evolution of the C2RCC Neural Network for Sentinel 2 and 3 for the Retrieval of Ocean Colour Products in Normal and Extreme Optically Complex Waters’, 2016. [Online]. Available: https://api.semanticscholar.org/CorpusID:199496625

[67] ESA - European Space Agency, ‘SNAP - Feature Highlights’, European Space Agency. Accessed: Jun. 08, 2024. [Online]. Available: https://step.esa.int/main/toolboxes/snap/

[68] L. Sá *et al.*, ‘Portable and Low-Cost Fluorometer for Phytoplankton Monitoring’, May 2023, pp. 96–99. doi: 10.1109/ENBENG58165.2023.10175351.

APPENDIX

Appendix A – Acquisition dates

Table 6 - Dates for the Aguieira Dam

Aguieira dam		
***In situ* measures**	**Satellite images**	**Difference**
2015-07-07	2015-07-15	8
2015-07-07	2015-07-25	18
2015-08-04	2015-08-04	0
2015-11-09	2015-11-12	3
2016-05-24	2016-05-20	-4
2016-06-28	2016-06-19	-9
2016-06-28	2016-06-29	1
2016-08-02	2016-07-29	-4
2016-08-02	2016-08-08	6
2016-09-06	2016-09-07	1
2016-11-08	2016-11-06	-2
2017-01-30	2017-01-25	-5
2017-03-28	2017-04-05	8
2017-06-19	2017-06-14	-5
2017-08-08	2017-08-08	0
2017-08-08	2017-08-13	5
2017-09-12	2017-09-12	0
2017-11-21	2017-11-21	0
2018-01-30	2018-01-30	0
2018-06-19	2018-06-19	0
2018-07-11	2018-07-09	-2
2018-07-11	2018-07-14	3
2018-09-12	2018-09-12	0
2018-10-23	2018-10-22	-1

Table 7 - Dates for the Castelo de Bode Dam

Castelo de Bode		
***In situ* mesaures**	**Satellite images**	**Difference**
2015-07-27	2015-07-25	-2
2015-08-24	2015-08-24	0
2016-06-22	2016-06-19	-3
2016-08-31	2016-08-28	-3
2017-02-21	2017-02-24	3
2017-04-18	2017-04-15	-3
2017-07-24	2017-07-24	0
2017-08-29	2017-09-02	4
2017-10-24	2017-10-22	-2
2018-02-26	2018-02-24	-2
2018-04-18	2018-04-25	7
2018-06-27	2018-06-24	-3
2018-08-29	2018-09-02	4
2018-10-10	2018-10-07	-3

Table 8 - Dates for the Alqueva Dam

Alqueva		
***In situ* mesaures**	**Satellite images**	**Difference**
2015-07-31	2015-08-01	1
2015-08-24	2015-08-21	-3
2015-11-26	2015-11-29	3
2016-04-27	2016-04-27	0
2016-07-05	2016-07-06	1
2016-08-26	2016-08-25	-1
2016-12-28	2016-12-26	-2
2017-01-24	2017-01-25	1
2017-06-21	2017-06-21	0
2017-08-24	2017-08-25	1
2018-11-13	2018-11-16	3
2019-01-15	2019-01-12	-3
2019-03-26	2019-03-26	0
2019-06-24	2019-06-21	-3
2019-08-20	2019-08-20	0
2020-12-02	2020-12-05	3
2021-03-23	2021-03-22	-1
2021-06-21	2021-06-23	2
2021-08-23	2021-08-22	-1
2021-11-17	2021-11-17	0
2022-01-24	2022-01-21	-3
2022-04-04	2022-04-06	2
2022-07-25	2022-07-25	0
2022-11-07	2022-11-07	0

Table 9 - Dates for the Odelouca Dam

Odelouca		
***In situ* mesaures**	**Satellite images**	**Difference**
2015-07-14	2015-07-15	1
2015-09-08	2015-09-03	-5
2015-11-17	2015-11-22	5
2016-05-16	2016-05-20	4
2016-07-21	2016-07-19	-2
2016-09-15	2016-09-17	2
2016-11-08	2016-11-16	8
2017-01-17	2017-01-15	-2
2017-06-08	2017-06-04	-4
2017-09-11	2017-09-12	1
2017-11-08	2017-11-06	-2
2018-01-08	2018-01-10	2
2018-06-11	2018-06-14	3
2018-09-10	2018-09-12	2
2018-11-19	2018-11-16	-3
2019-01-28	2019-01-25	-3
2019-07-15	2019-07-14	-1
2019-09-16	2019-09-17	1
2020-01-13	2020-01-10	-3
2020-05-25	2020-05-24	-1
2020-07-13	2020-07-13	0
2020-09-21	2020-09-21	0
2021-01-15	2021-01-14	-1
2021-04-05	2021-04-04	-1
2021-07-05	2021-07-08	3
2021-09-06	2021-09-06	0
2021-11-15	2021-11-15	0
2022-01-31	2022-01-29	-2
2022-06-06	2022-06-08	2
2022-07-04	2022-07-08	4
2022-09-05	2022-09-06	1
2022-11-07	2022-11-05	-2

Appendix B – Chlorophyl concentrations values

Table 10 - Chlorophyl concentrations for MCI and BandRatio - Aguieira Dam

Date	MCI est1	R705_R655 est1	*In situ* est1	MCI est2	R705_R655 est2	*In situ* est2
2015-07-15	1,453668475	1,438301	0	1,471639	1,475306	0
2015-07-25	1,4853338	1,479979	1,6	1,524152	1,519857	1,2
2015-08-04	1,81292212	1,562539	1,7	1,925944	1,567547	2,3
2015-11-12	1,450440168	1,429497	2,4	1,458858	1,523051	1,2
2016-05-20	1,487441301	1,480594	3,2	1,551019	1,529711	2,4
2016-06-19	1,465721488	1,468278	0	1,46242	1,464396	0
2016-06-29	1,460241318	1,462143	1	1,453048	1,434411	1
2016-07-29	1,45856905	1,469418	0	1,460904	1,475439	0
2016-08-08	1,473885417	1,491727	1	1,472943	1,484192	1
2016-09-07	1,475266218	1,473939	1,2	1,458517	1,456998	1,1
2016-11-06	1,461493015	1,529179	2,7	1,475785	1,615496	2,4
2017-01-25	1,449424624	1,418164	1,5	1,453966	1,493437	0
2017-04-05	1,449667454	1,41235	1,3	1,453652	1,436126	0
2017-06-14	1,455024719	1,452475	1	1,454958	1,449898	0
2017-08-08	1,516404033	1,490903	1,2	1,639846	1,519363	0
2017-08-13	1,465337515	1,478168	0	1,462533	1,47397	1,1
2017-09-12	1,504301786	1,491677	2,3	1,59918	1,528662	0
2017-11-21	1,743048191	1,707428	1	1,637705	1,656472	0
2018-01-30	1,557977796	1,773571	1,3	1,474119	1,618193	1
2018-06-19	1,4632442	1,463715	1	1,46849	1,471485	1
2018-07-09	1,501565456	1,498882	0	1,495154	1,490804	0
2018-07-14	1,467972517	1,456917	1	1,477158	1,471034	1
2018-09-12	1,472877622	1,474371	1,2	1,476004	1,47815	1,2
2018-10-22	1,460495353	1,515476	2	1,475021	1,59004	2,3

Table 11 - Chlorophyl concentrations for MCI and BandRatio – Castelo de Bode dam

Date	MCI est1	R705_R655 est1	*In situ* est1	MCI est2	R705_R655 est2	*In situ* est2
2015-07-25	0,986502	0,988915	1	0,990948	0,99201	1
2015-08-24	1,027829	1,036653	1	0	0	1
2016-06-19	1,022162	1,019943	1	1,014178	1,000526	1
2016-08-28	1,002317	0,989092	1	1,015218	1,001928	1
2017-02-24	1,027794	1,037087	1,3	1,025923	1,024133	0
2017-04-15	1,026843	1,033625	1	1,020029	1,014836	0
2017-07-24	0,994221	0,993004	1	0,986645	0,992296	0
2017-09-02	0,99674	0,989617	0	0,996505	0,991255	1
2017-10-22	1,023527	1,018801	1	1,023932	1,022086	0
2018-02-24	1,027858	1,038131	1	1,027472	1,036141	1
2018-04-25	1,026579	1,032477	1	1,026544	1,032075	1
2018-06-24	1,024672	1,025519	1	1,023853	1,023169	1
2018-09-02	0	0	1	0	0	1
2018-10-07	1,011826	1,006347	1	1,002223	1,002463	1

Table 12 - Chlorophyl concentrations for MCI and BandRatio – Alqueva dam

Date	MCI MONTANTE	R705_R655 MONTANTE	*In situ* MONTANTE
2015-08-01	7,840458	5,014999	19,5
2015-08-21	13,16162	5,432555	17,3
2015-11-29	2,237266	4,941881	1
2016-04-27	2,124423	4,006136	0,1
2016-07-06	2,432184	4,42965	1,2
2016-08-25	7,889504	5,206491	0,5
2016-12-26	7,750412	6,647476	2
2017-01-25	6,878741	6,508973	2,1
2017-06-21	2,3288	4,299095	0,1
2017-08-25	2,304923	4,259435	3,9
2018-11-16	3,723111	6,648553	1,6
2019-01-12	2,386368	4,414465	1,5
2019-03-26	2,079376	3,961422	1
2019-06-21	2,437248	4,353075	6,3
2019-08-20	3,758407	4,677737	1,6
2020-12-05	5,636905	6,925854	1,2
2021-03-22	2,045649	3,700298	4,1
2021-06-23	4,1059	6,238665	8,4
2021-08-22	18,94469	6,389443	19
2021-11-17	2,046132	3,735398	1,5
2022-01-21	2,045696	3,742377	1,5
2022-04-06	2,088607	3,840789	1
2022-07-25	3,105376	4,604041	1,7
2022-11-07	2,05366	3,766213	9,9

Table 13 - Chlorophyl concentrations for MCI and BandRatio – Odelouca dam

Date	MCI (S)	R705_R655 (S)	*In situ* (S)	MCI INT (C)	R705_R655 INT (C)	*In situ* INT (C)
2015-07-15	1	1	1	1,384375	1,246722	1
2015-09-03	1,453868	1,274767	1	1,502725	1,536573	1
2015-11-22	1,397711	1,466711	1	1,402007	1,314603	1
2016-05-20	1	1	1	1	1	1
2016-07-19	1,388867	1,294194	1	1,397114	1,385391	1
2016-09-17	1,389726	1,341034	1	1,410069	1,609601	1
2016-11-16	1,446715	1,65957	1	1,450443	1,57386	1
2017-01-15	1	1	1	1	1	1
2017-06-04	1,404073	1,369391	1	1,403217	1,421289	2
2017-09-12	1,385445	1,284392	1	1,413034	1,597773	1
2017-11-06	1,385288	1,353406	1	1	1	1
2018-01-10	1	1	1	1	1	1
2018-06-14	1,399302	1,386826	1	1	1	1
2018-09-12	1	1,117008	1	1,395896	1,702666	2
2018-11-16	1,416692	1,680079	1	1,424232	1,63832	2
2019-01-25	1,388072	1,282889	1	1,389506	1,29482	1
2019-07-14	1,38764	1,281252	1	1,388853	1,312565	1
2019-09-17	1,504194	1,609053	1	1,53932	1,651238	1
2020-01-10	1,383889	1,230893	2	1,388964	1,301842	2
2020-05-24	1,387733	1,283684	1	1,387662	1,279251	1
2020-07-13	1,384651	1,235327	1	1,384711	1,23595	2
2020-09-21	1,419722	1,713563	1	1,420455	1,661078	2
2021-01-14	1,38175	1,128701	1	1,381759	1,131706	1
2021-04-04	1,394697	1,352202	2	1,389207	1,309085	1
2021-07-08	1	1	1	1	1	1
2021-09-06	1,394313	1,462471	2	1,394344	1,464389	1
2021-11-15	1,383844	1,371554	4	1	1	1
2022-01-29	1,39189	1,30528	1	1,392976	1,291017	2
2022-06-08	1,392879	1,302867	1	1,387788	1,260036	1
2022-07-08	1,398986	1,315425	1	1,398103	1,322796	0
2022-09-06	1,397561	1,443869	1	1,409147	1,545406	2
2022-11-05	1	1	3	1	1	4

Appendix C – TSM concentrations values

Table 14 - TSM concentrations – Agueira dam

Date	est1	est2	Mean
15/07/2015	0,123708	0,422016	0,272862
25/07/2015	0,780877	1,023599	0,902238
04/08/2015	2,715349	2,830474	2,772912
12/11/2015	0,019118	0,019481	0,0193
20/05/2016	0,768672	1,346848	1,05776
19/06/2016	0,310281	0,261328	0,285804
29/06/2016	0,224401	0,113232	0,168816
29/07/2016	0,163362	0,205711	0,184537
08/08/2016	0,230905	0,36955	0,300227
07/09/2016	0,609441	0,204494	0,406967
06/11/2016	0,013984	0,047215	0,0306
25/01/2017	0,014348	0,007628	0,010988
05/04/2017	0,018519	0,087527	0,053023
14/06/2017	0,14647	0,118455	0,132462
08/08/2017	1,259753	2,655198	1,957476
13/08/2017	0,221462	0,189989	0,205725
12/09/2017	0,982972	2,005287	1,494129
21/11/2017	0,333744	0,539533	0,436639
30/01/2018	0,143157	0,038399	0,090778
19/06/2018	0,345078	0,467467	0,406273
09/07/2018	1,003887	0,921933	0,96291
14/07/2018	0,535847	0,740259	0,638053
12/09/2018	0,526126	0,600265	0,563196
22/10/2018	0,014453	0,026864	0,020659

Table 15 - TSM concentrations – Castelo de Bode dam

Date	est1	est2	Mean
25/07/2015	0,406966	0,394434	0,4007
24/08/2015	0,00257	0,002	0,002285
19/06/2016	0,086717	0,168234	0,127475
28/08/2016	0,222103	0,135925	0,179014
24/02/2017	0,002694	0,024484	0,013589
15/04/2017	0,023769	0,118012	0,07089
24/07/2017	0,397605	0,53287	0,465238
02/09/2017	0,293133	0,351749	0,322441
22/10/2017	0,022416	0,035525	0,028971
24/02/2018	0,005251	0,013113	0,009182
25/04/2018	0,013571	0,009777	0,011674
24/06/2018	0,04778	0,056526	0,052153
07/10/2018	0,279437	0,516965	0,398201

Table 16 - TSM concentrations – Alqueva dam

Date	MONTANTE
01/08/2015	2,789646
21/08/2015	2,201797
29/11/2015	0,036189
27/04/2016	0,144523
06/07/2016	0,412919
25/08/2016	1,443196
26/12/2016	0,465203
25/01/2017	0,324461
21/06/2017	0,428805
25/08/2017	0,440193
16/11/2018	0,302117
12/01/2019	0,433407
26/03/2019	0,04474
21/06/2019	0,660364
20/08/2019	1,263538
05/12/2020	0,239099
22/03/2021	0,015789
23/06/2021	0,259864
22/08/2021	2,207712
17/11/2021	0,002027
21/01/2022	0,001678
06/04/2022	0,113718
25/07/2022	0,704638
07/11/2022	0,025812

Table 17 - TSM concentrations – Odelouca dam

Date	(S)	INT (C)	Mean
15/07/2015	0,3	0,395684	0,347842
03/09/2015	0,06	0,063614	0,061807
22/11/2015	2,101913	3,170442	2,636177
20/05/2016	1,816158	1,749538	1,782848
17/09/2016	0,815951	1,150952	0,983452
16/11/2016	0,970874	0,659208	0,815041
15/01/2017	0,67382	0,875507	0,774663
12/09/2017	1,557939	1,070904	1,314422
06/11/2017	0,443232	0,642863	0,543048
10/01/2018	0,140298	0,1	0,120149
12/09/2018	0,701149	0,7	0,700574
16/11/2018	0,3	0,332356	0,316178
25/01/2019	0,559454	1,162538	0,860996
14/07/2019	1,050116	0,938671	0,994393
17/09/2019	0,737118	0,653332	0,695225
10/01/2020	1,631495	3,073727	2,352611
24/05/2020	0,378552	0,479975	0,429264
13/07/2020	0,678434	0,668313	0,673374
21/09/2020	0,576575	0,560932	0,568754
14/01/2021	0,727487	0,799245	0,763366
04/04/2021	0,006001	0,007281	0,006641
08/07/2021	1,093099	0,744998	0,919048
15/11/2021	1,178983	0,657463	0,918223
29/01/2022	0,073094	0,07	0,071547
08/06/2022	0,716111	0,871619	0,793865
08/07/2022	0,709839	0,847419	0,778629
06/09/2022	1,936425	1,900242	1,918334
05/11/2022	0,792047	0,803899	0,797973

Appendix D – CDOM absorption values

Table 18 - CDOM absorption values - Aguieira Dam

Date	est1	est2	Mean
15/07/2015	0,019329	0,075856	0,047593
25/07/2015	0,167098	0,421034	0,294066
04/08/2015	0,51355	0,491937	0,502743
12/11/2015	0,096861	0,039018	0,06794
20/05/2016	0,210711	0,500249	0,35548
19/06/2016	0,033711	0,038181	0,035946
29/06/2016	0,021136	0,021256	0,021196
29/07/2016	0,015108	0,014972	0,01504
08/08/2016	0,057595	0,134763	0,096179
07/09/2016	0,133897	0,075629	0,104763
06/11/2016	0,250186	0,232146	0,241166
25/01/2017	0,00054	0,002876	0,001708
05/04/2017	0,022784	0,129857	0,07632
14/06/2017	0,01844	0,011633	0,015036
08/08/2017	0,290977	0,514827	0,402902
13/08/2017	0,058324	0,056164	0,057244
12/09/2017	0,351204	0,547881	0,449543
21/11/2017	0,129649	0,337523	0,233586
30/01/2018	0,084978	0,049685	0,067331
19/06/2018	0,103405	0,139666	0,121535
09/07/2018	0,235401	0,16851	0,201955
14/07/2018	0,085324	0,176899	0,131111
12/09/2018	0,135016	0,190201	0,162608
22/10/2018	0,193377	0,256078	0,224727

Table 19 - CDOM absorption values - Castelo de Bode Dam

Date	est1	est2	Mean
25/07/2015	0,04456	0,047848	0,046204
24/08/2015	0,000125	0,000125	0,000125
19/06/2016	0,009904	0,020629	0,015267
28/08/2016	0,043383	0,021403	0,032393
24/02/2017	0,00166	0,00144	0,00155
15/04/2017	0,007383	0,026539	0,016961
24/07/2017	0,053769	0,071779	0,062774
02/09/2017	0,050937	0,088955	0,069946
22/10/2017	0,116255	0,120301	0,118278
24/02/2018	0,005319	0,010426	0,007873
25/04/2018	0,003699	0,002298	0,002999
24/06/2018	0,013533	0,011532	0,012532
07/10/2018	0,10729	0,156801	0,132046

Table 20 - CDOM absorption values - Alqueva Dam

Date	MONTANTE
01/08/2015	0,29557097
21/08/2015	0,414353922
29/11/2015	0,032510118
27/04/2016	0,01114967
06/07/2016	0,165030997
25/08/2016	0,408267751
26/12/2016	0,075287081
25/01/2017	0,087901399
21/06/2017	0,101596948
25/08/2017	0,107189823
16/11/2018	0,171887562
12/01/2019	0,388207272
26/03/2019	0,000865252
21/06/2019	0,205970339
20/08/2019	0,147571824
05/12/2020	0,035981571
22/03/2021	0,00440493
23/06/2021	0,293089718
22/08/2021	0,792728245
17/11/2021	6,90688E-05
21/01/2022	5,37602E-05
06/04/2022	0,020041282
25/07/2022	0,119481571
07/11/2022	0,01447129

Table 21 - CDOM absorption values - Odelouca Dam

Date	(S)	INT (C)	Mean
15/07/2015	0,1	0,107208	0,103604
03/09/2015	0,01	0,01772	0,01386
22/11/2015	0,574585	0,463029	0,518807
20/05/2016	0,329692	0,392474	0,361083
17/09/2016	0,365825	0,534963	0,450394
16/11/2016	0,590339	0,283705	0,437022
15/01/2017	0,093455	0,287165	0,19031
12/09/2017	0,495896	0,549754	0,522825
06/11/2017	0,387379	0,236616	0,311997
10/01/2018	0,070024	0,07	0,070012
12/09/2018	0,363937	0,3	0,331969
16/11/2018	0,1	0,117138	0,108569
25/01/2019	0,092435	0,146616	0,119525
14/07/2019	0,273787	0,299766	0,286776
17/09/2019	0,327354	0,411487	0,369421
10/01/2020	0,237212	0,266611	0,251912
24/05/2020	0,062522	0,226748	0,144635
13/07/2020	0,212175	0,181854	0,197015
21/09/2020	0,160389	0,166518	0,163453
14/01/2021	0,091005	0,110315	0,10066
04/04/2021	0,00092	0,000269	0,000594
08/07/2021	0,45954	0,348835	0,404188
15/11/2021	0,526393	0,38481	0,455602
29/01/2022	0,043415	0,04	0,041707
08/06/2022	0,190181	0,219871	0,205026
08/07/2022	0,210274	0,137361	0,173818
06/09/2022	0,350519	0,401953	0,376236
05/11/2022	0,546524	0,535083	0,540803

Appendix E – Water quantity values

Table 22 – Water volume – Aguieira Dam

Date	Volume (dam^3)	Volume (%)
2012-01-01	356660	84,31%
2012-02-01	378530	89,48%
2012-03-01	383110	90,56%
2012-04-01	376500	89,00%
2012-05-01	406690	96,14%
2012-06-01	410580	97,06%
2012-07-01	399980	94,55%
2012-08-01	355820	84,11%
2012-09-01	313950	74,21%
2012-10-01	283200	66,95%
2012-11-01	273880	64,74%
2012-12-01	331780	78,43%
2013-01-01	369000	87,23%
2013-02-01	321650	76,03%
2013-03-01	328690	77,70%
2013-04-01	349740	82,67%
2013-05-01	410190	96,96%
2013-06-01	408800	96,64%
2013-07-01	395340	93,45%
2013-08-01	348880	82,47%
2013-09-01	300870	71,12%
2013-10-01	273750	64,71%
2013-11-01	314140	74,26%
2013-12-01	314060	74,24%
2014-01-01	303390	71,72%
2014-02-01	322280	76,18%
2014-03-01	314920	74,44%
2014-04-01	307430	72,67%
2014-05-01	400960	94,78%
2014-06-01	417830	98,77%
2014-07-01	403490	95,38%
2014-08-01	370820	87,66%
2014-09-01	327670	77,46%
2014-09-30	298000	70,44%
2014-10-31	304000	71,86%
2014-11-30	310000	73,28%
2015-01-01	279510	66,07%
2015-02-01	330310	78,08%

2015-03-01	336890	79,64%
2015-04-01	310160	73,32%
2015-05-01	342920	81,06%
2015-06-01	386830	91,44%
2015-07-01	361190	85,38%
2015-08-01	323870	76,56%
2015-09-01	281420	66,52%
2015-10-01	261490	61,81%
2015-11-01	268590	63,49%
2015-12-01	295190	69,78%
2016-01-01	310310	73,35%
2016-02-01	286530	67,73%
2016-03-01	293890	69,47%
2016-04-01	328850	77,74%
2016-05-01	401150	94,83%
2016-06-01	409790	96,87%
2016-07-01	391700	92,59%
2016-08-01	358810	84,82%
2016-09-01	309250	73,10%
2016-10-01	280190	66,23%
2016-11-01	265020	62,65%
2016-12-01	293320	69,34%
2017-01-01	321020	75,89%
2017-02-01	269280	63,66%
2017-03-01	286250	67,67%
2017-04-01	344780	81,50%
2017-05-01	369000	87,23%
2017-06-01	370270	87,53%
2017-07-01	345970	81,78%
2017-08-01	297360	70,29%
2017-09-01	262350	62,02%
2017-10-01	239260	56,56%
2017-11-01	223940	52,94%
2017-12-01	213580	50,49%
2018-01-01	240870	56,94%
2018-02-01	330800	78,20%
2018-03-01	304130	71,89%
2018-04-01	321170	75,92%
2018-05-01	416570	98,47%
2018-06-01	410780	97,10%
2018-07-01	402710	95,20%
2018-08-01	363070	85,83%
2018-09-01	315070	74,48%

2018-10-01	276950	65,47%
2018-11-01	258470	61,10%
2018-12-01	301170	71,19%
2019-01-01	295910	69,95%
2019-02-01	318030	75,18%
2019-03-01	326110	77,09%
2019-04-01	338380	79,99%
2019-05-01	413170	97,67%
2019-06-01	397660	94,00%
2019-07-01	389200	92,00%
2019-08-01	357570	84,53%
2019-09-01	316160	74,74%
2019-10-01	281970	66,65%
2019-11-01	264770	62,59%
2019-12-01	351470	83,08%
2020-01-01	307730	72,74%
2020-02-01	278700	65,88%
2020-03-01	319750	75,59%
2020-04-01	355470	84,03%
2020-05-01	391510	92,55%
2020-06-01	405850	95,94%
2020-07-01	395340	93,45%
2020-08-01	354590	83,82%
2020-09-01	312300	73,82%
2020-10-01	276010	65,25%
2020-11-01	288920	68,30%
2020-12-01	284310	67,21%
2021-01-01	305330	72,18%
2021-02-01	288770	68,26%
2021-03-01	291890	69,00%
2021-04-01	330960	78,24%
2021-05-01	404470	95,61%
2021-06-01	402320	95,10%
2021-07-01	403690	95,43%
2021-08-01	380200	89,88%
2021-09-01	328690	77,70%
2021-10-01	293030	69,27%
2021-11-01	313680	74,15%
2021-12-01	287650	68,00%
2022-01-01	302650	71,54%
2022-02-01	286810	67,80%
2022-03-01	305630	72,25%
2022-04-01	359340	84,94%

2022-05-01	421610	99,66%
2022-06-01	410380	97,01%
2022-07-01	386010	91,25%
2022-08-01	342070	80,86%
2022-09-01	302790	71,58%
2022-10-01	278290	65,78%
2022-11-01	276140	65,28%
2022-12-01	290470	68,66%
2023-01-01	298090	70,47%
2023-02-01	303690	71,79%
2023-03-01	299840	70,88%
2023-04-01	354600	83,82%
2023-05-01	377610	89,26%
2023-06-01	375580	88,78%
2023-07-01	392200	92,71%
2023-08-01	352510	83,33%
2023-09-01	308340	72,89%
2023-10-01	281230	66,48%
2023-11-01	273930	64,75%
2023-12-01	280270	66,25%
2024-01-01	283340	66,98%
2024-02-01	298410	70,54%
2024-03-01	375760	88,83%
2024-04-01	362000	85,57%
2024-05-01	397890	94,06%

Table 23 - Water volume – Castelo de Bode Dam

Date	Volume (dam^3)	Volume (%)
2012-01-01	890850	81,36%
2012-02-01	878400	80,22%
2012-03-01	858250	78,38%
2012-04-01	843200	77,00%
2012-05-01	835390	76,29%
2012-06-01	872150	79,65%
2012-07-01	860860	78,62%
2012-08-01	830640	75,86%
2012-09-01	819210	74,81%
2012-10-01	817260	74,64%
2012-11-01	831070	75,90%
2012-12-01	850430	77,66%
2013-01-01	885500	80,87%
2013-02-01	989300	90,35%
2013-03-01	985400	89,99%
2013-04-01	1061680	96,96%
2013-05-01	995060	90,87%
2013-06-01	1016790	92,86%
2013-07-01	973340	88,89%
2013-08-01	942040	86,03%
2013-09-01	896400	81,86%
2013-10-01	875650	79,97%
2013-11-01	899700	82,16%
2013-12-01	852480	77,85%
2014-01-01	916200	83,67%
2014-02-01	975030	89,04%
2014-03-01	1019490	93,10%
2014-04-01	973000	88,86%
2014-05-01	969330	88,52%
2014-06-01	1032470	94,29%
2014-07-01	1012190	92,44%
2014-08-01	923450	84,33%
2014-09-01	867320	79,21%
2014-10-01	820150	74,90%
2014-11-01	838570	76,58%
2014-12-01	894740	81,71%
2015-01-01	821580	75,03%
2015-02-01	882640	80,61%
2015-03-01	931700	85,09%
2015-04-01	944350	86,24%

2015-05-01	921490	84,15%
2015-06-01	867290	79,20%
2015-07-01	878880	80,26%
2015-08-01	879760	80,34%
2015-09-01	839440	76,66%
2015-10-01	795270	72,63%
2015-11-01	779490	71,19%
2015-12-01	762920	69,67%
2016-01-01	761560	69,55%
2016-02-01	918420	83,87%
2016-03-01	1036470	94,65%
2016-04-01	1036860	94,69%
2016-05-01	1048170	95,72%
2016-06-01	1057570	96,58%
2016-07-01	1006890	91,95%
2016-08-01	904920	82,64%
2016-09-01	881780	80,53%
2016-10-01	860570	78,59%
2016-11-01	832800	76,05%
2016-12-01	818140	74,72%
2017-01-01	858250	78,38%
2017-02-01	808720	73,86%
2017-03-01	878590	80,24%
2017-04-01	855070	78,09%
2017-05-01	802760	73,31%
2017-06-01	833370	76,11%
2017-07-01	846670	77,32%
2017-08-01	849270	77,56%
2017-09-01	878010	80,18%
2017-10-01	837700	76,50%
2017-11-01	786430	71,82%
2017-12-01	751790	68,66%
2018-01-01	767300	70,07%
2018-02-01	771700	70,47%
2018-03-01	763190	69,70%
2018-04-01	1015630	92,75%
2018-05-01	1052250	96,10%
2018-06-01	1009530	92,19%
2018-07-01	935760	85,46%
2018-08-01	912610	83,34%
2018-09-01	895570	81,79%
2018-10-01	871870	79,62%
2018-11-01	840300	76,74%

2018-12-01	835110	76,27%
2019-01-01	828190	75,63%
2019-02-01	823880	75,24%
2019-03-01	839440	76,66%
2019-04-01	840300	76,74%
2019-05-01	877420	80,13%
2019-06-01	879170	80,29%
2019-07-01	870130	79,46%
2019-08-01	897230	81,94%
2019-09-01	884070	80,74%
2019-10-01	870420	79,49%
2019-11-01	846670	77,32%
2019-12-01	875060	79,91%
2020-01-01	1044520	95,39%
2020-02-01	1037260	94,73%
2020-03-01	937220	85,59%
2020-04-01	906020	82,74%
2020-05-01	978450	89,36%
2020-06-01	938100	85,67%
2020-07-01	908210	82,94%
2020-08-01	909700	83,08%
2020-09-01	887200	81,02%
2020-10-01	852460	77,85%
2020-11-01	903820	82,54%
2020-12-01	922890	84,28%
2021-01-01	927410	84,69%
2021-02-01	919530	83,98%
2021-03-01	1021050	93,25%
2021-04-01	959870	87,66%
2021-05-01	945860	86,38%
2021-06-01	957320	87,43%
2021-07-01	956060	87,31%
2021-08-01	937220	85,59%
2021-09-01	907390	82,87%
2021-10-01	855930	78,17%
2021-11-01	777790	71,03%
2021-12-01	750980	68,58%
2022-01-01	707160	64,58%
2022-02-01	646700	59,06%
2022-03-01	651510	59,50%
2022-04-01	715890	65,38%
2022-05-01	763470	69,72%
2022-06-01	790620	72,20%

2022-07-01	776130	70,88%
2022-08-01	744800	68,02%
2022-09-01	720550	65,80%
2022-10-01	704350	64,32%
2022-11-01	690470	63,06%
2022-12-01	744800	68,02%
2023-01-01	1016020	92,79%
2023-02-01	1002400	91,54%
2023-03-01	986110	90,06%
2023-04-01	974020	88,95%
2023-05-01	963090	87,95%
2023-06-01	944050	86,21%
2023-07-01	936630	85,54%
2023-08-01	885210	80,84%
2023-09-01	801630	73,21%
2023-10-01	749360	68,43%
2023-11-01	882590	80,60%
2023-12-01	930430	84,97%
2024-01-01	906570	82,79%
2024-02-01	931990	85,11%
2024-03-01	964070	88,04%
2024-04-01	1062430	97,03%
2024-05-01	1016400	92,82%

Table 24 - Water volume - Alqueva Dam

Date	Volume (dam^3)	Volume (%)
2012-01-01	3098870	74,67%
2012-02-01	3148990	75,88%
2012-03-01	3094870	74,58%
2012-04-01	3097360	74,64%
2012-05-01	3123570	75,27%
2012-06-01	3102500	74,76%
2012-07-01	3076420	74,13%
2012-08-01	3039480	73,24%
2012-09-01	2974810	71,68%
2012-10-01	2972370	71,62%
2012-11-01	3019910	72,77%
2012-12-01	3394200	81,79%
2013-01-01	3452190	83,19%
2013-02-01	3646580	87,87%
2013-03-01	3754000	90,46%
2013-04-01	4047910	97,54%
2013-05-01	4010360	96,64%
2013-06-01	4062160	97,88%
2013-07-01	3998320	96,35%
2013-08-01	3824080	92,15%
2013-09-01	3675600	88,57%
2013-10-01	3560800	85,80%
2013-11-01	3523750	84,91%
2013-12-01	3437880	82,84%
2014-01-01	3423710	82,50%
2014-02-01	3521620	84,86%
2014-03-01	3933610	94,79%
2014-04-01	3987000	96,07%
2014-05-01	3983550	95,99%
2014-06-01	3903900	94,07%
2014-07-01	3750970	90,38%
2014-08-01	3622670	87,29%
2014-09-01	3464640	83,49%
2014-10-01	3381510	81,48%
2014-11-01	3395780	81,83%
2014-12-01	3622700	87,29%
2015-01-01	3590130	86,51%
2015-02-01	3579340	86,25%
2015-03-01	3535100	85,18%
2015-04-01	3427650	82,59%

2015-05-01	3326900	80,17%
2015-06-01	3260230	78,56%
2015-07-01	3177780	76,57%
2015-08-01	3099060	74,68%
2015-09-01	3033430	73,09%
2015-10-01	3014250	72,63%
2015-11-01	3114350	75,04%
2015-12-01	3079950	74,22%
2016-01-01	3087640	74,40%
2016-02-01	3174300	76,49%
2016-03-01	3152710	75,97%
2016-04-01	3102880	74,77%
2016-05-01	3160100	76,15%
2016-06-01	3433460	82,73%
2016-07-01	3330950	80,26%
2016-08-01	3250790	78,33%
2016-09-01	3170290	76,39%
2016-10-01	3114350	75,04%
2016-11-01	3102880	74,77%
2016-11-30	3204837	77,22%
2017-01-01	3123930	75,28%
2017-02-01	3112430	75,00%
2017-03-01	3250790	78,33%
2017-04-01	3185870	76,77%
2017-05-01	3211320	77,38%
2017-06-01	3148970	75,88%
2017-07-01	3083840	74,31%
2017-08-01	2962480	71,39%
2017-09-01	2920550	70,37%
2017-10-01	2868450	69,12%
2017-11-01	2850670	68,69%
2017-12-01	2812770	67,78%
2018-01-01	2800820	67,49%
2018-02-01	2760330	66,51%
2018-03-01	2673310	64,42%
2018-04-01	3455780	83,27%
2018-05-01	3549310	85,53%
2018-06-01	3610480	87,00%
2018-07-01	3547430	85,48%
2018-08-01	3387310	81,62%
2018-09-01	3397270	81,86%
2018-10-01	3353980	80,82%
2018-11-01	3315280	79,89%

2018-12-01	3391050	81,71%
2019-01-01	3405570	82,06%
2019-02-01	3360140	80,97%
2019-03-01	3331520	80,28%
2019-04-01	3203470	77,19%
2019-05-01	3155360	76,03%
2019-06-01	3118530	75,15%
2019-07-01	2957350	71,26%
2019-08-01	2875410	69,29%
2019-09-01	2768680	66,72%
2019-10-01	2691820	64,86%
2019-11-01	2740330	66,03%
2019-12-01	2678940	64,55%
2020-01-01	2799930	67,47%
2020-02-01	2794700	67,34%
2020-03-01	2847200	68,61%
2020-04-01	2694780	64,93%
2020-05-01	2890900	69,66%
2020-06-01	2761940	66,55%
2020-07-01	2669540	64,33%
2020-08-01	2577020	62,10%
2020-09-01	2481030	59,78%
2020-10-01	2386630	57,51%
2020-11-01	2388610	57,56%
2020-12-01	2537120	61,14%
2021-01-01	2735360	65,91%
2021-02-01	2812170	67,76%
2021-03-01	3613940	87,08%
2021-04-01	3759900	90,60%
2021-05-01	3755370	90,49%
2021-06-01	3641260	87,74%
2021-07-01	3460490	83,39%
2021-08-01	3328330	80,20%
2021-09-01	3192440	76,93%
2021-10-01	3229410	77,82%
2021-11-01	3274620	78,91%
2021-12-01	3229410	77,82%
2022-01-01	3276600	78,95%
2022-02-01	3280560	79,05%
2022-03-01	3250970	78,34%
2022-04-01	3221600	77,63%
2022-05-01	3204080	77,21%
2022-05-31	3078000	74,17%

2022-07-01	2970320	71,57%
2022-08-01	2842760	68,50%
2022-09-01	2724780	65,66%
2022-10-01	2658950	64,07%
2022-11-01	2612480	62,95%
2022-12-01	2584600	62,28%
2023-01-01	3564920	85,90%
2023-02-01	3682640	88,74%
2023-03-01	3573380	86,11%
2023-04-01	3485330	83,98%
2023-05-01	3382730	81,51%
2023-06-01	3300400	79,53%
2023-07-01	3161190	76,17%
2023-08-01	3025580	72,91%
2023-09-01	2867550	69,10%
2023-10-01	2828670	68,16%
2023-11-01	2890020	69,64%
2023-12-01	2952080	71,13%
2024-01-01	2984980	71,93%
2024-02-01	3427580	82,59%
2024-03-01	3579740	86,26%
2024-04-01	3942220	94,99%
2024-05-01	3955040	95,30%

Table 25 - Water volume - Odelouca Dam

Date	Volume (dam^3)	Volume (%)
2012-01-01	101400	64,59%
2012-02-01	102400	65,22%
2012-03-01	102600	65,35%
2012-04-01	103400	65,86%
2012-05-01	104700	66,69%
2012-05-31	105804	67,39%
2012-06-30	99555	63,41%
2012-07-31	91247	58,12%
2012-08-31	82946	52,83%
2012-10-01	78080	49,73%
2012-09-30	78210	49,82%
2012-10-31	74750	47,61%
2013-01-01	96300	61,34%
2013-02-01	113370	72,21%
2013-03-01	116440	74,17%
2013-04-01	127720	81,35%
2013-05-01	129420	82,43%
2013-06-01	126150	80,35%
2013-07-01	120810	76,95%
2013-08-01	114140	72,70%
2013-09-02	107870	68,71%
2013-10-01	103830	66,13%
2013-11-01	102490	65,28%
2013-12-01	98300	62,61%
2014-01-01	97420	62,05%
2014-02-01	100310	63,89%
2014-03-01	115550	73,60%
2014-04-01	115250	73,41%
2014-05-01	132310	84,27%
2014-06-01	127890	81,46%
2014-07-01	112530	71,68%
2014-08-01	116660	74,31%
2014-09-01	110310	70,26%
2014-10-01	106140	67,61%
2014-11-01	102750	65,45%
2014-12-01	118680	75,59%
2015-01-01	118500	75,48%
2015-02-01	120910	77,01%
2015-03-01	120570	76,80%
2015-04-01	118250	75,32%

2015-05-01	116720	74,34%
2015-06-01	111980	71,32%
2015-07-01	106040	67,54%
2015-08-01	99370	63,29%
2015-09-01	92750	59,08%
2015-09-30	87830	55,94%
2015-11-01	84280	53,68%
2015-12-01	88270	56,22%
2016-01-01	85010	54,15%
2016-02-01	86890	55,34%
2016-03-01	86440	55,06%
2016-04-01	84380	53,75%
2016-05-01	83630	53,27%
2016-06-01	95550	60,86%
2016-07-01	89930	57,28%
2016-08-01	83240	53,02%
2016-09-01	76518	48,74%
2016-10-01	70962	45,20%
2016-11-01	66955	42,65%
2016-12-01	64336	40,98%
2017-01-01	71883	45,79%
2017-02-01	77700	49,49%
2017-03-01	88746	56,53%
2017-04-01	92841	59,13%
2017-05-01	90432	57,60%
2017-06-01	86436	55,05%
2017-07-01	80778	51,45%
2017-08-01	74165	47,24%
2017-09-01	67521	43,01%
2017-10-01	63114	40,20%
2017-11-01	59293	37,77%
2017-12-01	56563	36,03%
2018-01-01	54214	34,53%
2018-02-01	51933	33,08%
2018-03-01	51075	32,53%
2018-04-01	98731	62,89%
2018-05-01	114351	72,84%
2018-06-01	111099	70,76%
2018-07-01	105270	67,05%
2018-08-01	98372	62,66%
2018-09-01	91025	57,98%
2018-10-01	85387	54,39%
2018-11-01	81144	51,68%

2018-12-01	78736	50,15%
2019-01-01	75345	47,99%
2019-02-01	73051	46,53%
2019-03-01	74502	47,45%
2019-04-01	72936	46,46%
2019-05-01	72776	46,35%
2019-06-01	70386	44,83%
2019-07-01	67455	42,96%
2019-08-01	64199	40,89%
2019-09-01	60484	38,52%
2019-10-01	57963	36,92%
2019-11-01	56187	35,79%
2019-12-01	55242	35,19%
2020-01-01	72641	46,27%
2020-02-01	82094	52,29%
2020-03-01	83010	52,87%
2020-04-01	84585	53,88%
2020-05-01	89998	57,32%
2020-06-01	91030	57,98%
2020-07-01	90271	57,50%
2020-08-01	86099	54,84%
2020-09-01	81916	52,18%
2020-10-01	78423	49,95%
2020-11-01	74584	47,51%
2020-12-01	78809	50,20%
2021-01-01	87146	55,51%
2021-02-01	87430	55,69%
2021-03-01	114128	72,69%
2021-04-01	118947	75,76%
2021-05-01	116804	74,40%
2021-06-01	112655	71,75%
2021-07-01	107369	68,39%
2021-08-01	101129	64,41%
2021-09-01	94756	60,35%
2021-10-01	90775	57,82%
2021-11-01	86680	55,21%
2021-12-01	83621	53,26%
2022-01-01	81831	52,12%
2022-02-01	79179	50,43%
2022-03-01	76744	48,88%
2022-04-01	75522	48,10%
2022-05-01	73612	46,89%
2022-06-01	69598	44,33%

2022-07-01	64880	41,32%
2022-08-01	59582	37,95%
2022-09-01	54626	34,79%
2022-10-01	51450	32,77%
2022-11-01	48883	31,14%
2022-12-01	48748	31,05%
2023-01-01	59232	37,73%
2023-02-01	60765	38,70%
2023-03-01	61465	39,15%
2023-04-01	60484	38,52%
2023-05-01	57315	36,51%
2023-06-01	54117	34,47%
2023-07-01	50783	32,35%
2023-08-01	46077	29,35%
2023-09-01	40898	26,05%
2023-10-01	37410	23,83%
2023-11-01	37751	24,05%
2023-12-01	37831	24,10%
2024-01-01	38677	24,64%
2024-02-01	45442	28,94%
2024-03-01	50974	32,47%
2024-04-01	68293	43,50%
2024-04-30	73051	46,53%